Technical Letter                                                    1 June 2010
No. 1110-2-566

EXPIRES 1 June 2015
Engineering and Design
**ADVANCED RELIABILITY ANALYSIS OF FATIGUE CRACKING
IN HORIZONTALLY FRAMED MITER GATES**

1. <u>Purpose</u>. A series of navigational locks and dams along the nation's inland waterways provide the ability to transport large tonnages of materials and goods efficiently over long distances. These facilities are operated and maintained by the U. S. Army Corps of Engineers and form a vital part of the transportation economy of this country. The lock miter gates, which are large steel structures that open and close to allow passage of vessels while maintaining required water pools at the dams, are critical components in this transportation system. Most of these miter gates are fabricated with welded steel plates using either horizontally framed or vertically framed designs. Cracking damage has become an increasing maintenance problem on these fabricated steel miter gates. The objective of this Engineer Technical Letter is to enhance and generalize the previously developed analytical methodology for fatigue crack evaluation with the goal of developing this methodology for miter gate fracture, fatigue, reliability, and repair.

2. <u>Applicability</u>. This Engineer Technical Letter is applicable to all HQUSACE elements and USACE commands having responsibilities for the planning, design, construction, and maintenance of civil works projects.

3. <u>Distribution Statement</u>. Approved for public release; distribution is unlimited.

4. <u>References</u>. References are included in Appendix A.


JAMES C. DALTON, P.E.
Chief, Engineering and Construction
Directorate of Civil Works

DEPARTMENT OF THE ARMY          ETL 1110-2-566
U.S. Army Corps of Engineers
CECW-EC          Washington, DC 20314-1000

Technical Letter          1 June 2010
No. 1110-2-566

EXPIRES 1 June 2015
Engineering and Design
ADVANCED RELIABILITY ANALYSIS OF FATIGUE CRACKING
IN HORIZONTALLY FRAMED MITER GATES

TABLE OF CONTENTS

**CHAPTER 1**
**INTRODUCTION**

1-1.  Background.

a.  A series of navigational locks and dams along the nation's inland waterways provide the ability to transport large tonnages of materials and goods efficiently over long distances.  These facilities are operated and maintained by the U. S. Army Corps of Engineers and form a vital part of the transportation economy of this country.  The lock miter gates, which are large steel structures that open and close to allow passage of vessels while maintaining required water pools at the dams, are critical components in this transportation system.  Most of these miter gates are fabricated with welded steel plates using either horizontally framed or vertically framed designs.  The horizontally framed design has evolved as the preferred configuration (Engineer Manual (EM) 1110-2-2105, EM 1110-2-2703) and consists of a series of horizontal girders with upstream and downstream flange plates welded to the web plate, as illustrated in Figure 1-1.  These horizontal girders are framed together with vertical diaphragms, again composed of welded plate sections, with skin plate attached across all the upstream flanges.  For each lock operation, the loading is cycled from the gate open, free-hanging condition to the mitered operating condition where the gate uses arch action through the girders to transmit the hydrostatic water loads into the lock walls.  In the load cycle, the gates are also pushed or pulled through the water, typically by means of a hydraulically actuated strut arm attached near the top of the gate.  This eccentric loading, from strut arm forces near the top of the gate and resistance on the submerged surfaces from the movement through the water, causes twisting or warping loads to develop in the gate.  Tensioned bars or diagonals are attached diagonally across the gate to help resist these torsion type loads and to help resist sagging at the miter end under the dead weight of the gate.

b.  Cracking damage has become an increasing maintenance problem on these fabricated steel miter gates.  Such problems have occurred at Bankhead Lock (1975), Upper St. Anthony's Falls, Poe Locks at the Soo (1968), Snell Locks (1959) on the St. Lawrence Seaway, Greenup (1959), Meldahl (1959), Markland (1960), and McAlpine (1961) Locks to name a few.  Damage to the gates caused by barge impact or an obstruction from debris caught on the sill is generally localized to the impacted area.  The damage from these type events usually is easily detected, either visually or from complications in gate operations, and is repaired as soon as practical.  Fatigue cracking, which typically originates at a welded connection and can generally be much more widespread in the gate, is also a serious problem.  This cracking occurs most frequently in the lower parts of the gates that remain covered by the lower pool and often requires unscheduled lock outages to make repairs when found during normal maintenance inspections.  Although the operating loads may be carried through compression in these components, the tensile residual stress at the welded connection, coupled with the geometric concentration and weld geometry, can cause fatigue cracking to develop at these connections.  Furthermore, in many cases and depending on the weld configuration, this cracking will extend beyond the weld zone and well into the base metal of the flanges.  This type of cracking can be widespread because all girders are essentially designed to carry similar loads, and all have the same welded connection configurations.  These miter gates are redundant structures because the framed design configurations allow loads to redistribute easily around damaged areas.  However, since the

flanges are major load-bearing components for the designs, widespread fatigue cracking affecting the flanges can eventually lead to structural failure or safety issues.  Many times, field repairs, such as gouging and rewelding or even welding on additional gusset plates, are instituted in an ad hoc manner when unexpected cracking is found during an inspection to complete repairs in a timely manner during the scheduled lock outage period.  It has also been found that historically these types of repairs are susceptible to re-cracking or causing cracks to start in a new location.  The residual stresses and less than optimal weld conditions in the field generally cause new cracks at the repaired locations to develop within a relatively small number of additional operating cycles.  Typically cracks can be found at any location on a miter gate, but commonly appear near the lower girders near the quoin and miter ends.



Figure 1-1.  Horizontally framed miter gates in lock chamber, downstream view

c.  In July 1994, the 1200-ft (366-m) chamber at the Markland Lock, Ohio River, was dewatered for scheduled maintenance, and significant structural damage was found in the lower portions of the gates especially near the quoin where the operating loads are carried in compression (Werncke and McClellan 1996).  The gates were repaired and returned to service, but because this damage was unexpected and more severe than previously encountered, an engineering study was undertaken to evaluate and better understand the root cause of the cracking.  In 1996, an analytical study was completed and showed that the residual tensile stress field at the welded flange connections, interacting with the high compressive stress during the

operation part of the load cycle, was sufficient to grow the cracks well into the base metal of the flanges (James and Zhang 1996).  The cracking was exacerbated by the stress concentrations at the welded connections, both from re-entrant corner geometry and from welding procedures leaving large weld beads, and also from increasingly elevated compressive stresses in the downstream flanges caused by mechanical wear of gate components.  This work developed analytical methodology for an engineering assessment of this complex problem, using global finite element models to understand overall gate performance, local modeling to establish residual stress fields and stress concentrations at the welded connection, and J-integral analyses to characterize crack extension within the residual stress field for use in calculating fatigue crack growth rates.  This methodology was later extended for use in the Ohio River Main Stem Systems Study by developing probabilistic-based reliability models to account for uncertainties (James et al. 2001) and subsequent coupling with economic consequence evaluations.

1-2.  Objectives and Scope.

a.  Similar cracking has been found to be a continuing problem at other navigational locks, sometimes with unscheduled maintenance needed for repairs causing extended and unplanned shutdowns of the lock system.  Recent examples of extensive cracking found on the miter gates occurred at Bankhead Lock in 1999, at Greenup Lock during the 2003 maintenance dewatering (Padula, Barker, and Kish 2005), and during an emergency closure of the 1200-ft (366-m) chamber at McAlpine Lock in 2004.  The objective of the work described herein is to enhance and generalize the previously developed analytical methodology for fatigue crack evaluation with the goal of developing this Engineer Technical Letter for miter gate fracture, fatigue, reliability, and repair.

b.  As a first step, the objective of this report is to highlight the problems through historical experiences, describe the current analytical methodology for evaluating fatigue cracking for several types of problematic connections, and provide example case studies where the methods have been used to evaluate project specific situations.  The ultimate goal is the development of an engineering tool for predicting and evaluating performance and reliability of long-term miter gates affected by fatigue cracking problems.  The current vision for such a tool is to integrate the Corps experience base in dealing with these problems with methods of extrapolating finite element results and field data using a probabilistic framework.  This tool would be intended as an aid in scheduling inspections, optimizing repairs, or developing maintenance versus rehabilitation strategies for welded lock miter gates.

**CHAPTER 2**
**FATIGUE CRACKING OF MITER GATES**

2-1.  Historical Perspective.

a.  An example of a typical experience with fatigue cracking on horizontally framed miter gates involves the cracking and repairs encountered at Markland Locks and Dam on the Ohio River.  The 1200-ft (366-m) chamber was operational in 1959, and the miter gates performed some 80,000 lock operations or load cycles with only minimal maintenance until the early 1980's.  In 1983 and 1984, the lock was scheduled for dewatering to perform maintenance and refurbishing of the pintles necessitated by normal mechanical wear over more than 24 years of operations.  During this dewatering and inspection, some small cracks were found at the welded joint connections of the downstream girder flanges with the vertical diaphragm flanges.  Most of these cracks were found near the quoin and miter ends of the gate where high compressive loads are transferred into the lock wall from the arch action of the miter gates.  This fatigue cracking was unexpected because the cracking components were loaded in compression and had experienced relatively few stress cycles.  For example, the typical downstream flange stress in horizontally framed miter gates in these regions during operation is around 10-15 ksi (44-67 kN) in compression, and structural steel, even experiencing a stress range of 20 ksi (89 kN) with tension (alternating stress of 10 ksi (44 kN)), should have an endurance limit of over 1 million cycles.  Thus, the stress range acting at the welded connection was greatly enhanced because of the geometric discontinuities, both from the re-entrant corner connection and the weld bead configuration, and also the residual stresses present from the weld operations.  In addition, the stress range for the load cycle may be exacerbated by higher compressive stress in the flanges under gate operations caused by mechanical wear in the gate components, especially those with high bearing loads.  Another factor in the development of these cracks was corrosion fatigue.  It is well known that cracks in carbon steels propagate more rapidly in aqueous environments than in air (American Society of Mechanical Engineers 1998).  Cracks found in 1983 and 1984 were repaired while the lock was dewatered by burning out the longer cracks with a torch and welding the resulting slit.  Figure 2-1 illustrates fatigue cracking at welded joints of the horizontal girder flanges near the quoin where operating loads are compressive.  Figure 2-2 illustrates fatigue cracking initiating in the corner of a welded joint and extending into the horizontal girder flange.

b.  During the next dewatering for inspection in 1987 and 1988 more extensive cracking was found. Some of the cracks that were repaired in the previous dewatering had already developed new cracks through completed repairs of the previous cracks welded 4 years prior. Gouging and rewelding of cracks in the field, even if performed properly, can increase the residual tensile stresses at the connections because the components being welded in this situation are generally highly constrained, especially near the quoin and miter ends where the plates are shorter and thicker.  This constraint will generate increased magnitudes and extents of the residual stresses at the welded joint.  This increases the cyclic stress range because of higher tensile stresses when the gate is open, and new cracks can initiate under very few additional cycles.  In addition, field welding can often leave microvoids or discontinuities that can coalesce into initial flaws that then propagate as fatigue cracks through the thickness of the plates.  For the repairs in 1987-1988, gusset plates were added in the corners of the flange connections where the cracking was developing, as illustrated in Figure 2-3.  These triangular shaped gusset plates with

Figure 2-1.  Fatigue cracking at welded joints of horizontal girders
loaded in compression



Figure 2-2.  Example of fatigue crack at welded joint extending
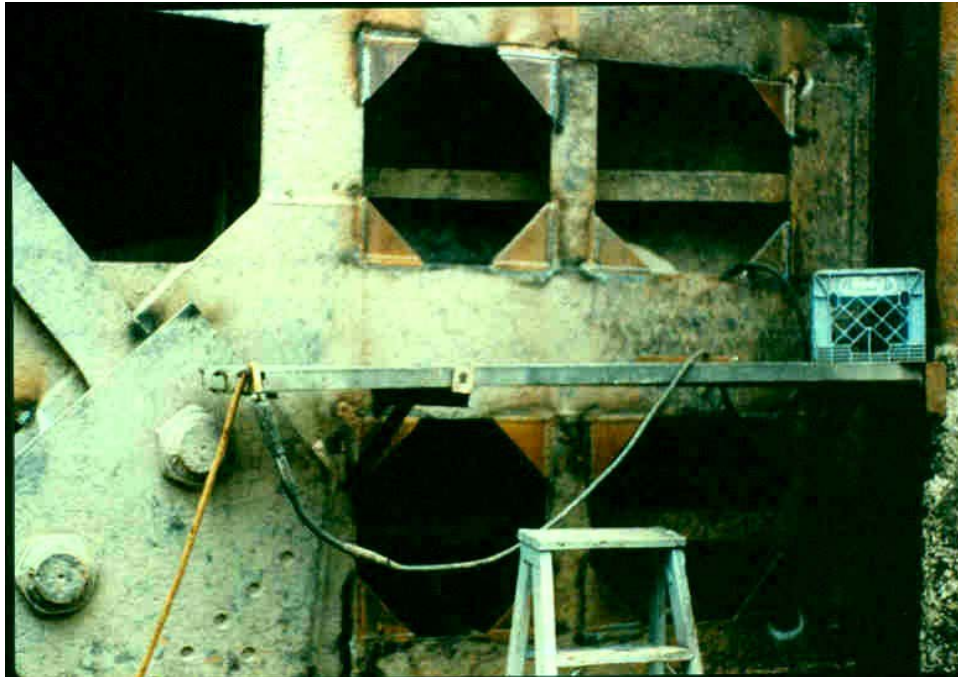into horizontal girder flange

Figure 2-3.  Addition of triangular gusset plates as part of
cracking repairs

a 45-deg angle across the free face were welded along the edges to the flanges in the corner
connections in hopes of reducing the stress concentration at the re-entrant corner of the flange
connection.  During the de-watering inspections in 1994, after 6 years and approximately 21,000
additional load cycles later, even more extensive cracking was discovered.  Many cracks had
initiated in the flanges where the tip of the gusset plates ends.  This cracking is illustrated in
Figure 2-4 and Figure 2-5.  Again, high residual tensile stresses and perhaps embedded voids
were introduced from the welding operations under constrained conditions.  Also, additional
cracking had initiated and grown into the flanges at other welded connections where gusset
plates had not been installed.  Cracks extending 2 to 4 in. (0.05 to 0.1 m) into the flanges were
found during the 1994 dewatering.  For this more extensive cracking in the regions near the
quoin and miter ends of the gates, a new repair procedure was developed.  In these regions, the
girder flanges framing into the vertical diaphragm flanges created rectangular openings.  This
repair procedure first removes any gusset plates previously installed in the corners and then
installs a prefabricated "window frame" having a rectangular outer perimeter to weld along the
edges of the flanges, as illustrated in Figure 2-6.  The interior of the window frame incorporates
radius corners.  This maintains an opening for inspection of the interior components while
providing relief in the stress concentrations at the welded corners.  In addition, the new welded
connections are now around the edges of the window frames away from the free surface where
cracks are more likely to initiate.  Another dewatering and lock outage was scheduled for 1996 to
complete the repairs using the window frame procedure.  Subsequent inspections have so far
confirmed that the window frame technique is effective in mitigating fatigue cracking at these
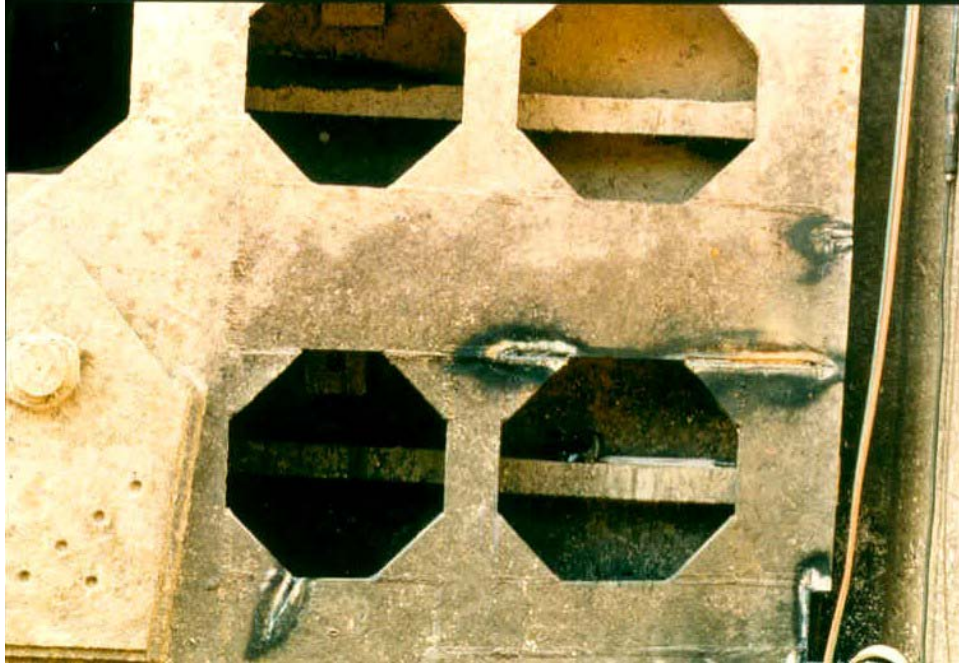welded joint connections.

Figure 2-4.  Cracking at toe of gusset plates added to flange connections
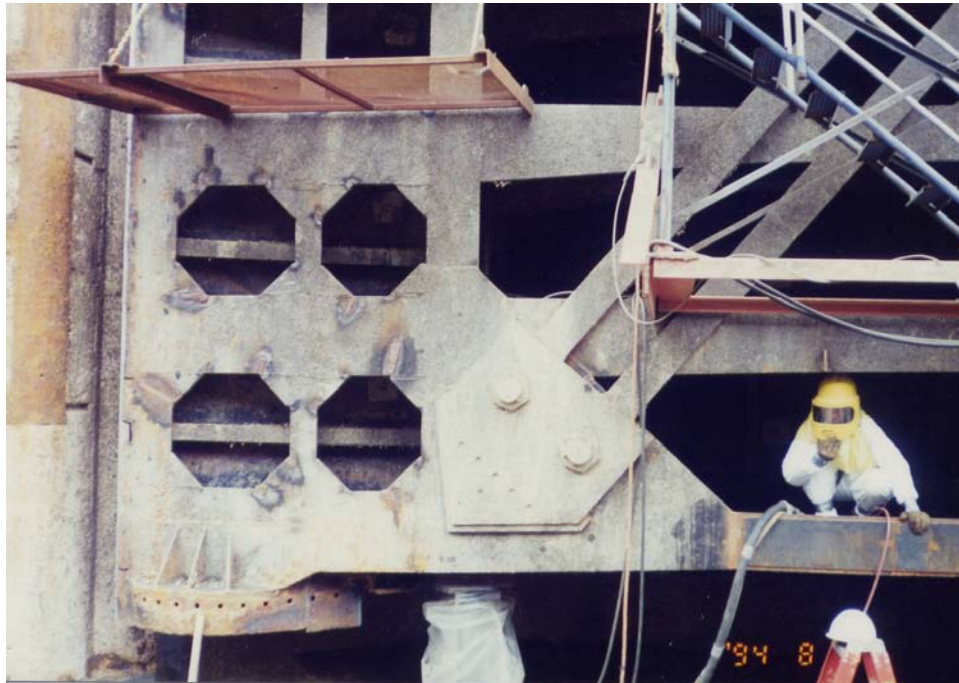


Figure 2-5.  New cracking at tips of welded gusset plates

Figure 2-6.  Example of window frame repair technique

2-2.  <u>Cracking Examples</u>.  Many factors contribute to fatigue cracking of miter gates such as gate geometry, joint details, applied loading, wear, weld sequence, weld quality, steel quality, initial joint fit-up tolerances, and number and magnitude of operating cycles.  Presented here are examples of some of the different types of cracking that have developed on horizontally framed miter gates.  These examples are categorized as shown below.

a.  Cracking in tension members.  Cracking in tension members include the downstream girder flanges near midspan, the pretensioned diagonal bars, anchor arms, and strut arms.  It has long been recognized that inspection and disposition of cracking in these members are essential because the initiation of cracks can quickly reach critical sizes leading to brittle failure of the component under tensile loads.  Figure 2-7 illustrates cracking found in downstream girder flange near midspan where some tension stress develops under operational conditions due to bending in the horizontal girders.  Figure 2-8 illustrates a fractured strut arm and subsequent tensile failure of the anchor arm resulting in loss of miter of the gate.

b.  Cracking in compression members.  As discussed in the previous section, fatigue cracking at connections on flanges, stiffeners, and thrust plates near the quoin or miter posts where operational loads are carried in compression has been a continuing problem.  These generally develop because of high compressive loads interacting with residual stress and stress concentrations at welded connections and generally have relatively stable ductile crack growth.  This type of cracking is of concern because it can be widespread and can affect the ability of the girders to carry the compressive loads during gate operations.  Loss of significant effective flange area can result in buckling or excessive gate movement during mitering operations.  In addition, if the quoin is worn to the point where the pintle is carrying the load, it will increase and further complicate the state of stress in the lower girders near the quoin.  Figures 2-9 and 2-10 illustrate this type of cracking.

Figure 2-7.  Cracking in girder flange connection near midspan
with tension loads



Figure 2-8.  Example of fractured strut arm and anchor arm

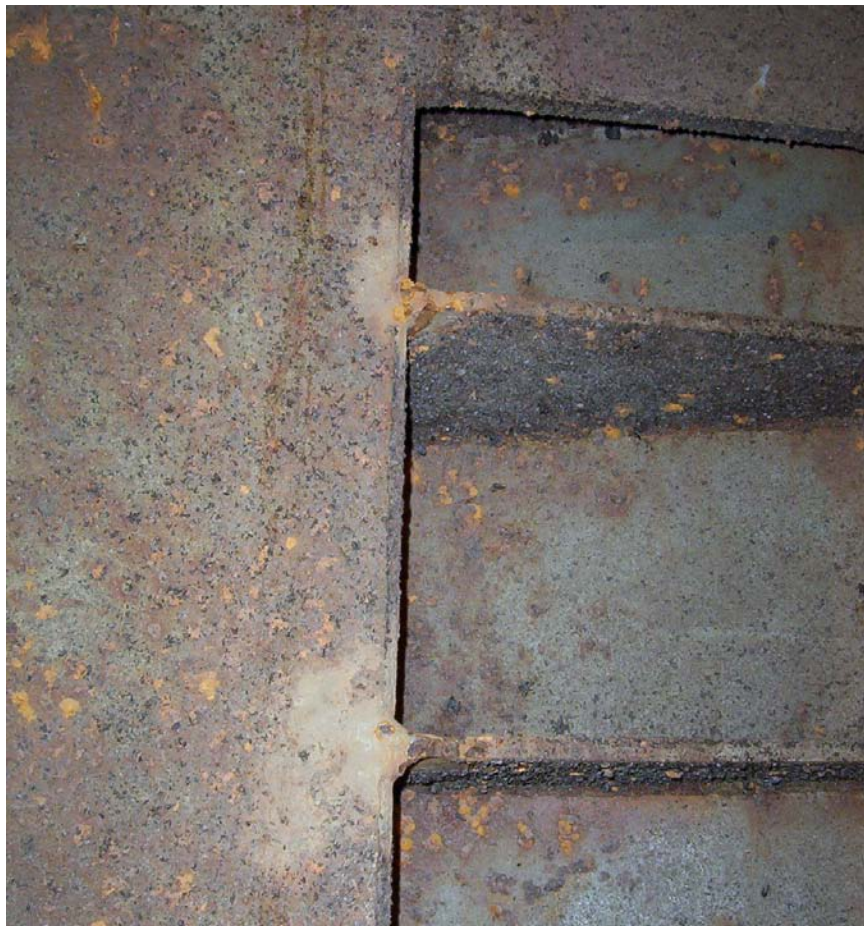Figure 2-9.  Cracking in girder and diaphragm flanges near quoin



Figure 2-10.  Cracking in stiffeners on thrust plate at miter end

c. Cracking at major connections. Cracking has been found in the connections of the girder flanges and the diagonal anchorage plates, as illustrated in Figure 2-11, and in the flanges where the pintle casting is connected, as illustrated in Figure 2-12. This cracking develops in areas having complex stress states and is of concern because the connections involve major components. Excessive movement in the pintle connection could result in problems in opening or closing the gate, problems in achieving correct miter upon closing, or even loss of the gate during miter operation.

d. Cracking in web plates. At some sites, significant cracking and loss of area have been found in the girder web plates. Examples are shown in Figures 2-13 and 2-14. In some cases, this cracking has propagated into the web plates from cracks initiating in the girder flanges. In other cases, the cracking has initiated directly in the web plate at some stress riser on the plate such as a hole or the welded connection of a stiffener on the plate. Crack propagation here could be exacerbated by the cyclic dishing in and out of plane of the web under operational loads. This cracking is a concern because the web plates support the flanges and carry the shear loads.

e. Miscellaneous cracking. Cracking in girder flanges initiating at holes or welded attachments has also been found, as illustrated in Figure 2-15. This cracking can initiate at midspan at bolt holes for bumper attachments or at holes or temporary welded attachments used during construction or repair. Generally, this type of cracking will be a local problem and is not considered a detriment to structural safety.

f. Pintle socket casting. Cracking has commonly occurred in pintle socket castings. This is likely caused by worn or improperly adjusted quoin blocks that do not make contact with the wall quoin when the gates are mitered and are carrying a hydrostatic load. This results in additional forces on the pintle, which can lead to cracking. If the casting is bolted to the bottom girder, bolts may fail because of this increased loading.

g. Cracking under concentrated loads. Cracking or tearing from plastic deformations under concentrated loads, such as barge impact or sill obstructions, also occurs. Figure 2-16. shows an example of damage sustained from sill obstruction during closing of the gate. However, these are abnormal loads that occur only infrequently, and the gate is generally repaired as soon as practical after such damage occurs. The effect of this type of damage is typically readily evident, either visually or in problems with gate operations, such as large strut arm forces generated during closure of the gate. Cracking damage from this type of loading is not considered in this effort for the evaluation of fatigue cracking.

h. Cracking in gudgeon anchor arms. Anchor arms are fracture critical members that hold the top hinge of the miter gate swing. Cracking that occurs in these arms can propagate quickly and result in catastrophic failure of the gate. Arms that have experienced problems in the past have been either undersized, causing low cycle fatigue failure, or geometry related, such as threaded bars or couplings. In both cases, analysis can be done by hand to estimate the fatigue life and critical crack size for the arms.

Figure 2-11.  Example of cracking at the diagonal anchorage
and pintle connection



Figure 2-12.  Example of cracking in the pintle connection

Figure 2-13.  Example of cracking in web plates



Figure 2-14.  Example of crack in girder flange propagating
into diaphragm web

Figure 2-15.  Example of miscellaneous cracking in girder flange



Figure 2-16.  Example of damage from sill obstruction

2-3.  <u>Repair Procedures</u>.  A wide range of welded repair procedures have been employed for controlling and mitigating fatigue cracking in horizontally framed miter gates.  Historical effectiveness, advantages and disadvantages, and relative efforts involved are identified for the

following repair procedures. In all cases, proper weld procedures and testing should be done to ensure a successful repair. Bolted repairs are not addressed in this list but certainly have merit in some repair applications.

a. Gouge out crack and reweld. Historically, this is the most common solution to repairing cracks on horizontally framed miter gates. The effectiveness of this repair depends largely on weld preparation, weld geometry, preheat, nondestructive testing, stress states, and quality of welds. In many cases, this procedure introduces high residual stress over a relatively large extent around the repair caused by the field welding procedures and welding components that are typically highly constrained against thermal-induced movement. It is recommended that the gates be jacked or supported during these repairs so that the components being welded do not accumulate mechanical (nonthermal) stresses that can also affect the residual stress distribution. In addition, if voids or discontinuities develop in the field welds, these can act as initial flaws for continued crack growth. Grinding the repaired weld surface smooth helps to alleviate surface discontinuities in the welds. If unexpected cracking is found that is extensive enough for concern about operational safety before the next dewatering, this type of repair may be necessary. If the cracking is extensive but not an immediate concern for structural integrity, an alternative may be to drill out the crack tips and reduce the interval between dewatering inspections.

b. Add triangular gusset plates to diaphragm/flange connection. This repair procedure, usually performed in conjunction with gouging and rewelding the cracks, has proven to be ineffective and can cause additional cracking problems. Gusset plates are added to strengthen a girder-to-diaphragm flange connection under the assumption that the added strength or support will reduce the stresses or stress concentrations that contribute to cracking. But the increased residual stresses from the welding of these added components usually cause additional cracks to develop under very few additional cycles. Typically, cracks at the connections of these gusset plates can develop and extend within 2-4 years after the repairs, and additional inspections are generally required to monitor the repair, resulting in more frequent dewaterings and outages. Figure 2-9 is a typical example of additional cracking that develops from the addition of gusset plates. Figure 2-17 shows an example of cracking developing again at the location previously repaired before adding the gusset plate.

c. Drill out crack tip. This is one of the easiest and perhaps best methods for dealing with fatigue cracking, especially if unexpected cracking is found during a scheduled dewatering. For this procedure, a hole is drilled through the component at the tip of the existing crack. This removes any residual stress around the crack and also mitigates the stress concentration at the crack tip. The disadvantage is that the tip of the crack must be located since drilling behind the tip will not prevent further propagation at the tip and drilling ahead of the tip may just cause the crack to change directions. Typically, a dye penetrant or magnetic particle testing procedure is used to find the crack tip. The rule of thumb for drill diameter is that the hole should be equal to the plate thickness being drilled. This procedure is most effective when the crack driving forces (change in stress intensity for the load cycle versus crack length) are decreasing. An example of drilling crack tips for fatigue control is illustrated in Figure 2-18.

Figure 2-17.  New cracking after gouging and rewelding a crack
and adding gusset plate



Figure 2-18.  Example of drilling out crack tips to control fatigue cracking

d. Construct window frame inserts. As discussed in paragraph 2-1, this repair procedure has been implemented and used with good success on the Markland miter gates. For situations where cracking generally develops at all connections between adjacent girders and vertical diaphragms, an efficient repair procedure is to prefabricate a window frame insert to be welded along the edges into the opening. This of course requires advance knowledge of the extent of cracking and the areas to be repaired. This type procedure is thus performed in a scheduled outage following a maintenance inspection. The frame provides some additional area for load distribution and uses radius corners to mitigate the stress concentrations. The field weld is also performed along the outer edge of the frame so that residual stresses are minimized on the inner free surface where cracking is more prone to initiate. An example of this repair procedure is shown in Figure 2-6. An improvement to the repair shown would have been to clip the corners of the window to avoid intersecting welds.

e. Add plate overlays on flanges. In some cases, fabricating large sections of plates to weld as an overlay on the affected flanges has been performed, as illustrated in Figure 2-19. This method is useful when the fatigue cracking is widespread and when additional flange area and new steel are needed for improved reliability. The overlays must be prefabricated, and the area must be prepared to ensure a smooth surface for attaching the plate. Additional cost will be incurred for fabrication, but the onsite labor should be more efficient than finding and repairing many individual cracks within the same area. This repair technique should provide for more effective control of fatigue cracking because of the additional steel area and strength provided. The weld sequence for adding these plates should be determined to minimize stresses during welding. The plates should fit up properly and within tolerance for root openings established by American Association of State Highway and Transportation Officials/American Welding Society (AASHTO/AWS) D1.5M/D1.5 Bridge Welding Code (AASHTO/AWS 2002). Nondestructive testing of the welds shall be done to make sure that the weld quality meets AASHTO/AWS D1.5M/D1.5 code requirements.

f. Remove and replace sections of flanges. For flanges that have cracked completely across the width or have separated from the webs, it may be necessary to remove and replace a complete section of the flange. This will provide new steel for the heavily damaged areas. The connections or splices should be far enough away from the crack-prone area to minimize the potential for new cracking at these spliced connections. Again, the plates should be properly fit, and the sections joined using proper weld or bolting procedures.

g. Remove and replace sections of girders. For extensive and repeated cracking that includes cracking into the webs of the girders, it may be necessary to remove and replace a section of a girder flange and web. The replacement section will provide new steel and should incorporate more fatigue-resistant configurations where possible. In addition, the spliced connection where the new section is attached to the old components will be a likely place for new cracking problems. Proper fit-up and weld procedures are critical for successful installation.

2-4. Problematic Configurations.

a. Problematic areas of miter gates are typically welded connections where geometric configurations create excessive stress concentrations, or fabrication fit-up procedures induce
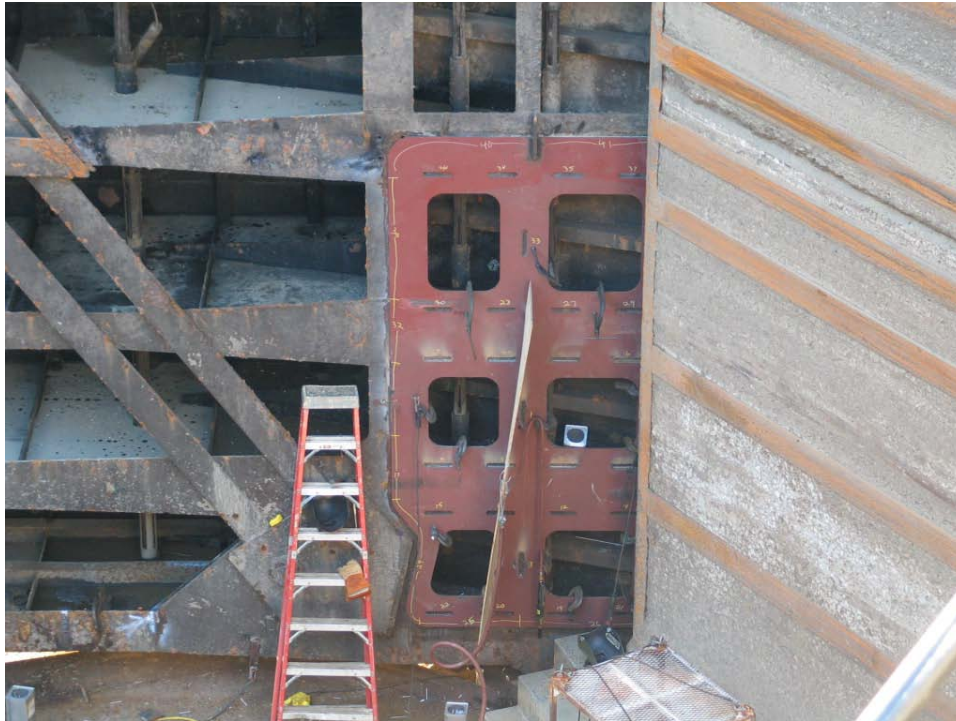
Figure 2-19.  Example of plate overlay attached to flanges with
extensive cracking

increased residual stresses, or operational conditions produce loads in excess of that considered in the design.  Historically, the welded connections of the horizontal girder flanges with the vertical diaphragm flanges, particularly near the quoin and miter ends of the gate, are problematic configurations.  The geometry generally consists of square, re-entrant corners connecting short thick plates joined with large welds (typically not ground smooth) that are highly constrained during fabrication.  The result is large stress concentrations and relatively large residual stresses that act as crack starters, especially if voids or discontinuities are present.  Mechanical wear in the gate quoin or pintle can exacerbate the compressive load in the flanges at these connections.  If vertical seals between the bottom girder and the sill are employed, a contact reaction force may develop with gate wear that can also affect the stress distributions in these areas.  These effects can combine to generate premature fatigue cracking at these welded connections.  Repair procedures to burn or gouge out the cracks and reweld or even install additional gusset or stiffener plates generally make matters worse because of the additional residual stresses imposed from field welding the constrained configurations.

b.  Another problematic configuration is attaching components such as anchor plates for the tensioned diagonal bars or fenders where welds are needed on flanges such that the weld geometry is perpendicular to the flow of stress in the flange.  This can create large stress ranges for the flange material at this location and also provide a mechanism for crack growth along the complete length of weld with the flange, which in many cases is the complete flange width.  Cracks in the pintle socket casting are also fairly common.  This may be attributed to the pintle taking loads beyond its original design caused by quoin block wear or improper adjustment.  Cracks in the pintle may be repaired by welding if its material properties are suitable.  Heat treatment or stress relieving is desirable if welding is done to minimize residual stresses.

2-5. <u>Summary</u>. While these horizontally framed miter gates have an outstanding pedigree for safety with countless hours of good performance on many sites for many years, they also historically have exhibited persistent fatigue cracking problems requiring many man-hours and outage hours for maintenance and repairs. The biggest maintenance problem is with fatigue cracks developing in the girder flanges at welded joint connections in the quoin and miter regions. This type of cracking can be widespread because the girders are designed to carry similar loads and have common welded joint configurations. The fatigue cracks in these regions typically extend past the heat-affected zone of the weld and well into the base metal of the flange, often extending across the flange and into the web of the girders. Because the flanges are major load-carrying components of the girders, this type of cracking is cause for concern about the continued operational reliability of the gate. The current policy is to repair these types of cracks as soon as they are detected. This has often led to delays in scheduled maintenance outages or even unplanned outages to complete the repairs. A more proactive method of predicting fatigue crack performance could help develop procedures that would minimize unscheduled repairs and outages while maintaining acceptable risks against unsatisfactory performance of the gates caused by fatigue cracking.

**CHAPTER 3**
**STRUCTURAL EVALUATION METHODOLOGY**

3-1.  Evaluation Procedures.

a.  EM 1110-2-6054 provides guidance for assessing fracture and fatigue cracking problems in miter gates and other hydraulic steel structures.  Procedures are provided for identifying critical locations that should be examined during inspections.  When cracking conditions are found that could compromise the integrity or serviceability of the structure, then an engineering evaluation is required to determine the criticality of the condition and the appropriate action.  Guidance is provided for material testing and structural evaluation procedures that may be required to help in the evaluation.  The evaluation procedures are concerned mainly with fracture-critical members where cracking develops in members that carry operational loads in tension.  Several examples are presented for establishing critical crack sizes and remaining fatigue life using tabulated fracture mechanics formulas for stress intensity on representative cracking geometries.  Consideration for various types of repair procedures is also discussed in this regard.  This manual also provides a good background and overview of fracture and fatigue principles (Rolfe and Barsom 1977) based on Linear Elastic Fracture Mechanics (LEFM) or Elastic-Plastic Fracture Mechanics (EPFM) and oriented for application to Corps hydraulic steel structures.

b.  The evaluation of fatigue cracking at welded joint connections can be difficult, especially in areas with detailed geometrical configurations and more complex loading conditions.  The usual fracture mechanics approach based on formulas involving far field stress and simplified cracking geometry is difficult to apply.  At welded connections, the cracking characteristics are governed by the complex local stress state under a cycle of loading.  In addition, the fracture mechanics formulas are based on test data and theories involving only Mode I crack growth where the crack extends perpendicular to a load that opens or pulls apart the crack surfaces.  In the more complex geometry and loading configurations where shear and out-of-plane deformations may be involved, the crack extension can also be significantly affected by Mode II or tearing forces on the crack.  The plate thickness of the sections involved in this cracking is almost always small enough to preclude brittle fracture, and the cracks behave in the ductile fatigue growth regime.  This discussion will focus on the structural analysis procedures that have been developed to evaluate fatigue cracking at these more complex welded joint connections.  The discussion of basic principles for fracture and fatigue evaluation is left to EM 1110-2-6054 or to relevant textbooks (Rolfe and Barsom 1977).

c.  The methodology that has been developed and used for evaluation of fatigue cracking at welded connections is based on detailed finite element modeling and advanced analytical methods.  The goal is to provide a basis for determining the critical characteristics of this cracking, including the number of cycles leading to crack initiation, the subsequent crack growth rate with operating cycles, and the ultimate effect on structural integrity or criticality.  How critical is the need for detection, repair, or prevention of such cracking?  How do changing operating conditions, such as pintle alignment, wear on the quoin and miter blocks, or stress relaxation in the diagonals, influence the cracking?  Because of uncertainties in this complex issue, key aspects of this evaluation procedure involve benchmarking the models to field data on

cracking history and establishing the effects caused by variations in problem parameters. A reliability model has been developed that characterizes the fatigue cracking in relation to these problem variables as a means of conducting an engineering evaluation of the cracking on the gate performance. The reliability model can also be integrated into a probabilistic based study to help assess the effect of uncertainties in a more quantitative manner.

d. The methods and procedures developed and used for evaluating fatigue cracking at welded connections are summarized as follows. These procedures are discussed in more detail below.

(1) Develop a three-dimensional (3-D) global model of one leaf of the miter gate pair using plate and beam elements. Perform nonlinear analysis using quoin and miter block contact springs and nonlinear geometric effects (P-Δ) but with linear material response to assess the performance of the gate.

(2) Establish the nominal stress range in the structural components near the welded connection of interest for a cycle of gate operation. Perform a matrix of analyses for variations in operational conditions to determine the variation in the stress range and the sensitivity of various parameters.

(3) Exercise the global model to determine potential failure modes and associated limit states caused by cracking damage at the connection(s) under investigation. For example, in areas of the gate where multiple cracks occur, there is less structural redundancy and the girder webs take on additional load. Elastic or bifurcation buckling analysis is performed on the model to determine if this is a potential failure mode limit state for cracking damage in areas that carry the operating loads in compression.

(4) Develop a local detailed model for each welded connection of interest. Establish the magnitude and extent of the residual stress in the connection caused by welding using nonlinear thermal stress analysis to simulate the weld process. Evaluate sensitivities of this residual stress distribution for variations in the material properties (yield stress) and for the constraint on the connection during the weld and establish a range for the residual stress.

(5) Evaluate the stress range using the local model, which includes the residual stress and stress concentrations caused by the geometric configuration. This stress range is evaluated by imposing boundary conditions that are extracted from the global analyses for the loading conditions that are found to govern the limits of the stresses during a cycle of operation. Use the principal stress vectors to establish the crack growth direction after crack initiation and benchmark with available field data.

(6) Determine the mean stress and the alternating stress for the load cycle and calculate the effective alternating stress using the Goodman relation to account for stress cycling about a nonzero mean stress.

(7) Use the American Society of Mechanical Engineers (ASME) (1998) fatigue curves to determine the number of cycles that would lead to the initiation of a fatigue crack for load cycles under the effective alternating stress. The reliability model will be constructed to account for

variations in the stress range and will employ Miner's rule for accumulating damage leading to crack initiation.

(8) Calibrate this crack initiation model with any available inspection reports for cracking and the number of operating cycles from operational logs. The nominal values of the parameters in the analytical model should provide the time (or number of cycles) to initiate cracking that is in agreement with the field data.

(9) Using the local model, extend a crack within the residual stress field with application of boundary conditions that represent both the minimum and maximum stress conditions from the global analysis. This is performed by setting up the model with duplicate nodes and surfaces that are initially constrained together and incrementally releasing pairs of nodes to simulate the crack extension. For each increment of crack length, use the J-integral procedure to calculate the energy released and the corresponding stress intensity factor for both limits of the imposed stress range in a load cycle. Develop a relation for the change in stress intensity (difference in the maximum and minimum values) as a function of the change in crack length.

(10) Use the Paris Equation, which relates the ratio of change in crack length to change in stress intensity with material property data, to evaluate crack growth. The nominal crack growth is benchmarked with available field data for observed crack lengths. The likely range in crack growth is established by considering the variations in problem parameters, such as change in stress intensity with crack length and initial crack size after initiation.

3-2. Global Modeling of Gate.

a. General.

(1) Global 3D finite element models are used to establish the overall structural performance and provide the boundary conditions for the more detailed local models of a welded connection. The intent is to evaluate the effect of variations in the operating conditions and identify the more important key parameters that influence the near-field stresses at the welded connection of interest. In addition, the global model is also used to assess the effect of the cracking on the structural performance and integrity of the gate. The goal here is to determine if some extent of cracking leads to any significant changes in the performance of the gate and identify possible limit states and failure modes caused by such cracking.

(2) For this effort, a 3D model of one leaf of the miter gate pair is developed using plate bending elements for all significant structural elements. Examples of this global modeling are provided in Appendixes B and C. Beam element modeling is typically used for intercostals or web plate stiffeners to help reduce the model size. Adequate mesh refinement is needed to capture stress distributions and deformations near the area of interest. Typically, a rather uniform mesh is employed since overall gate performance is at issue, and local modeling will be used for much better refinement at the connections of interest. A "stiff beam" for the pintle support is usually employed with one end rigidly attached to the bottom girder for the pintle casting and the other end representing the pintle ball with the correct standoff for boundary conditions. For floating pintle designs, the pintle ball base is explicitly modeled at the end of the

stiff beam with a contact surface representing the embedded pintle support geometry to better capture movement and reaction forces at the pintle. Nonlinear spring elements are employed to model the contact along the quoin and miter blocks. This allows contact reaction forces to develop as required along the length of the blocks. This modeling also allows representations for worn quoin or miter blocks or variations in contact along the blocks to be considered. For example, the contact springs are oriented normal to the miter block surface so that allowing additional "free" displacement in the spring before developing resistance from contact will simulate a worn surface on the miter block and allow the gate to displace somewhat farther downstream before achieving miter and load transfer.

(3) Typically, linear material response is used in the global model to study gate performance under variations in operating conditions. However, the calculations are performed as nonlinear analyses, requiring equilibrium iterations, because of the nonlinear springs for contact surfaces and because nonlinear geometry effects are included to capture P-Δ effects. Nonlinear material response can also be included for the evaluation of limit states, if necessary, such as for progressive failure or buckling, formation of a plastic hinge, or plastic deformations caused by interferences. If this level of analysis is needed, additional refinement in the global model may be necessary.

   b. Gate performance.

(1) Analyses are performed to establish the structural performance of the gate under operational conditions. The intent is to establish the stress range at the connection of interest for a cycle of loading that represents a lock operation. The variation in this stress range caused by variations in the operational conditions is also needed for developing a probabilistic-based reliability model. Baseline analyses are first performed on the global model for normal operational conditions. Gravity and diagonal prestressing is applied, and gate analyses for free hanging, opening and closing with the strut arm, and mitered operation under the normal lower and upper pool elevations are performed. Typically, for the gate configurations considered, the stress range is governed by the free-hanging condition and the mitered operational condition. The torsion loads during the push and pull through the water for closing and opening the gate generally develop stresses that fall somewhere between those for the free-hanging and mitered operation conditions. The magnitude of these torsional loads is typically a function of the gate height-to-width ratio. If gate opening and closing conditions are considered, these analyses are typically performed as static cases based on the design basis load specifications. The strut arm connection is fixed in the correct geometry for the gate just as miter and pressure loads are applied to the elements on the wetted upstream surface for opening and to the wetted downstream elements for closing. The pressure load is typically 30 psf (0.2 MPa) (45 psf (0.3 MPa) for deep draft) representing the resistance of pushing the gate through the water per the design requirements for normal load cases (EM 1110-2-2105, EM 1110-2-2703).

(2) The global model is then exercised for a variety of conditions to establish a variation on the performance and identify the sensitivity of various parameters. Typically, operational history at the site and known problematic conditions will determine the types and magnitudes of variations to consider in this part of the study. Normally, only operational conditions that are likely to occur over an extended time are considered, such as mechanical wear or gate

misalignment over time. Barge impact or sill obstructions that cause local damage but are short lived are not of interest in the evaluation for gate reliability affected by fatigue cracking. However, gravel or silt buildup on the sill where nominal interference may occur over long time periods without detection from operation of the gate would be something to consider. The stress variation caused by corrosion is typically not evaluated through the global model. This effect is accounted for by adjusting the component stress as a ratio of cross-section area reduction based on a given corrosion rate as part of the reliability model. The corrosion rate will have a randomly applied uncertainty in the evaluation. The following conditions may need consideration depending on the gate history and site operational conditions.

(a) Variation in diagonal prestressing. The tensioned bar diagonals help stiffen the gate for torsion loads during opening and closing. They are also used to resist the sagging deformations under free-hanging weight and keep the gate plumb for achieving good miter contact. Because the diagonals are anchored near the corners of the gate, the diagonal reaction loads can also influence the stress distributions in nearby flange connections. The actual stress level achieved during the diagonal tensioning is often uncertain, and the diagonals can lose tension over time caused by stress relaxation or even plastic yielding in the threaded connections. Thus, variations in the diagonal prestressing are needed to establish the effect on the stress distribution near the connections of interest. This can affect the flange stresses in the free-hanging and opening/closing conditions as part of the stress range in the load cycle. Thermal effects of diagonal stresses are not considered in this model.

(b) Variation in differential head. In probabilistic studies, change in the head differential, caused by seasonal changes in the upper or lower pool elevations, is often a required parameter for variation. Typically, reasonable changes in the head differential produce correspondingly linear changes in the flange stresses. Variations in the applied pressure loads for variations in head differential can be performed with the global model to confirm and characterize the change in flange stress.

(c) Variation in opening and closing loads. As discussed in paragraph 3-1 above, the stress range governing fatigue near a welded connection may not be affected by the opening and closing conditions. For cracking near the quoin or miter, the free hanging conditions typically provides the highest tension in the cycle from the residual stresses at the welded connection (in absence of other loads), and the mitered operating condition provides the highest compressive load in the cycle. However, performing variations in these loads should be considered if the normal cases indicate that opening and closing loads are important in determining the stress range for the type of cracking under consideration. Variations in the diagonal prestressing for the opening or closing conditions would be needed. Variations on the pressure load to represent wave surge or prop wash may also be necessary for certain sites if these occur on a regular basis.

(d) Miter block or quoin block wear. It has been found that wear on the miter and quoin contact blocks will increase the compressive loads in the downstream flanges near the quoin. Because this wear shortens the overall length of the gate leaf, the miter end will be pushed further downstream to miter with the other leaf, and this will induce additional bending in the girders. While also shortening the gate, wear on the quoin block is somewhat more complicated because of the restraints at the pintle and anchor arms. This can cause more load to be reacted

through the pintle and its connection with the bottom girder and perhaps also create gaps in the contact with the embedded quoin block in the lock wall. The change in flange stresses near the connections of interest caused by miter or quoin block wear must be determined through parametric analyses.

(e) Pintle wear and gate misalignment. Pintle wear and gate misalignment can also develop over time and will cause stress variations that can affect the fatigue cracking. Pintle wear can develop on the pintle ball surface or bushing in the pintle casting, or be caused by wear on the base or in the embedded support. The general result is possible movement so that the center line is not in line with the gudgeon pin at the top of the gate. Some vertical settlement of the gate may also develop in the first case.

(f) Sill obstructions or other interferences. As mentioned in paragraph 2-2g, infrequent sill obstructions, impacts, or interferences causing local plastic deformation and damage are not of interest in the fatigue cracking evaluation. Damage caused by these excessive and local loads is usually apparent during gate operations, and normal operations are stopped to repair or correct the situation. However, less severe sill obstructions causing additional stresses but without visible or evident effects on gate operation may need consideration because this condition could be in effect over significant time periods and load cycles. If this condition is known or thought to be a problem for a particular site, then the variation of stresses near the connection of interest should be characterized for this operating condition. If a frequency or time dependence for occurrence of such a condition can be assigned, the effect on the cracking can be included through the probabilistic based assessment.

(g) Temperature variations. Miter gates are exposed to a range of temperatures from variations in air and water temperature. These variations can cause additional stresses in the gate especially the diagonals but are not considered in this analysis.

c. Limit states.

(1) The global model is also exercised to identify possible limit states that would compromise the structural integrity of the gate from fatigue cracking. The miter gates are very redundant structures, and loads can easily redistribute for localized damage. This is evident from the many examples when substantial damage has been found during normal maintenance dewatering when gate operations were being performed without any apparent difficulties. The limit state will depend on the location and function of the components that experience the cracking damage. For cracking at welded connections on the girder flanges near the quoin or miter posts, where these structural components are in compression under the mitered operating loads, a possible limit state will be buckling of girders if the flanges become detached or ineffective in carrying the loads. This is evaluated by imposing increasing levels of cracking damage in the global model and performing elastic buckling calculations for the gate under the mitered operational loads. These buckling analyses are based on eigenvalue extractions where loading and deformation increments are found that result in a stiffness singularity representing an elastic bifurcation condition. The mode shapes are the buckling deformation patterns, and the associated eigenvalues are the factors that would be applied on the load state for that buckling shape to develop. Thus, the effect of increasing cracking damage on "global" buckling of a

girder can be established. Typically there is a large factor of safety on this type of buckling for miter gates in the absence of damage, and a limit state can be established as the extent of cracking that causes the factor for this buckling to approach a value of 1.0. Note that many local buckling modes will be present for these structures, such as skin plate or even web plate dishing between supports, but these are not considered for structural limit states. This type of dishing, even with permanent deformations, is very common and widespread in gate operations.

(2) For cracking in components that develop tension during the operating loads, such as the diagonals or a downstream flange near the middle of a horizontal girder, the limit state may be the crack length that would lead to brittle extension or rapid fracture of the component. This type of limit state could be determined through fracture mechanics formulas as described in EM 1110-2-6054. Other limit states caused by cracking, such as increased deformations that lead to interferences, concerns about successful mitering of the gates, or other problems with operation of the gate, may also need to be investigated. It may be necessary to set limit states based on these operational concerns or even public perception that would occur before structural integrity limits. For example, visible cracking that is not yet structurally significant, but apparent to public observers during use might be cause for establishing a limit state to avoid loss of public confidence and the associated economic consequences. In general, limit states based on structural failure and safety are absolute but usually require extensive damage because of the redundant nature of the structures. In any case, it must then be determined how fast the structure could reach a specified level of damage and the nature of the process. Is it a slow and relatively constant progression, or more likely is there a point when increasingly rapid deterioration will develop? The information needed to answer these questions is accomplished with local modeling.

3-3. <u>Local Modeling of Welded Connections</u>.

a. General. For cracking at a welded connection, it is usually necessary to conduct a local model analysis to evaluate the load distributions and crack growth with the effects of the residual stress field and better refinement for local stress concentrations. The local model is constructed using 3-D solid elements for a section around the joint of interest. A nonlinear thermal stress analysis is used to establish the residual stress distribution in the local model caused by the weld operation. Boundary conditions, extracted from the global model, are imposed on the cut surfaces of the local model to apply loads for the different operating conditions of interest. Local models developed for first generation investigation are given in Figures 3-1 through 3-3.

b. Residual stress.

(1) The first step in the local modeling is to establish the extent and magnitude of the residual stress field at the welded connection. For butt-welded joints, the residual stress parallel to the weld is known to peak in tension at a value near the yield strength of the material and then dip into compression as one moves transverse to the weld line. This distribution, illustrated in Figure 3-4 (Masubuchi 1980), is due to the self-equilibrating nature of these thermal induced stresses since the net force must be zero. The figure also illustrates the distribution of transverse stress for butt-welded plates, a self-equilibrated distribution for unrestrained plates, and a net
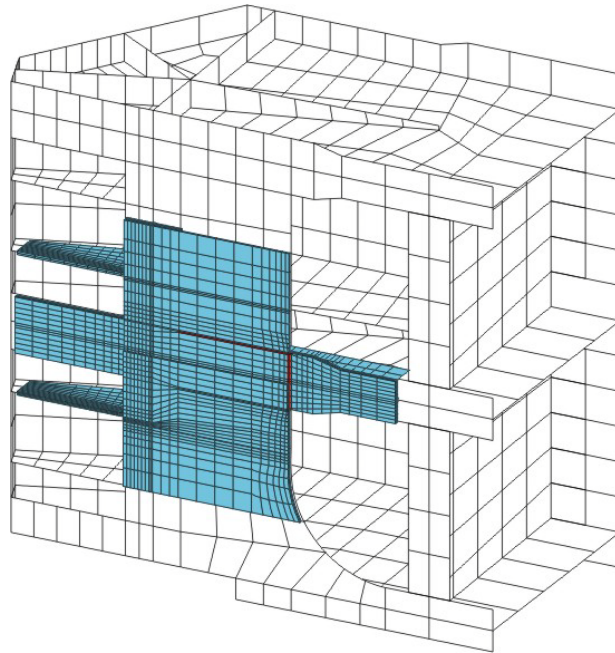
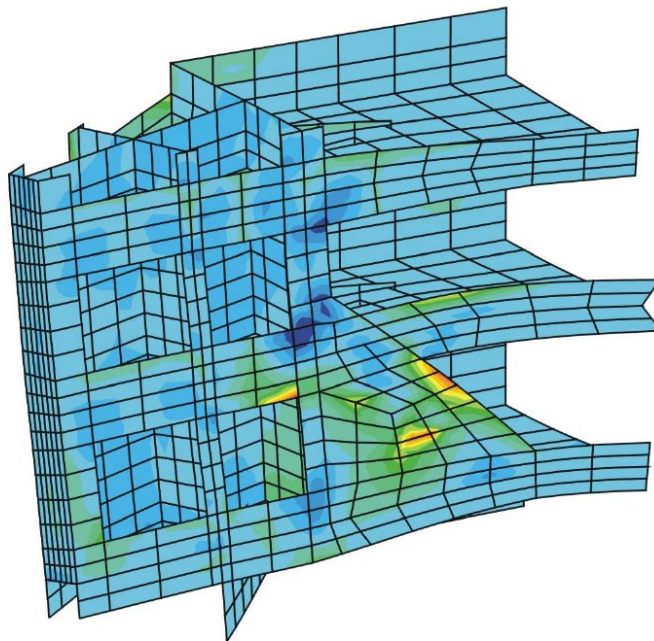Figure 3-1.  Local model of cover plate, flange and horizontal stiffeners



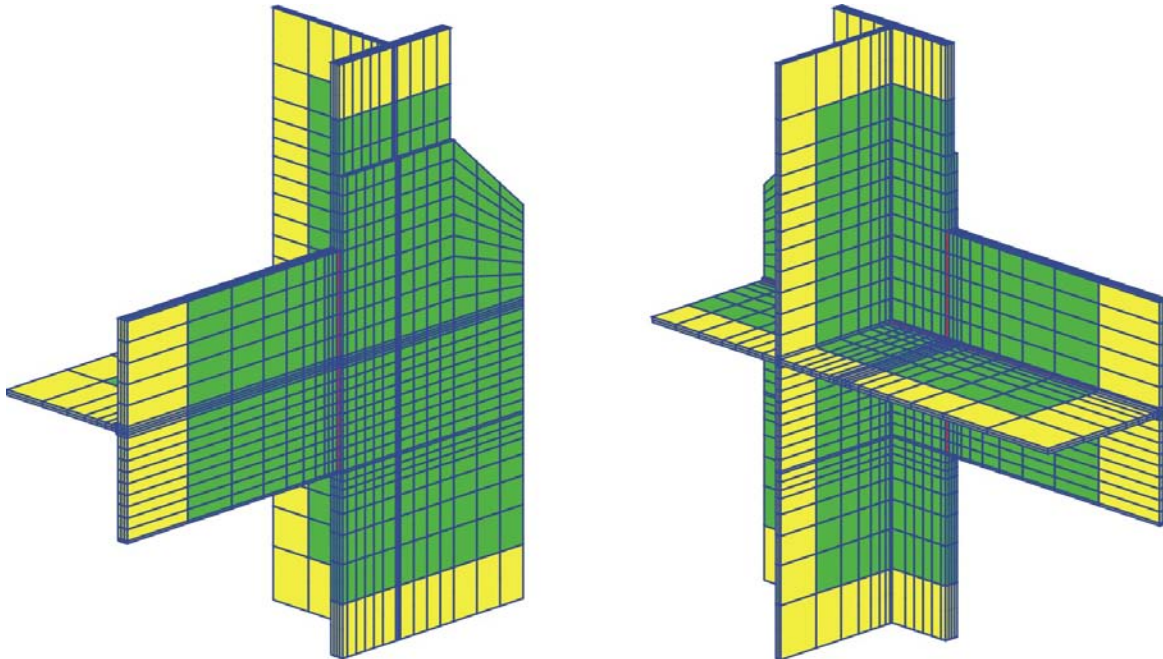Figure 3-2.  Local model of diagonal plate, girders, diaphragms and quoin post

Figure 3-3.  Local model of diaphragm to girder flange connection

tensile force distribution for plates restrained during the weld procedure.  Computing residual stresses caused by the weld process is a difficult procedure and has been the subject of intense research projects over a number of years.  Since the stresses develop from the rapid heating, melting, and subsequent solidification under cool-down, precise calculations depend not only on highly nonlinear material properties, but also on the details of the welding process, including type of electrode; power input; fit-up geometry (i.e., weld root opening); base metal thickness; and the number and velocity of welding bead passes.  Much of the research has been concerned with these types of details (for example, see Tall 1964).  These types of details affect mainly the magnitude and distributions of the stresses in the immediate vicinity of the weld.  Because this study is concerned with crack growth beyond the vicinity of the weld, the general magnitude and distribution of stresses away from the weld zone are the main interest.  These types of weld details are not available for the welded connections to be evaluated in any case.  The approach used here is to model the weld process in a broader sense, without the localized exactness of individual weld passes, but with enough detail to establish representative stress magnitudes and distributions.  In addition, the uncertainty can be included through probabilistic methods.

(2) A methodology for calculating residual stress is developed and benchmarked with test data reported in the literature.  Masubuchi (1980) reports residual stresses calculated from strain measurements for welding along a slit in a carbon steel plate.  The test specimen is a 47- by 31- by 3/4-in.- (1.2- by 0.8- by 0.02-m-) thick plate with a slit machined in the center.  The slit is welded with approximately an 0.5-inch (0.01-m) weld bead, and strain measurements are taken as functions of distance from the weld.  Figure 3-5, extracted from Masubuchi, illustrates the test specimen.  The material, plate thickness, and even the geometric configuration are all very similar to that of welded connections at flange intersections in miter gates.
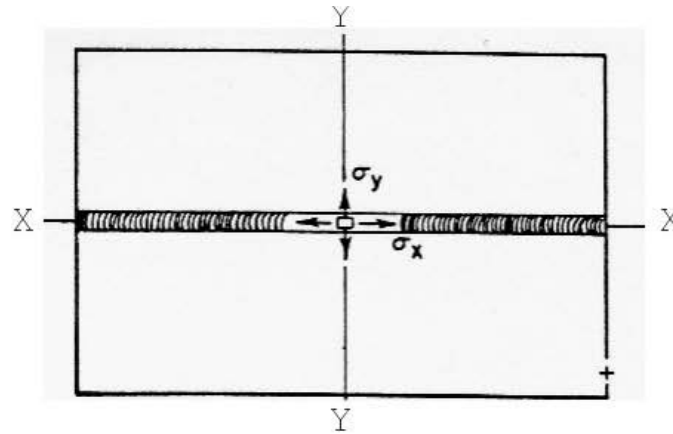
a. Butt Weld
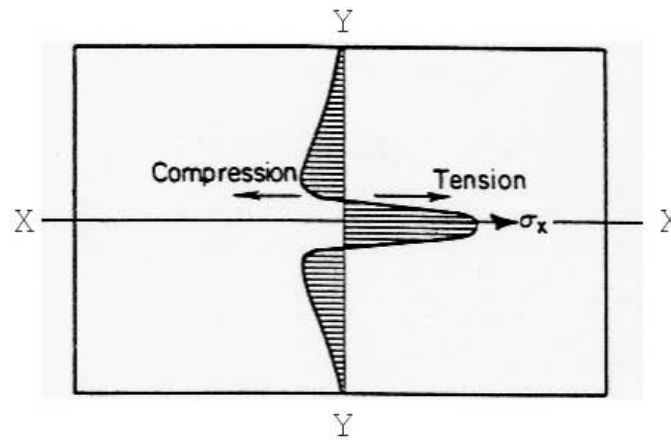


b. Distribution of $\sigma_x$ Along YY
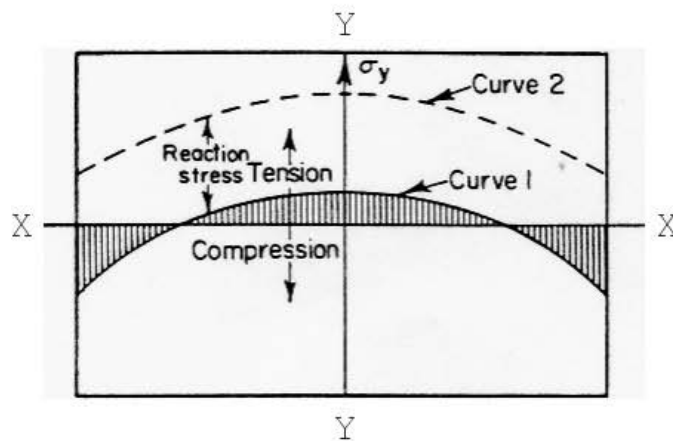


c. Distribution of $\sigma_y$ Along XX

Figure 3-4.  Typical distributions of residual stress in
butt weld (from Masubuchi 1980;
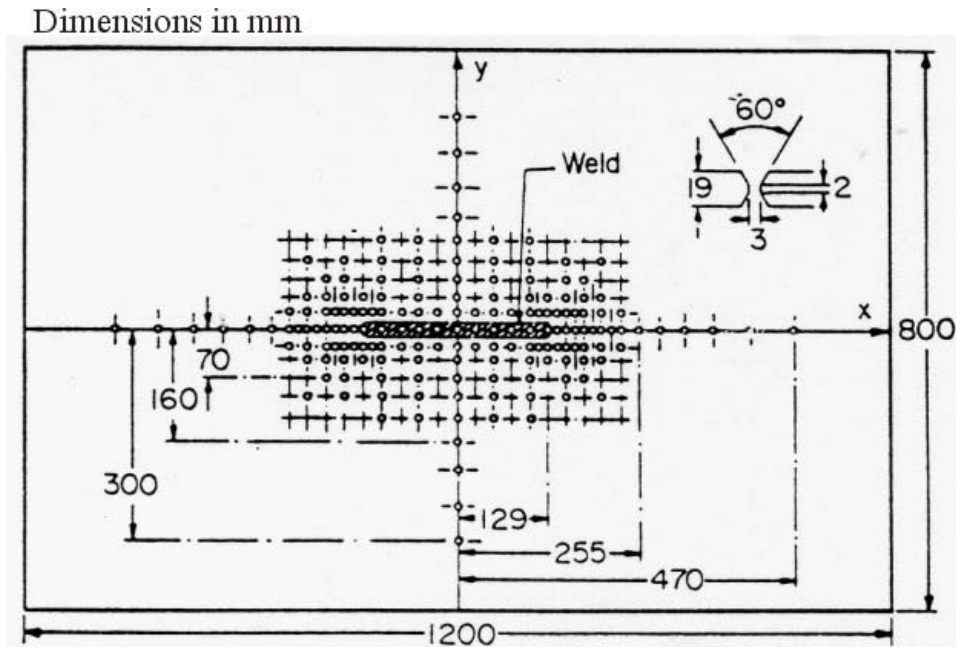courtesy of Koichi Masubuchi)

Dimensions in mm



Figure 3-5.  Slit type specimen used to measure residual welding stresses
(from Masubuchi 1980; courtesy of Koichi Masubuchi)

(3) Figure 3-6 illustrates the finite element mesh for a quarter symmetric 3D model used for the numerical simulation of the test.  The analysis uses temperature dependent material properties for the elastic modulus and yield stress with strain hardening, as shown in Figure 3-7.  This material characterization is based on data collected by Idaho National Engineering Laboratory (INEL) on SA533 carbon steel (Rempe et al. 1993) needed for research in evaluating the creep rupture failure of lower heads on nuclear reactor pressure vessels after the Three Mile Island accident.  The shape of the temperature dependence for this data was scaled for the yield stress of A36 structural steel used in the test and in miter gates.  A nonlinear thermal stress analysis is performed by applying volumetric heating rate to the material forming the weld so that the peak temperatures reach 1600 to 1800 °F (871 to 982 °C) in about the time required to lay down the weld bead.  Figure 3-8 illustrates the thermal contours that develop in the plate during the weld simulation to establish the residual stresses.  The heat source is then removed, and conduction and heat convection from the free surfaces are modeled to return the material to room temperature, which follows the classic exponential decay response.  The corresponding thermal-induced stresses and plastic strains are accumulated through the incremental nonlinear stress solution for each step in the analysis.  As the materials are rapidly heated, compressive stresses build up in the weld area caused by restraint against expansion.  As the temperatures approach the melting range, the material softens substantially and these stresses are dissipated.  Then, as the materials cool down, the reverse process occurs and tensile stresses develop in the welded connections as the material regains strength and is restrained from contraction.  Figure 3-9 compares the stress distributions calculated with this procedure for the test specimen with the stresses determined from the strain measurements taken during the experiment.  This figure indicates that this simulation provides a good indication of both the distribution and magnitude of the residual stresses caused by the welding.
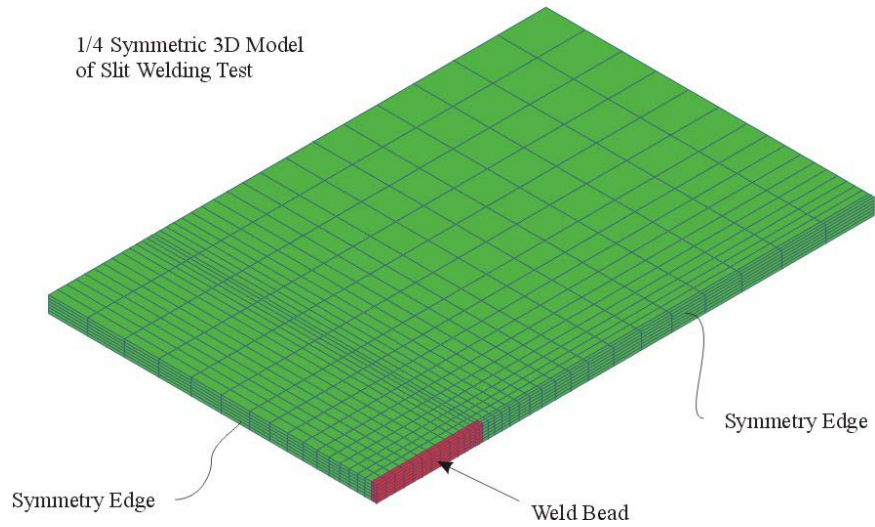
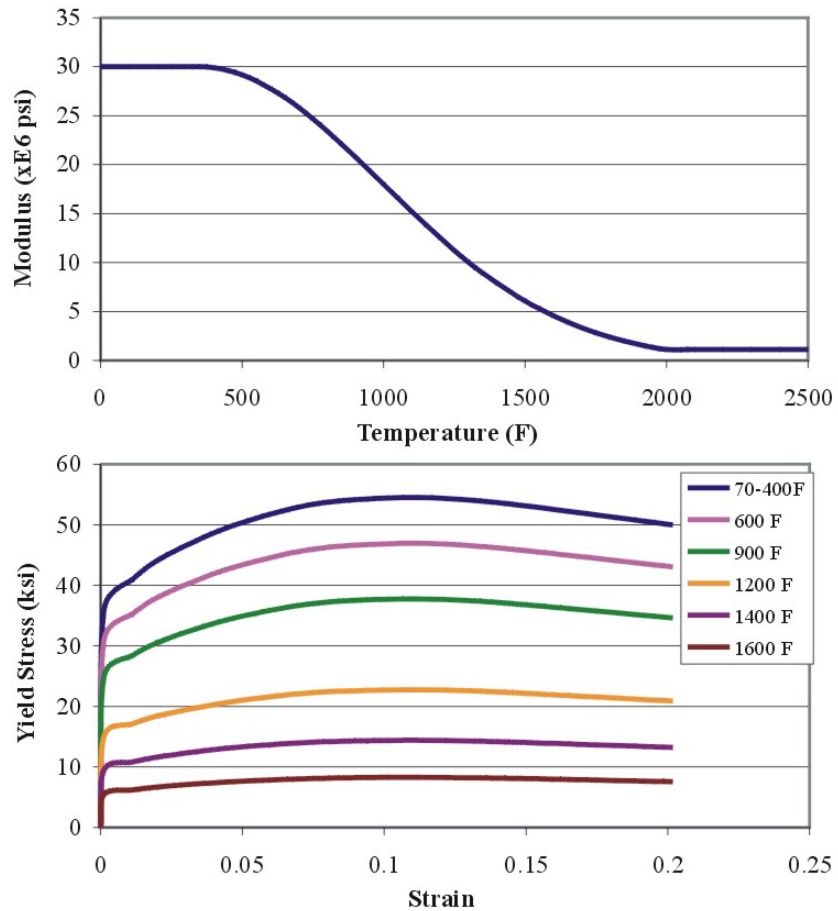Figure 3-6. Finite element model for simulation of slit welding test



Figure 3-7. Example of temperature-dependent, nonlinear material
properties used for weld simulation (Note: to convert ksi to MPa,
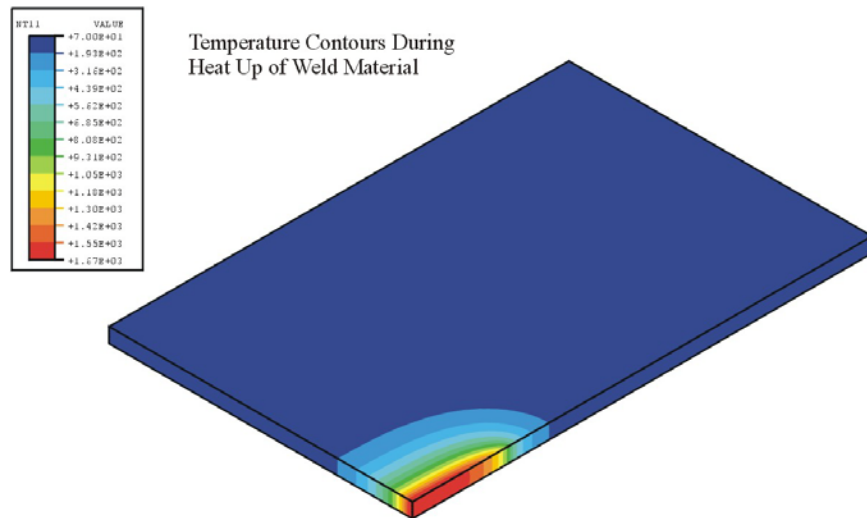multiply by 6.9; to convert psi to MPa, multiply by 0.0069)

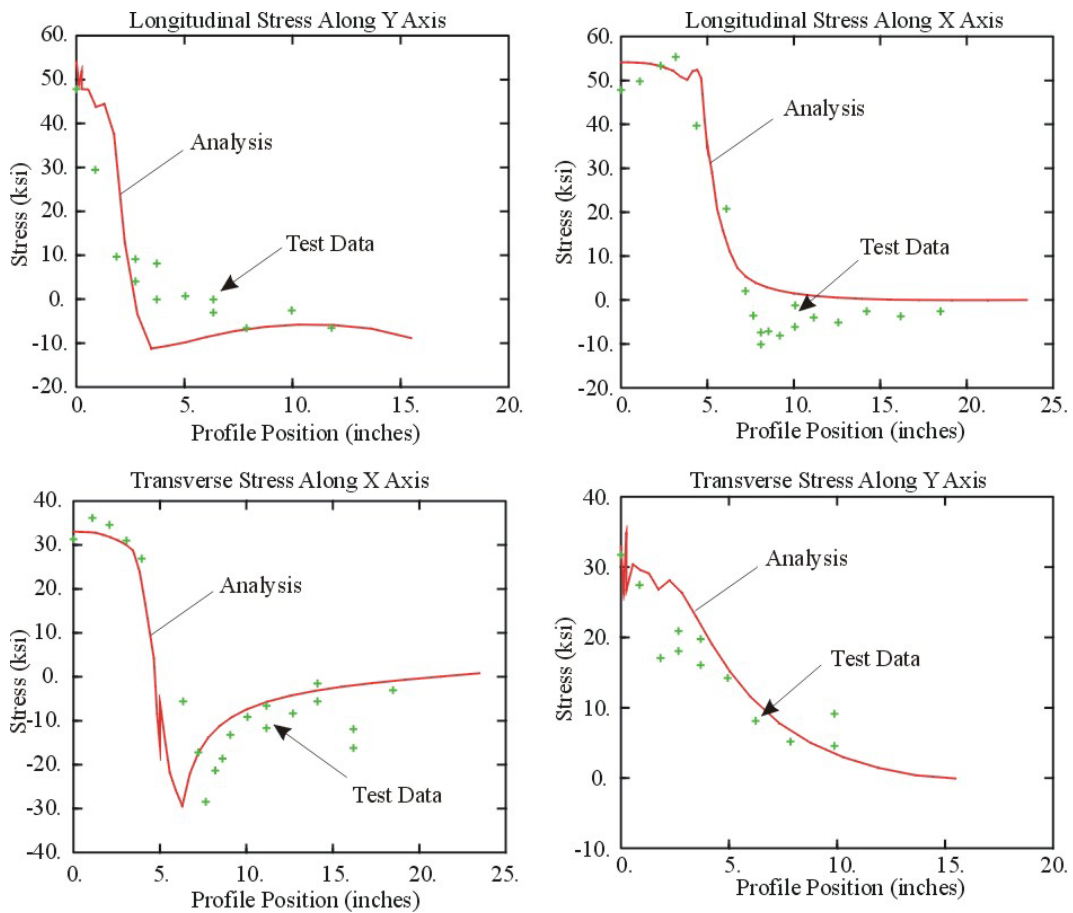Figure 3-8. Example of temperature contours for simulating weld in test plate



Figure 3-9. Comparison of residual stress calculation with test data (Note: to convert ksi to MPa, multiply by 6.9; to convert inches to meters, multiply by 0.03)

(4) This procedure is applied to the local model of the welded connection of interest to establish the extent and magnitude of the residual stress field. Variations in parameters, such as the material yield stress and the constraint during the weld procedure, are performed to assess the effect on the residual stress distribution.

c. Fatigue crack initiation.

(1) The following steps are used in the evaluation for the initiation of a fatigue crack:

(a) Determine the stress range for a cycle of load from the global and local modeling.

(b) Calculate mean stress and alternating stress for the stress range.

(c) Use the Goodman relation to define the effective alternating stress.

(d) Establish the number of cycles that will cause fatigue cracking using the ASME fatigue relations.

(e) Accumulate fatigue damage through a damage index.

(f) Benchmark with field data for cracking history.

(2) The first step is to define the maximum and minimum stresses in the stress range for a cycle of loading at the connection. This can be done in either of two ways. The minimum and maximum stresses can be established directly from the local model. The boundary conditions from the global models that represent the limits of the stress range are imposed on the local model after the nonlinear thermal analysis is conducted to establish the residual stresses in the local model. Alternatively, the stress range can be determined by establishing the minimum and maximum flange stresses near the connection from the global modeling analysis, scaling these based on the stress concentration at the connection, and superimposing the residual welding stress. This second method has the advantage that the flange stresses can then be characterized directly from the global analyses for variations in operating conditions. For this second method, define $\sigma_1$ to be the maximum flange stress at the welded connection for a cycle of loading, and let $\sigma_2$ be the minimum flange stress during the load cycle. These are determined from the global analyses for the gate performance under the various loading conditions that occur in the operating cycle for the gate. A local stress concentration $C$ is determined from the local modeling as the factor that multiplies the nearby flange stress in the local model to develop the stress at the geometric location in the connection where the cracking initiates. Using the local model, define $\sigma_w$ as the residual stress at this location from the welding procedure. These stresses will be characterized for variations in key parameters as part of the reliability modeling. The maximum and minimum stresses in the load cycle are then determined as

$$\sigma_{max} = C \cdot \sigma_1 + \sigma_w \tag{3-1}$$

$$\sigma_{min} = C \cdot \sigma_2 + \sigma_w \tag{3-2}$$

(3) After the minimum and maximum stresses at the cracking location are established, the alternating stress and mean stress for the load cycle are calculated as

$$\sigma_{alt} = \frac{1}{2}\left(\sigma_{max} - \sigma_{min}\right)$$

(3-3)

$$\sigma_{mean} = \frac{1}{2}\left(\sigma_{min} - \sigma_{max}\right)$$

(3-4)

(4) In fatigue cracking, it has been established that load cycling about a tensile mean stress is more damaging than cycling about a zero or compressive mean stress (Rolfe and Barsom 1977). To account for the effects of the mean stress, an effective alternating stress is computed from the Goodman equation as

$$\sigma_{eff} = \frac{F_b \cdot \sigma_{alt}}{1 - \dfrac{\sigma_{mean}}{\sigma_{ult}}}$$

(3-5)

where $\sigma_{ult}$ is the ultimate tensile strength of the material. Here, $F_b$ is included as a modeling factor to account for other uncertainties, such as stress corrosion cracking effects, surface roughness, possible void inclusions or discontinuities in the weld, and component size and configuration effects compared with fatigue test laboratory specimens. The nominal value of this factor is determined from benchmarking or correlation with field data. Note that this factor could instead be applied to the number of allowable cycles to be calculated below.

(5) A damage index is used to accumulate fatigue cycles to establish crack initiation. The damage index is defined as the summation of the ratios of the applied cycles to the allowable cycles for all the increments in stress range over time. Note that $\sigma_1$ and $\sigma_2$ will be functions of time so that the stress range as well as the number of operating cycles will change with time. When the damage index reaches a value of 1, initiation of a fatigue crack is predicted:

$$D = \Sigma\left(\frac{n_k}{N_k}\right)$$

(3-6)

where

$D =$ damage index

$n_k =$ number of cycles imposed at a stress level of $\sigma_{eff}$

$N_k =$ allowable number of cycles at that stress level

The allowable number of cycles is calculated from the following equation:

$$N_k = \left\{ \frac{E \cdot Ln[100/(100 - RA)]}{4 \cdot (\sigma_{eff} - \sigma_z)} \right\}^2$$ (3-7)

where

$E =$ Young's modulus, psi

$RA =$ 68.5%

$\sigma_z =$ 21,645 psi

This is the Langer equation as the best fit to the fatigue data that is used as the basis for the ASME design fatigue relations (ASME 1998a). Figure 3-10 plots this fatigue data for air environment at room temperature along with the Langer equation (ASME best fit) and the ASME design fatigue curve. This plot shows number of cycles versus the strain amplitude, which is just the stress amplitude divided by the elastic modulus. Note that the stress range to cycles (S-N) curve defined for the ASME fatigue design curve bounds the data to allow for margin in the design and account for uncertainties. In the low cycle fatigue range, this margin is typically a factor of 20 on cycles, and in the high cycle fatigue range, the factor of safety is usually a factor of 2 on the stress (or strain) amplitude. As discussed above, the model described herein uses the factor $F_b$ on the effective alternating stress as a means of accounting for uncertainties in the fatigue data for differences in the actual structural component and the laboratory test specimen. In addition, $RA$ in Equation 3-7 is multiplied by a factor $F_w$ to provide a band on the fatigue data for uncertainty in the steel properties. This factor is also used to multiply the yield stress and the ultimate strength with a typical range of 0.85 to 1.2. This common factor provides a direct correlation between the yield stress, ultimate strength, and fatigue resistance in this model.
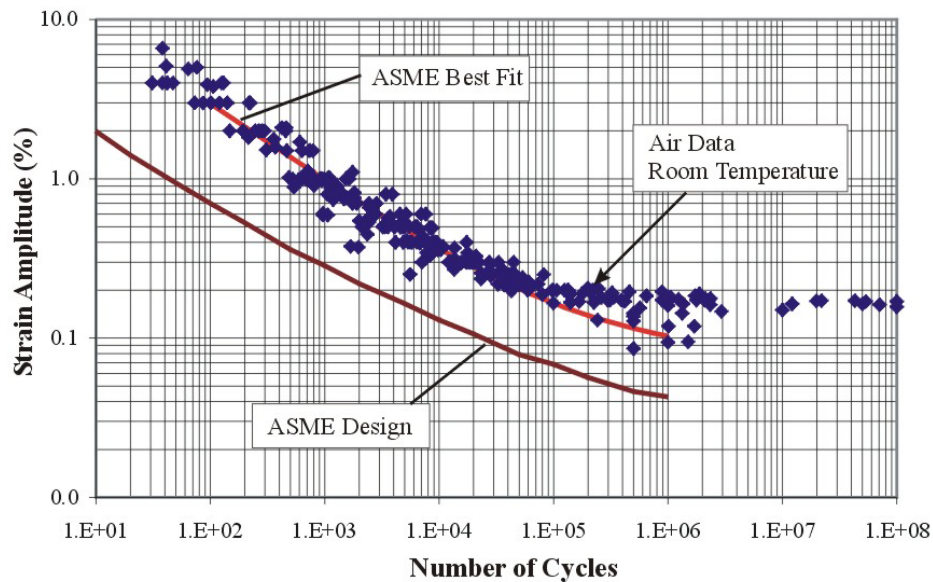


Figure 3-10. ASME fatigue data and representative correlations

d. Fatigue crack growth

(1) The following steps are used to establish the growth rate of the fatigue crack:

(a) Incrementally extend a crack within the residual stress field and for stress conditions representing the extremes of the load cycle.

(b) Use the J-integral procedure to calculate the stress intensity for varying crack lengths for the open and closed load conditions.

(c) Characterize this change in stress intensity with change in crack length

(d) Use the Paris equation to calculate crack growth with load cycles with appropriate material properties.

Note that the J-integral is independent of local plasticity and considers both Mode I and Mode II crack growth driving forces because it is based on energy principles.

(2) The fatigue relations, paragraph 3-3b above, are based on data for cyclic loading on specimens where the number of cycles correlates to complete failure of the specimen. Here, the number of cycles to initiate a crack is assumed to correlate to an initial crack that extends through the thickness of the plate. Thus, when a crack initiates, an initial crack length $a_o$ for that crack is assumed as the starting point for the crack growth study. Typically, a nominal initial crack length of 0.10 in. (2.54 mm) is assumed with a range from 0.05 to 0.20 in. (1.3 to 5 mm) This initial crack length also corresponds to minimum crack sizes that are typically found from visual inspections.

(3) The crack growth under subsequent stress cycles is characterized using the Paris equation (Rolfe and Barsom 1977):

$$\frac{da}{dN} = C\left(\Delta K\right)^n \tag{3-8}$$

where

$da = $ change in crack length per cycle $dN$

$C$ and $n = $ material parameters

$\Delta K = $ change in stress intensity at the crack as a function of crack length and loading:

$$\Delta K = K_{max} - K_{min} \tag{3-9}$$

where $K_{max}$ and $K_{min}$ are the maximum and minimum values of stress intensity at the crack front for a cycle of loading, respectively. Furthermore, the values of $C$ and $n$ also depend on the ratio of the stress intensity values, $R = K_{min}/K_{max}$.

(4) The correlation for this crack growth rate is based on the following ASME relations for fatigue crack growth in carbon steels exposed to water environments (ASME 1998b):

(a) First, define

$$\overline{\Delta K} = 17.75 \qquad\qquad\qquad\qquad\qquad \left(0 \leq R \leq 0.25\right)$$
$$= 17.74\left[(3.75R + 0.06)/(26.9R - 5.725)\right]^{0.25} \left(0.25 < R < 0.65\right)$$
$$= 12.04 \qquad\qquad\qquad\qquad\qquad \left(0.65 \leq R \leq 1.0\right)$$

(b) For a calculated $\Delta K < \overline{\Delta K}$, $n = 5.95$, and $C = S \cdot 1.02\text{ E} - 12$ where

$$S = 1.0 \qquad\qquad \left(0 \leq R \leq 0.25\right)$$
$$= 26.9R - 5.725 \quad \left(0.25 \leq R \leq 0.65\right)$$
$$= 11.76 \qquad\qquad \left(0.65 < R \leq 1.0\right)$$

(c) For a calculated $\Delta K \geq \overline{\Delta K}$, $n = 1.95$, and $C = S \cdot 1.01\text{ E} - 7$, where

$$S = 1.0 \qquad\qquad \left(0 \leq R \leq 0.25\right)$$
$$= 3.75R + 0.0625 \; (0.25 \leq R \leq 0.65)$$
$$= 2.5 \qquad\qquad (0.65 \leq R \leq 1.0)$$

(5) The characterization for $\Delta K$ as a function of crack length and loading (i.e., $K_{max}$ and $K_{min}$) is based on detailed local modeling for crack extension within a residual stress field under a cycle of loading. The local model of the welded connection is configured so that a crack can be extended along a known direction or in a direction normal to the principal stress vectors. This is generally accomplished by including duplicate nodes and separate element surfaces along the crack front. These nodes and element surfaces are constrained together to perform the weld simulation and establish the residual stress field. Then the nodes can be incrementally released to simulate the extension of the crack. For each increment in crack extension, the model is subjected to both the maximum and minimum near-field stress conditions for the range in operating conditions by imposing the appropriate boundary conditions. At each of these loading states, the stress intensity at the crack is calculated using the J-integral procedure to evaluate the energy release rate for an infinitesimal crack extension. This provides $K_{max}$ and $K_{min}$ (and thus $\Delta K$ and $R$) as a function of crack length. Typically this procedure is then performed for variations in the residual stress field and operational conditions affecting the maximum and minimum stress values to ascertain the possible variations in stress intensity versus crack length.

3-4.  Structural Reliability Model.

a.  General.  It is generally desirable to develop a structural reliability model for use in the evaluation of fatigue cracking at welded connections.  This is a way of incorporating the variations performed in the global and local analyses into a consistent evaluation procedure and to provide a better understanding of the range of performance and the effects of uncertainties.  It also provides an easy path for constructing a true probabilistic assessment and establishing probabilities that a given structural condition will develop.  This extension for probabilistic assessment is covered in the next chapter.  Constructing the reliability model involves conducting an engineering assessment of the analytical data generated from the global and local analyses to characterize the crack initiation and growth relative to variations in the key variables that are identified in the global and local modeling.  The objective is to develop response surfaces for the various structural performance measures as functions of the key response variables.  A response surface is a functional representation for the behavior of some structural parameter such as the number of cycles of various stress magnitudes needed to initiate a crack or the increment in crack length for some number of cycles with a given stress level.  The response surface is constructed from the deterministic analyses that use combinations of variations to define discrete points on this response surface.  Engineering judgment is then employed as necessary to construct functions or equations that will define a continuous representation of this response surface as functions of the key variables.

b.  Key response variables.

(1) An important aspect of reliability modeling is establishing the key response variables so that a response surface can be characterized with respect to these variables.  The key response variables are those that have a significant impact on the response of interest.  Generally, a key response variable is one for which reasonable variations will directly or significantly change the response of interest, especially if the nature of the response can also be affected.  However, a key response variable can also be one in which there is an unusually large uncertainty compared to other parameters or that is difficult to adequately include in determining the structural response of interest.  The following variables are generally considered key response variables in developing a reliability model for fatigue cracking at welded connections in horizontally framed miter gates*:*

(a) The head differential acting on the gate, which can vary with the seasons.

(b) The stress level in the diagonals, which typically relaxes with time and can be re-tensioned during maintenance dewatering.

(c) The rate of corrosion, which causes section thinning with time.  The rate of corrosion can also be changed in time by painting or other coating measures for maintenance.  The corrosion rate can also vary by site and by location on the gate.  For example, the corrosion rate for a component that is continually wetted and dried (splash zone) is typically higher than that for a component that is continually submerged.

(d) Mechanical wear on miter blocks, quoin blocks, or pintle, which will generally increase the near-field flange stresses with time. This effect is typically site dependent as a function of miter block design and also operating environment. A significant rehabilitation, such as quoin or miter block replacement, may be necessary to reset the effect of this variable.

(e) Other unusual operational conditions, such as sill obstructions or other closure interferences that gradually develop over time and last for a significant number of operating cycles before repairs.

(f) Mechanical properties of base metal and weld metal. Variations in the yield stress can directly affect the peak residual stress. Variations in the ultimate strength can affect the effective alternating stress. These properties generally have a direct correlation; a higher yield stress also implies a higher ultimate strength.

(2) The restraint on the connection during the welding procedure can significantly affect the extent and distribution of the residual stress field. Increased restraint that resists the thermal contraction during cool down after welding causes residual stresses to develop over a larger extent.

(3) Variations in several parameters affecting fatigue crack initiation also contribute to the uncertainty. For example, surface roughness, environment, and specimen geometry of the actual components are much different from those of the laboratory specimens that are used in establishing the allowable S-N relations. These types of uncertainties are typically incorporated into one parameter with a nominal value determined from benchmarking the analysis results with field data. An appropriate variation is needed because of the uncertainty and the approximate method of including these effects in the analysis. If S-N design fatigue curves are used as a basis for the reliability model, then additional factors and uncertainties may be needed because the design curves are constructed with factors of safety on the data to account for uncertainties and to allow for margin in the design. Thus, the allowable number of cycles from the design-based curve would typically underpredict the actual number of cycles that could accumulate before developing a fatigue crack.

(4) Similarly, variations in the parameters affecting the fatigue crack growth used in the Paris equation need to be considered. Again, the fatigue growth equation is an empirical relation developed from data, and there is some uncertainty in the form and data fitting employed. A single parameter is typically introduced in the modeling to deal with this uncertainty, and the nominal value is determined by benchmarking with field data.

(5) The limit state can also have uncertainty, and appropriate variations should be considered in the reliability model.

c. Response surfaces.

(1) As mentioned previously, a response surface is a functional representation for the behavior of some structural response relative to variations in the key parameters. A continuous representation for the response surface is constructed from the results of the deterministic

analyses that use combinations of variations to define discrete points on this response surface. For fatigue cracking at welded connections, it is desirable to construct response surfaces for the initiation of the fatigue crack and for the subsequent crack growth with continued operating cycles. In most cases, the reliability modeling is performed after cracking has developed as a means of evaluating how critical the problem is and what steps should be taken. In this situation, the initiation of the fatigue crack is known to occur, and the corresponding number of cycles can be determined from operational logs. Thus, it may seem that this crack initiation response surface is not required, and the associated effort can be eliminated. However, development of the local model and the residual stress distribution is still required for establishing the response surface for the crack growth, and only a few extra steps are needed to also characterize the crack initiation. This also provides an opportunity to benchmark the local model (and the associated residual stresses) to known structural performance. This benchmarking provides a good sanity check and additional confidence in the local modeling for the residual stresses, which are critical in predicting the fatigue crack growth.

(2) The response surface for initiation of fatigue cracking is defined by the damage index discussed in paragraph 3-3a(5), and the limit state is defined when the index reaches a value of 1.0. The damage index assumes that any stress cycle will contribute a proportionate share to the accumulating damage that eventually leads to fatigue cracking. The damage, based on the magnitude of the stress range, is proportional to the ratio of the subjected number of cycles at a given stress range to the allowable cycles before cracking at that stress range. Thus, this response surface must be characterized with respect to the effective alternating stress for a load cycle, which in turn is a function of the stress range under varying operating conditions and the weld residual stress. For example, the operating stress range can be characterized as a function of head, diagonal prestress, corrosion rate, and miter block wear rate. The welding residual stress could be characterized as a function of yield stress and constraint in the connection during the weld. Typically the response surface is developed as a product of several functions, one that incorporates the actual magnitude of the variable, and the others as multipliers accounting for variations in individual key variables.

(3) The response surface for the crack growth is typically defined using the Paris Equation. The increment in crack growth is calculated for some sequence of load cycles that provide a range of stress intensity on the crack with appropriate material parameters. This change in stress intensity, which is a function of stress range and crack length, is characterized for variations in operating conditions and loading from the local modeling. Typically, a range of stress intensity is defined for a given crack length that accounts for variations in load and the residual stress distribution. A limit state for this crack growth is typically defined using a "critical" crack length that would cause structural safety or operational concerns as determined from the global model study on the extent of such cracking.

**CHAPTER 4**
**PROBABILISTIC ASSESSMENT**

4-1.  Structural Performance.

a.  General.  The previous chapter discusses the development of a structural reliability model that allows assessment of structural performance relative to variations in key parameters. Because of the uncertainties involved in many of these key parameters, it is often necessary and usually desirable to establish the structural performance relative to specific limit states within a probabilistic framework.  In general, the desired result is the probability of failure with time or operating cycles and the comparison of such curves for different operational, maintenance, or repair options.  Failure is typically defined as reaching some limit state, such as an extent of cracking damage, that would be cause for concern on the structural integrity or operational safety of the gate or otherwise cause operational problems.  Other questions, such as "What is the probability of an existing crack reaching a given length over a given number of years or cycles?" can also be addressed through this procedure.  The method that has generally been used for this type of assessment of fatigue cracking on Corps hydraulic structures, such as the Ohio River Main Stem System Study, is commonly called the Response Surface Method.  The implementation for this problem is described below.  Some other methods that can be used to perform a probabilistic assessment of structural performance affected by fatigue cracking are also briefly described.

b.  Response surface analysis.

(1) For a probabilistic assessment of structural performance using the reliability model as a response surface, the idea is to define a set of randomly selected values for the key variables from an allowable range and distribution of values and determine the response of interest over time for this set of variables.  This evaluation is repeated for many iterations or trials of randomly selected sets of variables.  For each random trial, a complete finite element analysis could be performed to assess the structural performance and determine if the desired limit state is reached.  This is generally computationally prohibitive for these types of problems, so a response surface, as described in paragraph 3-4, is used to assess the structural behavior for each set of random variables and determine if and when a given limit state is reached in the probabilistic assessment.  A probabilistic-based loop for generating random trials, typically a Monte Carlo procedure, is constructed around the structural reliability model.  The response surface allows efficient evaluation of the structural performance for the random trials within this probabilistic framework.  Some key variables or even the criteria defining the limit state can also have time-dependent variations for the probabilistic assessment.  The first step in the probabilistic assessment is to develop distributions of values for all the key parameters.  This involves assigning the type of distribution that best describes the variation in the parameter and identifying any limits on the range of the values within that distribution.  Limits on the values of parameters can be due to physical limits or operational restrictions.  For example, mechanical material properties generally have a normal distribution with a mean and standard deviation that can be derived from test data, and a minimum value based on required minimum specifications that must be met by the material.  The distributions for most operational parameters, such as differential head or diagonal prestress levels, are typically normal distributions based on known operational conditions for a site along with any physical limitations.  The lognormal distribution

is generally recognized as the most appropriate distribution for structural response or limit states because it limits parameters to positive values and incorporates more uncertainty as the values become larger. For example, the length of a fatigue crack cannot be negative and small fatigue cracks are not likely to cause structural failure. However, as fatigue cracks get longer and longer, failure becomes more likely and additional uncertainty develops because of possible synergism or changes to the structural performance because of the crack.

(2) The Monte Carlo procedure, usually employing the Latin hypercube method for focusing the selected random trails, selects random values for each key variable from the assigned distributions, and the response surface is evaluated for the associated structural performance. The number of times a given limit state, such as a critical crack length (which can also be part of the random selection), is reached during these trials is counted; and the probability of this structural state occurring is then the number of occurrences found divided by the number of trials. A hazard rate or conditional probability can also be defined as the probability of reaching the limit state in the current year given that the structure has satisfactory performance up to the start of the current year (or other time period). The number of random trails or iterations is repeated until convergence is satisfied. Convergence here generally means sufficient trials such that the calculated results are "stable" in a probabilistic sense, for example, when the mean and standard deviation of response variables change very little with additional iterations.

c. Fragility analysis.

(1) The method referred to here has been developed based on the total probability theorem over the years as part of probabilistic risk assessments of major structural systems to seismic hazards, especially at nuclear power plants. Other applications of this method are in life cycle management of bridges (Zhang et al. 2004). The key random parameters are identified, and an appropriate probability distribution is assigned to each key random parameter, as discussed in b above. Finite element analysis combined with Latin hypercube sampling to represent the uncertainties in the key random parameters is performed to predict the fatigue cracking probabilistically. In particular, the range of each key random parameter is divided into a certain number of segments, typically about 20, with equal probability. From each segment, one representative sample, generally taken as the median value of the segment, is selected. The samples of all key parameters are randomly matched into sets containing one sample from each key parameter and without duplication of any of the key parameter values; that is, once one of the sampled values is selected, it is removed from the pool of remaining values for that parameter. A deterministic finite element analysis is performed with each of these parameter combinations, and a crack length over time is calculated. This gives 20 curves of predicted crack lengths with time (or cycles). At selected points in time, say every 5 or 10 years, the probability density function (PDF) for the crack length at that time can be constructed from the 20 sample points at that time. At each time of interest, the 20 predicted crack lengths for that year are collected from the 20 sample analyses curves. The cumulative probability for each crack length found is then the number of times that the calculated length equals or is greater than that length divided by the number of trials plus 1. The corresponding lognormal PDF can then be determined by fitting the integral of the PDF to this cumulative probability function. For each time slice selected, a lognormal PDF is constructed that defines the relative frequency that a given crack length will develop by that time.

(2) At the same time, the uncertainty in the capacity or limit-state function can be characterized by defining a PDF for the critical crack size. This PDF can be based on global modeling to identify the extent of cracking that compromises operational safety or on engineering judgment for the crack length that can be tolerated before repairs are needed for operational concerns and reliability. In some applications, this PDF can be obtained by comparing capacity model predictions with real world observations, either in the field or in the laboratory. For example, limit states for beam-column connections for bridges or buildings can be established using data developed from pushover capacity tests for various configurations of these critical connections.

(3) The fragility or probability of failure (exceeding a critical crack length) over time is then calculated from the convolutions of the limit state PDF and the fitted probability distributions of the predicted crack length according to the total probability theorem. At each time point, the cumulative probability of failure is determined by calculating the area of intersection of the PDF that a given crack will develop by that time with the PDF for the critical crack length. The probability of failure for each of these time points is plotted to define the probability of failure over time. This method sounds complicated, but is quite straightforward and well accepted as standard practice. However, an extensive analysis effort is needed for each simulation to obtain an accurate estimation of the probability distribution with time of the crack lengths for the application to fatigue cracking in welded steel miter gates.

d. Stochastic crack growth analysis.

(1) Stochastic crack growth methods have been developed and used for many years to predict fatigue cracking in critical components of airframes (see Yang and Manning 1996). Ellingwood and others (McAllister and Ellingwood 2001a, 2001b; Zheng and Ellingwood 1998) have applied these stochastic-based methods for predicting fatigue cracking in welded steel miter gates to assess reliability and establish in-service inspection intervals. These efforts have focused on treating the fatigue cracking at welded connections as a purely stochastic process. The details associated with specific welded joint connections, including geometry, residual stresses from fabrication or repair, or flow of stress through the joint during a cycle of gate operation, are not explicitly considered. Rather, a stochastic function is employed, which is intended to account for all sources of uncertainty. In addition, this work considered the failure criteria or limit state to be when a crack extends through the thickness of the flange at the welded connection. The intent was to establish inspection intervals to find and repair fatigue cracks as soon as they are detectable in the field. This approach assumes initial flaws (voids) are always present from the welding operation of the joint, and uses a probabilistic-based evaluation of the Paris equation, factored by the stochastic function, to predict the number of cycles needed for these initial flaws to coalesce and propagate through the flange thickness. The probability of such a condition developing is then primarily a function of the ability to detect flaws, either during fabrication or during in-service inspections, and the inspection period where such flaws are to be found and repaired.

(2) A summary description of this approach, taken from McAllister and Ellingwood (2001a, 2001b), is presented here for reference. This model for fatigue cracking in welded steel miter gates augments the Paris equation for fatigue crack growth with a lognormal stochastic

function to account for uncertainty in crack growth prediction based on the work by Yang and Manning (1996), as

$$\frac{da}{dN} = C(\Delta K)^m X(N) \qquad (4\text{-}1)$$

The stochastic function *X(N)* has a median value of 1.0 and a covariance defined as $\sigma_x^2 \exp(-\zeta_x \Delta N)$, where $\sigma_x^2$ is the variance of *X(N)* and $\zeta_x$ is a correlation scale factor. This form is chosen because closed-form solutions can then be developed to describe the distribution of the number of cycles needed for any particular crack size or for the probability that a crack length will be reached for a given number of cycles. The correlation scale factor was assumed to be 2.5 E-6/cycle based on crack propagation in mild steel (Zheng and Ellingwood 1998). The variance is defined as

$$\sigma_x^2 = \sigma_d^2 + m^2 \sigma_{\log \Delta K}^2 \qquad (4\text{-}2)$$

with

$$\sigma_{\log \Delta K}^2 = \sigma_{\log Y}^2 + \sigma_{\log \Delta \sigma}^2 \qquad (4\text{-}3)$$

where

$Y =$ a geometry factor (stress concentration factor)

$\Delta\sigma =$ the far-field stress range

and *m* and *ΔK* are as defined in the Paris equation and $\sigma_d^2$ represents uncertainty or variance in the data for measured crack growth rates. Values for the various coefficients of variations are then estimated from finite element modeling or from literature sources. For example, the uncertainty in the stress range is based on the assumption that the associated finite element modeling gives flange stresses that are within 30 percent of in situ values, the variation for the geometric factor *Y* is based on an assumed distribution of stress concentration factors for fillet welds taken from literature sources, and the variation for measured crack growth rates is based on regression analysis of data for mild steel baseplate specimens and then adjusted for the effects of welding. The basis for this adjustment for welded connections is not clear. The assumed overall variance of the stochastic multiplier function was determined to be about 60 percent around the median value of 1.0 for the welded steel connections under consideration. The change in stress intensity, *ΔK*, is apparently determined based on linear fracture mechanics formulas for an edge crack in a plate with *Δσ* based on the compressive flange stress under gate operation.

(3) The number of cycles required for fatigue cracking using this model is determined by integrating the stochastically factored Paris equation. This requires a determination for the initial and final flaw sizes. The final flaw size, or failure criteria, is taken to be the thickness of the

flange. The initial flaw size was estimated based on a literature survey for flaw size detection from visual and magnified inspection methods and then finalized through benchmarking the model with laboratory welding conditions and fatigue test data. Benchmarking of the model with fatigue test data for fillet-welded cover plate beams provided median values for times to failure within 12 percent of the test data, correlation of lower bound values within 20 percent, and correlation of upper bound values within 30 percent. Application of this model for known fatigue cracking in miter gates indicated that large initial flaws (up to 45 percent of the flange thickness) would likely be required to produce the cracks found for the number of operational cycles and stress ranges that had occurred. It was considered somewhat unlikely that these initial flaws (roughly 0.5-in.(12.7-mm) surface lengths) would not have been previously detected. This inconsistency was attributed to the possibility that previous repairs to the joints had slag inclusions or incomplete fusion from the weld repair procedures in the field.

(4) The probability of fatigue failure (cracking through the flange thickness) can be constructed using this method by establishing the PDFs for initial flaws at the start of each service period. This function depends on the initial flaw size at fabrication, the quality of the detection and repair of flaws in the field, and the inspection interval or number of cycles for each service period.

(5) This procedure appears to be amenable for correlation with laboratory test data for initiation of fatigue cracking, but not very satisfactory for predicting known fatigue cracking at welded connections on miter gates in service. This could imply that the connection details, such as residual stresses and local stress distributions under cyclic operation, which were not considered in the procedure, are important in the modeling for fatigue cracking at these types of connections. The reported work using the stochastic crack growth method correlates roughly to the crack initiation phase of the current effort. The current effort is also concerned with the growth of these cracks well into the flanges and webs of the structural components as part of the guidance for evaluation and repair of fatigue cracking in horizontally framed miter gates.

4-2. Economic Considerations. The probabilistic-based assessment for structural reliability can also be coupled with economic considerations for projecting maintenance costs, optimizing maintenance budgets over systemwide projects, and identifying when rehabilitation or replacement is more cost effective than continued maintenance. The goal of an optimal inspection and repair strategy is to minimize the lifetime maintenance/repair cost of a miter gate while ensuring that its probability of failure remains below an acceptable level throughout its expected service life (Frangopol, Lin, and Estes 1997; Mori and Ellingwood 1994). This analysis must account for the quality of inspection technologies with different detection capabilities, the effects of the crack propagation and the various repair techniques on the structural reliability, the cost of the inspection and repair, and the time value of money. The ability of an inspection technique to detect a crack is dependent on its quality. A higher quality inspection method will provide a more dependable assessment of the crack propagation. In addition, the repair work, if based on high-quality inspection, can be more effective, since even a small defect can be detected and repaired. The quality of an inspection technique is generally characterized probabilistically. The reliability aspect of this optimization consists of two elements: reliability degradation caused by the fatigue crack propagation and reliability update from repair. The probabilistic fatigue crack propagation model is applied to predict the

reliability decrease. Finite element analysis is performed or historical data is used to estimate the effects of a repair technique on the structural reliability. An event tree model provides a systematic means to investigate all possible repair events associated with the inspections. Each branch of the event tree corresponds to a specific inspection/repair strategy, together with a lifetime history of the probability of failure and an expected total cost. The optimal inspection/repair strategy leads to the minimum present value of the expected total inspection and repair cost while keeping the probability of failure below the acceptable level throughout the service life.

4-3. <u>Summary</u>. Because there are many uncertainties in the parameters controlling fatigue crack initiation and growth for the configurations and loading environment of horizontally framed miter gates, the evaluation and prediction of fatigue cracking must be performed in a probabilistic framework. Several methods that allow treatment of the probabilistic aspect of this problem have been discussed. The response surface method, based on detailed modeling and benchmarking of specific cracking problems, has been used with apparent success on past Corps projects. However, the modeling and analysis effort can be quite extensive in developing the response surface. The fragility approach is also a well-defined and accepted method for probabilistic assessment, but the underlying analyses again rely on detailed modeling and analyses that require extensive efforts. Procedures using stochastic crack growth methods, which treat the cracking as a purely random process without considering specific details of the welded joint, have also been applied to welded steel miter gates. While this procedure is much easier to implement, it has not proved very reliable in predicting fatigue cracking in actual welded joint configurations on working miter gates.

# CHAPTER 5
# SUMMARY AND CONCLUSIONS

5-1.  The designs for horizontally framed, welded steel miter gates used on navigational locks along the nation's inland waterways have a long and exemplary performance record for structural safety.  Many sites have gates in operation well past the original design life with appropriate maintenance for corrosion, component wear, fatigue, fracture, and extended cycles.  There have been many cases of gates sustaining significant damage from extreme load conditions, such as barge impact, without structural failure or loss of miter.  Because these types of extreme loads are part of the design basis, and because the Corps also requires additional load and resistance factors (over normal steel design procedures) because of the importance of these structures and the uncertainty associated with the hydraulic environment, the gates tend to have large margins for normal operating loads.  Typically, a horizontally framed miter gate will have a factor greater than 4 on global buckling and factors of at least 2 on tensile yielding under normal mitered operational loads.

5-2.  Historically records show that the typical welded steel gate has suffered premature fatigue cracking at welded connections of girder flanges, generally around only 20 to 40 percent of the anticipated fatigue endurance limits for the types of connections used.  The fatigue cracking generally seems to develop after about 15-20 years of normal operations, somewhere around 100,000 loading cycles.  The general policy is to repair fatigue cracks when found to maintain structural reliability.  Once this fatigue cracking initiates, significant maintenance efforts for inspections, evaluations, and repairs are expended in controlling the fatigue cracks.  Some maintenance resources are generally required every 3 to 5 years after cracking develops.  Over the past 25 years, the Corps has gained extensive experience in repair techniques and in understanding the cause for this premature and persistent problem with fatigue cracking.  Still, there seems to be a continuing occurrence of extended shutdowns and unplanned delays for repairs when unexpected cracking or an unexpected severity of cracking is found on these types of miter gates during scheduled maintenance dewatering.

5-3.  As described herein, detailed analytical methods have been developed and used for engineering evaluations of cracking problems at specific sites.  These analytical studies have been effective in isolating the causes, in helping develop effective repair procedures, and in planning major rehabilitation efforts for particular sites.  The analyses have also helped guide new design philosophies that minimize re-entrant corner geometries and welded connections for the upstream and downstream flange plates near the quoin and miter ends of the gates.  However, the effort required, in terms of engineering and analysis time, for these detailed studies is often quite significant.  New projects have benefitted from lessons learned and experience gained in previous efforts.  However, the analysis procedures using these detailed modeling methods are not easily transitioned into a production mode that can be more readily applied on a widespread or even time-critical basis.  On the other hand, purely stochastic methods, while much easier to implement, have not yet been satisfactory in providing a reliable basis for fatigue crack evaluations.  The fatigue cracking problem and thus any associated evaluation methods have inherent uncertainties that generally require probabilistic treatment and often engineering judgment.  A procedure is needed that combines the best of both  these approaches, a generally stochastic crack initiation and growth framework enhanced with knowledge gained and lessons learned from detailed analytical studies of gate behavior and welded joint performance.  This

ETL provides the basis for the development of such a simplified procedure for the evaluation of fatigue cracking on horizontally framed welded steel miter gates.

5-4.   A simplified tool or procedure that is effective in predicting and evaluating fatigue cracking and establishing inspection intervals will greatly enhance the ability to optimize maintenance and repair strategies for both cost and structural reliability.  Reliable predictions for potential fatigue cracking problems that allow planned inspections and minimize maintenance resources can provide greater efficiency and reliability in the inland waterways transportation infrastructure.  Significant industry costs for transportation delays, as well as Corps maintenance costs, can also be avoided, for example, if it can be determined that unexpected cracking found during a dewatering can wait for repairs until a subsequent scheduled shutdown.  More effective repairs, in terms of cost and longevity, could also be planned and developed for the scheduled repair effort.  Fatigue cracks that have just penetrated the thickness of a flange are not likely to compromise the structural performance of the gate, and immediate repairs would not seem to be necessary.  The important issues are how fast they will extend, and how critical they are to structural integrity or gate operations.

5-5.   The stochastic cracking model approach enhanced with improved correlations based on detailed modeling results may provide the basis for a good simplified procedure with more robust predictive capabilities.  This procedure may be especially effective in considering the incremental improvement in reliability after field repairs of cracking are performed. Development of extensions to this procedure are needed for predicting the first initiation of fatigue cracking after fabrication or major rehabilitation, and especially for predicting the extent and rate of continued crack growth into flanges and webs.  While such a simplified tool may have more inherent uncertainty in predicting fatigue cracking, it would have the advantage of continually improving the predictions and removing uncertainty as field data is collected without having to return to the complex models and analyses.  Ultimately, once the simplified tool is benchmarked for a wide variety of configurations, it could then also serve as a screening tool that could identify potential problematic configurations where the more detailed investigations may be warranted.  For example, if an unexpected or specific problem develops where the field experience is in obvious conflict with the predictions of the simplified tool, then that may be a warning sign that additional issues could be involved, and a more detailed investigation would be needed to flush out the cause of the problem.

5-6.   The simplified tool can also be augmented with knowledge of problematic configurations and operating conditions from past experiences that are likely to develop fatigue cracking issues. A sampling of these configurations and conditions applicable to that under consideration can identify weighting factors on the probabilistic projections.  For any specific site, ongoing data entry for in-service inspections will allow continual improvements in these predictions through checkpoints and benchmarks with field data. Perhaps, ultimately, if the tool is web based and used on a Corps-wide basis, then ongoing data entry at each specific site can also enhance a shared knowledge base for continual "learning" by the software and overall improvement of predictions.  As such a global resource, the tool could then also be used to optimize maintenance, repair, or rehabilitation efforts on a systemwide basis by balancing the structural reliability across numerous lock systems.

# APPENDIX A
# REFERENCES

**EM 1110-2-2105**
Design of Hydraulic Steel Structures

**EM-1110-2-2703**
Lock Gates and Operating Equipment

**EM-1110-2-6054**
Inspection, Evaluation, and Repair of Hydraulic Steel Structures

**American Association of State Highway and Transportation Officials/American Welding Society 2002**
American Association of State Highway and Transportation Officials/American Welding Society, 2002. *Bridge Welding Code,* D1.5M/D1.5, Washington DC.

**American Society of Mechanical Engineers 1998**
American Society of Mechanical Engineers. 1998. Boiler and Pressure Vessel Code, Section III, Rules for Construction of Nuclear Power Plant Components, Division 1, Appendix I.

**American Society of Mechanical Engineers**
American Society of Mechanical Engineers. Boiler and Pressure Vessel Code, Section XI, Rules for Inservice Inspection of Nuclear Power Plant Components, Appendix A.

**Bjorhovde et al. 1972**
Bjorhovde, R., Brozzetti, J., Alpsten, G. A., and Tall, L. 1972. "Residual Stresses in Thick Welded Plates," *Welding Research Supplement* of the *Welding Journal,* August 1972, 3925-4055.

**Brozzetti, Alpsten, and Tall 1971**
Brozzetti, J., Alpsten, G. A., and Tall, L.. 1971. "Welding Parameters, Thick Plates, and Column Strength," *Welding Journal,* 50(8), August 1971.

**Frangopol, Lin, and Estes 1997**
Frangopol, D. M., Lin, K. Y., and Estes, A. C. 1997. "Life-cycle Cost Design of Deteriorating Structures," *Journal of Structural Engineering,* ASCE, 123(10), 1390-1401.

**James and Zhang 1996**
James, R. J., and Zhang, L. 1996. "Fatigue Cracking Evaluation of the Markland Miter Gates," ANATECH Report ANA-96-0201 to Corps of Engineers, Louisville District, ANATECH Corporation., San Diego, CA.

**James et al. 2001**
James, R. J., Schaaf, D. M., Werncke, G. A., and Patev, R. C. 2001. "Finite Element Modeling for Reliability Evaluation of Fatigue Cracking at Welded Connections," *Proceedings of the 8th*

*International Conference on Structural Safety and Reliability,* Newport Beach, CA, June 17-21, 2001.

**Masubuchi 1980**
Masubuchi, K.  1980.  "The Magnitude and Distribution of Residual Stresses in Weldments," *Analysis of Welded Structures*, Chapter 6, Pergamon Press, New York.

**McAllister and Ellingwood 2001a**
McAllister, T. P., and Ellingwood, B. R.  2001.  "Reliability-based Condition Assessment of Welded Miter Gate Structures," *Journal of Infrastructure Systems,* 7(3), 95-106.

**McAllister and Ellingwood 2001b**
McAllister, T. P., and Ellingwood, B. R.  2001.  "Reliability-based Condition Assessment of Welded Steel Miter Gates with Fatigue Damage," *Proceedings of the 8th International Conference on Structural Safety and Reliability,* Newport Beach, CA, June 17-21, 2001.

**Mori and Ellingwood 1994**
Mori, Y., and Ellingwood, B. R.  1994.  "Maintaining Reliability of Concrete Structures; I: Role of Inspection/Repair, and II: Optimum Inspection/Repair," *Journal of Structural Engineering,* ASCE, 120(3), 824-862.

**Padula, Barker, and Kish 2005**
Padula, J., Barker, B., and Kish, D.  2005.  "Greenup L&D Miter Gate Repair and Instrumentation," *Re-Energizing Engineering Excellence,* 2005 Tri-Service Infrastructure Systems Conference and Exhibition, St. Louis, MO, 2-4 August 2005.  PowerPoint presentation available from http://www.dtic.mil/ndia/2005triservice/2005triservice.html, Track 12.

**Rempe 1993**
Rempe, J. L., Chávez, S. A., Thinnes, G. L., Allison, C. M., Korth, G. E., Witt, R. J., Sienicki, J. J., Wang, S. K., Stickler, L. A., Heath, C. H., Snow, S. D.  1993.  "Light Water Reactor Lower Head Failure Analysis," NUREG/CR-5642, INEL Report EGG-2618 for U. S. Nuclear Regulatory Commission, Washington, DC.

**Rolfe and Barsom 1977**
Rolfe, S. T. and Barsom, J. B.  1977.  *Fracture and Fatigue Control in Structures*, Prentice-Hall, Englewood Cliffs, NJ.

**Tall 1964**
Tall, L., "Residual Stresses in Welded Plates – A Theoretical Study," *Welding Research Supplement,* January 1964.

**Werncke and McClellan 1996**
Werncke, G. A., and McClellan, B. K.  1996.  "Ohio River Markland Miter Gates, A Case History," Corps of Engineers Structural Engineering Conference, San Antonio, TX, 28-30 August 1995.

**Yang and Manning 1996**
Yang, J. N., and Manning, S. D. 1996. "A Simple Second Order Approximation for Stochastic Crack Growth Analysis," *Engineering Fracture Mechanics,* 53(5), 677-686.

**Zhang et al. 2004**
Zhang, Y., Acero, G., Conte, J. P., Yang, Z., and Elgamal, A. 2004. "Seismic Reliability Assessment of a Bridge Ground System," *Proceedings of 13th World Conference on Earthquake Engineering,* Vancouver, B.C., Canada, August 1-6, 2004.

**Zheng and Ellingwood 1998**
Zheng, R., and Ellingwood, B. R. 1998. "Stochastic Fatigue Crack Growth in Steel Structures Subjected to Random Loading," Contract Report ITL-98-1, U. S. Army Engineer Waterways Experiment Station, Vicksburg, MS.

**APPENDIX B
CASE STUDY FOR SNELL LOCKS**

B-1.  Introduction.  This case study highlights the reliability modeling and analysis performed for fatigue cracking on the miter gates at Snell Lock as part of the Great Lakes and St. Lawrence Seaway Navigation Study.  These gates are a key component in the reliability of the overall Great Lakes and St. Lawrence Seaway navigation system.  After some 35 years of operation, widespread cracking was found on stiffener plates attached to the thrust plates on the quoin and miter posts.  This cracking initiated at the welded connection of these horizontal stiffener plates to the downstream vertical flanges of the quoin and miter end diaphragm and was very widespread, essentially at most all girder locations in the lower half of the gate.  The cracks tended to grow toward the thrust plates and were generally 1 to 2 in.(0.03 to 0.05 m) long.  An engineering evaluation was required to establish the cause, future growth rates, and criticality of this cracking.  Figure B-1 illustrates the gate construction and cracking in the stiffener plates.
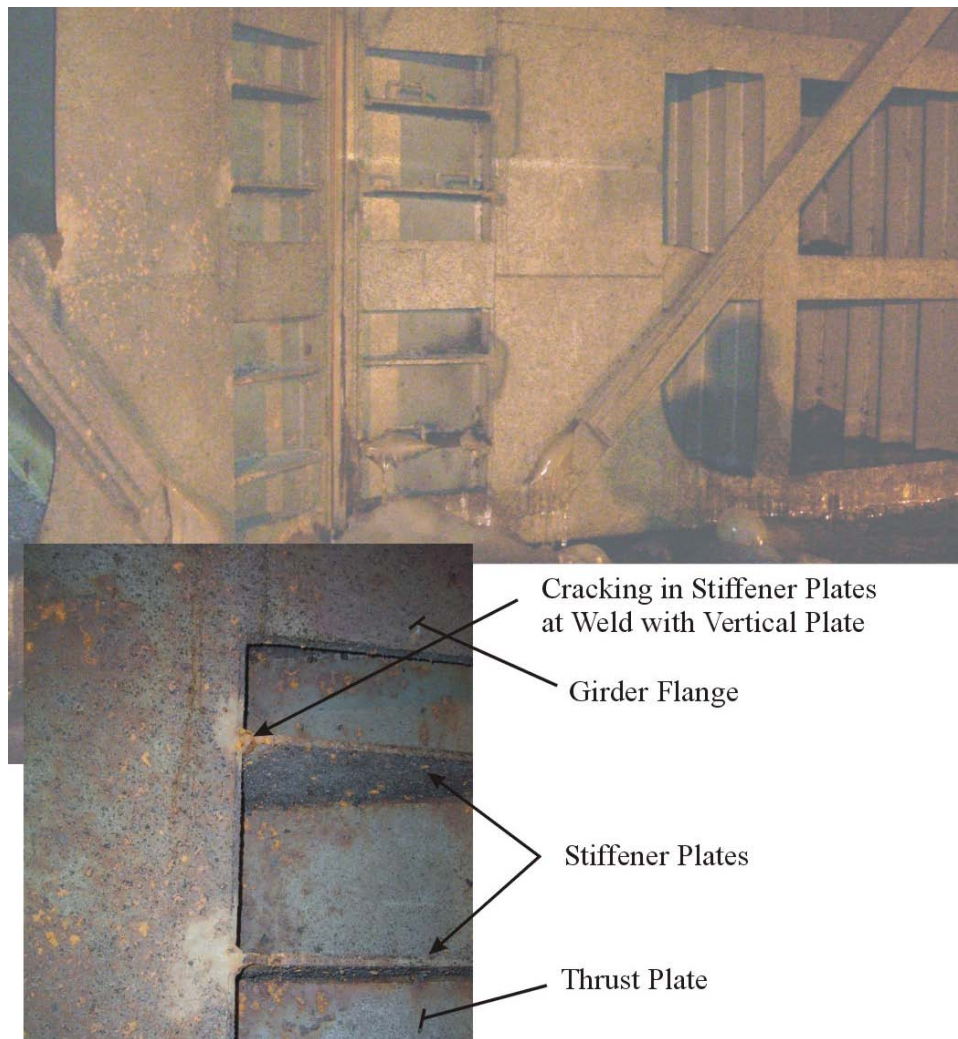


Figure B-1.  Illustration of fatigue cracking in stiffener plates at Snell Lock

B-2.  Global Modeling of Gate Performance.

    a.  A global model for the Snell Lock miter gate was developed and exercised to establish the working stress distribution at the joint connection of interest and to characterize the variation of this stress with variations in operational conditions.  This global model was also used to evaluate the consequences of this fatigue cracking (if left unattended) and identify possible limit states based on structural integrity of the gate.  Figure B-2 shows the downstream side of the gate, illustrating the global finite element model of the gate along with basic overall dimensions. The global model employs 8-node plate bending elements for the primary structural components, and beam elements for most of the secondary components, such as intercostals for the skin plate. Figure B-3 illustrates the beam element modeling and also the nonlinear springs used to model the contact along the quoin and miter blocks.  This figure also shows the tension-only truss elements used for the prestressed diagonal bars.  Figure B-4 isolates the modeling for the downstream flanges and cover plates, and Figure B-5 shows the plate element modeling for the girder webs and thrust plates, including the horizontal stiffeners, with the upstream and downstream flanges and skin plate removed for clarity.  These plots use colors to identify the various plate thicknesses used in the construction.

    b.  Figure B-6 provides blowup views to further illustrate the modeling details for the gudgeon and anchor arms, the strut arm connection, and the floating pintle.  The base of the pintle, attached to the bottom girder through a rigid beam element, is explicitly modeled and restrained in the horizontal plane with a rigid contact surface representing the shape of the base embedded in the concrete sill.  This contact surface allows the pintle to move as necessary during the miter as the hydrostatic load is transferred into the wall of the monolith and better capture the reaction loads acting on the pintle.

    c.  The vertical displacement at the base of the pintle and all translational displacements at the ends of the anchor arms are fixed as displacement boundary conditions.  The horizontal displacements at the base of the pintle are also restrained to remain within the fixed contact surface described in b above.  The diagonals are pretensioned with the gate in a free-hanging state using several analysis steps to simulate the physical steps taken in the field to pretension the diagonals.  The steps for pretensioning the diagonals are summarized in Table B-1.  Following this procedure, the nominal value of prestress in the negative diagonals is 10-11 ksi (69-76 MPa), and the nominal value of prestress in the positive diagonals is 12-13 ksi (83-90 MPa) with an out-of-plumb displacement of about 0.10 in. (2.5 mm) along the miter in a free-hanging state.

**Table B-1.  Summary of Steps for Pretensioning Diagonals
on Snell Miter Gates**

| | |
|---|---|
| Step 1 | Support gate at pintle and top anchorage. Apply dead loads with slack in all diagonals. |
| Step 2 | Twist top of gate downstream until out of plumb by 3 in. (0.7 m). Remove slack from negative diagonals. |
| Step 3 | Twist top of gate upstream until out of plumb by 3.1875 in. (0.08 m). Remove slack from positive diagonals. |
| Step 4 | Release top of gate.  Adjust diagonals if necessary to keep miter post within 0.25 in. (6 mm) plumb top to bottom. |
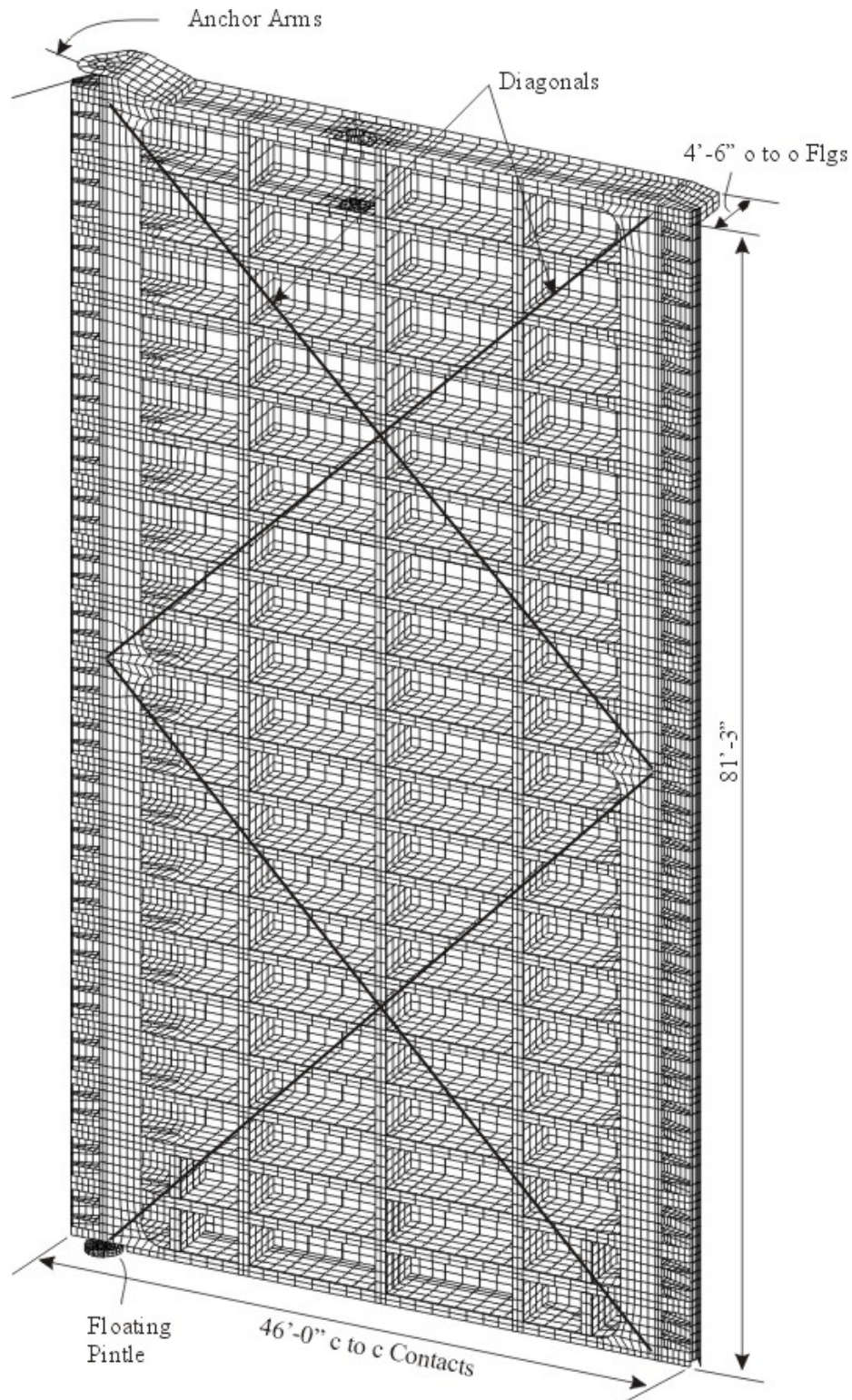
Figure B-2.  Global model of Snell lock miter gate leaf, view from
downstream (Note:  to convert feet to meters, multiply by 0.3048;
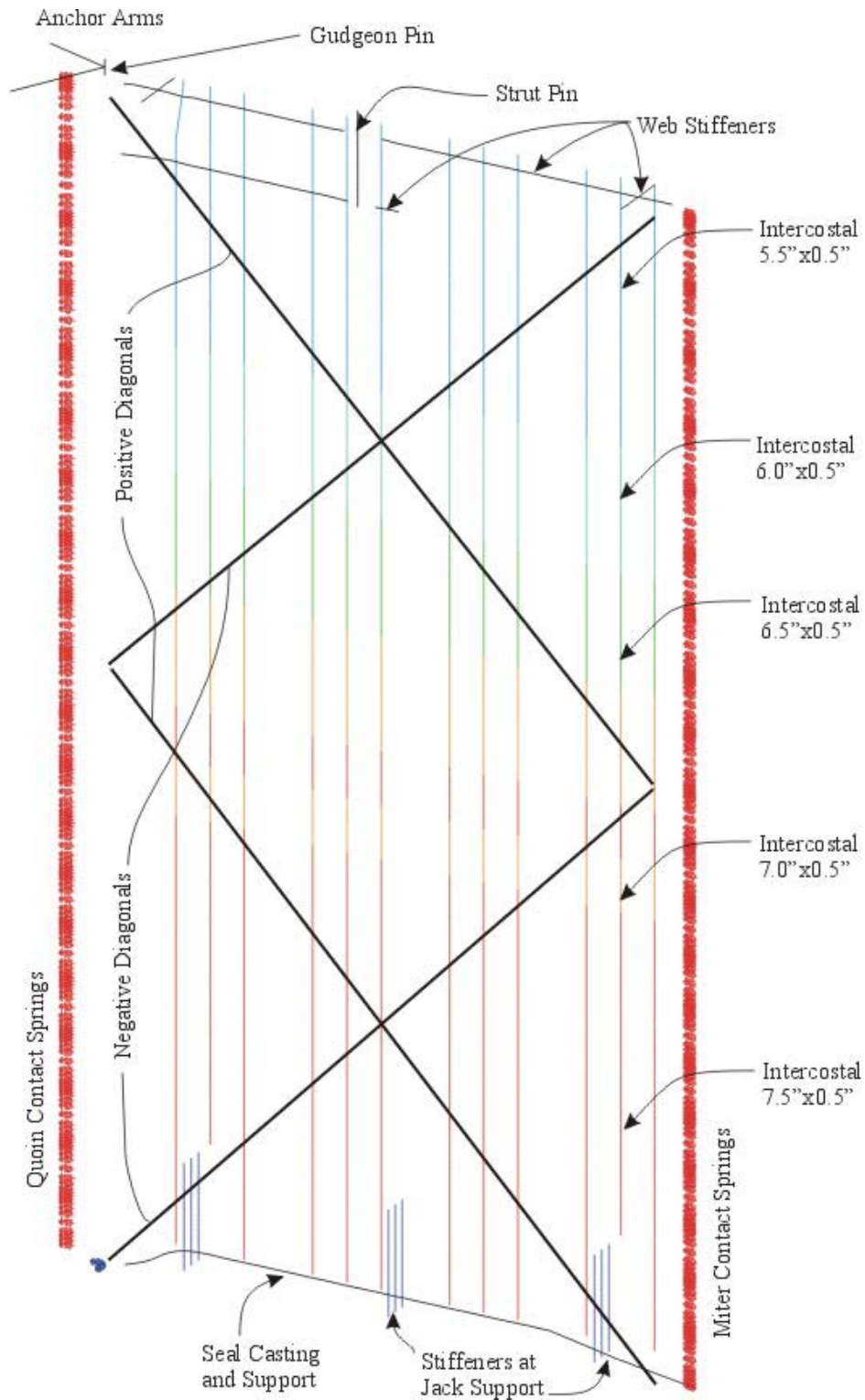to convert inches to millimeters, multiply by 25.4)

Figure B-3.  Beam element and contact spring modeling, Snell miter
gate (Note:  to convert feet to meters, multiply by 0.3048;
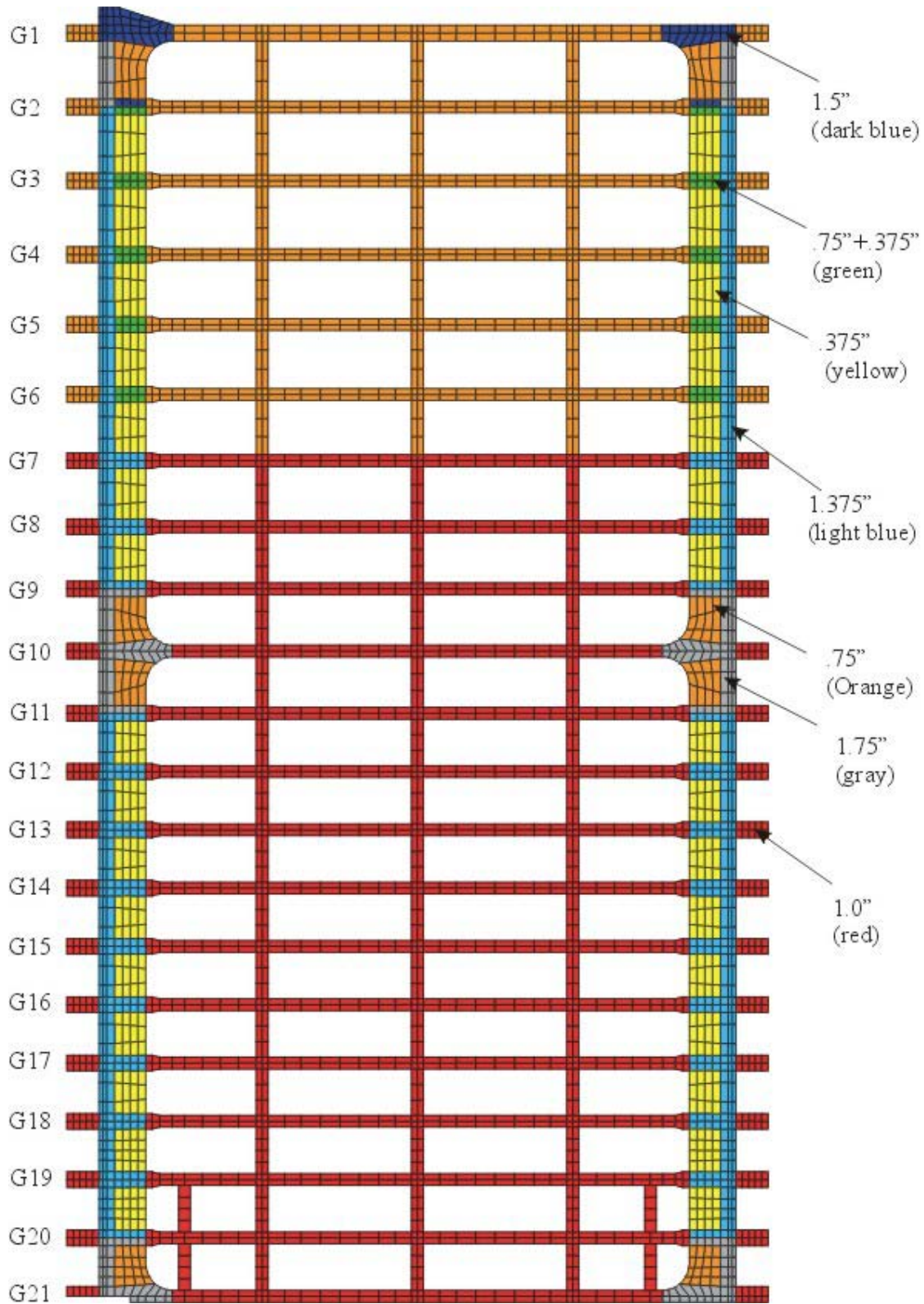to convert inches to millimeters, multiply by 25.4)

Figure B-4. Plate element modeling for downstream flanges and plates, Snell miter gate
(Note: to convert inches to millimeters, multiply by 25.4)
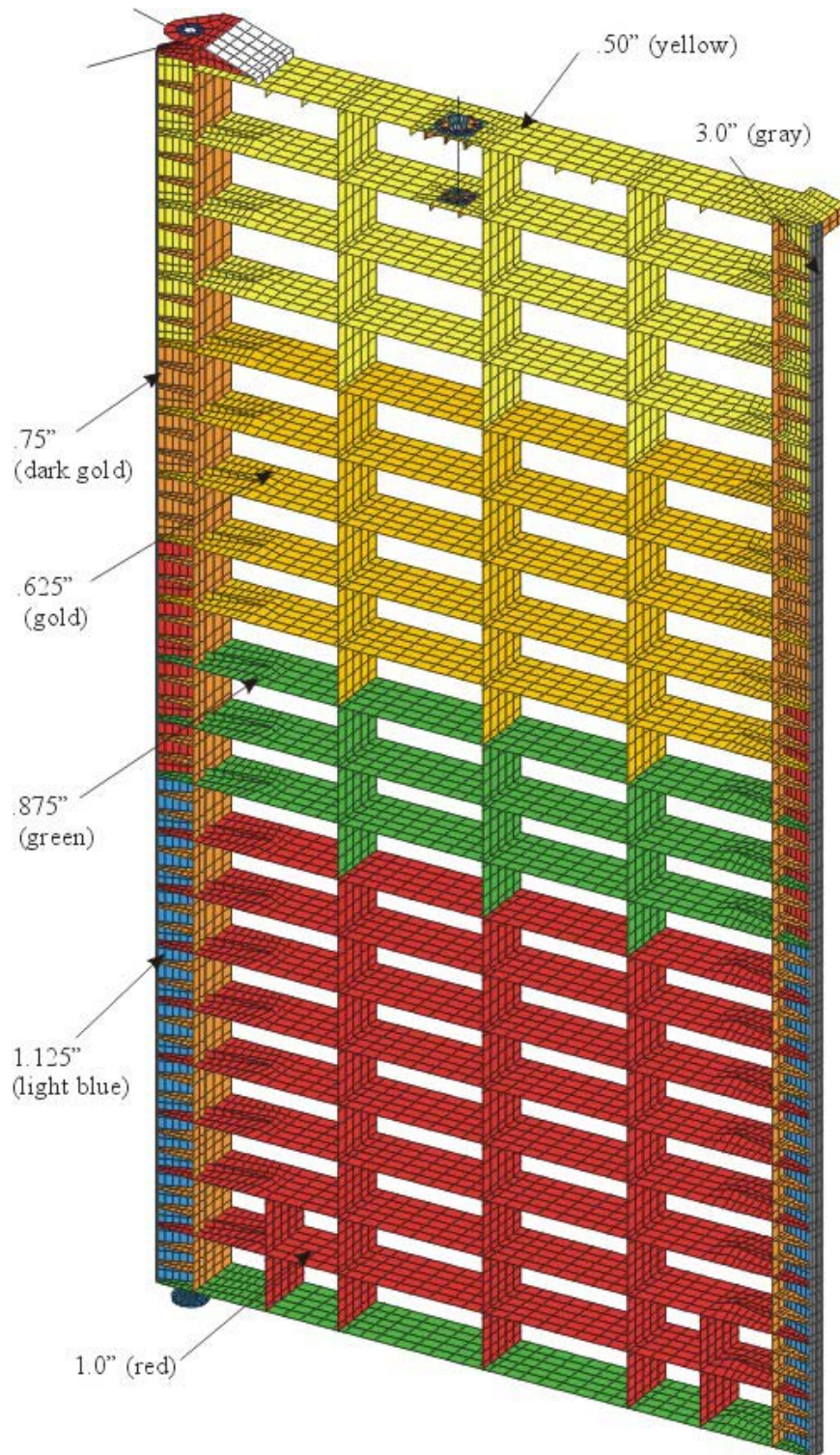
Figure B-5.  Plate element modeling for girder webs and trust plates,
Snell miter gate (Note:  to convert inches to millimeters,
multiply by 25.4)
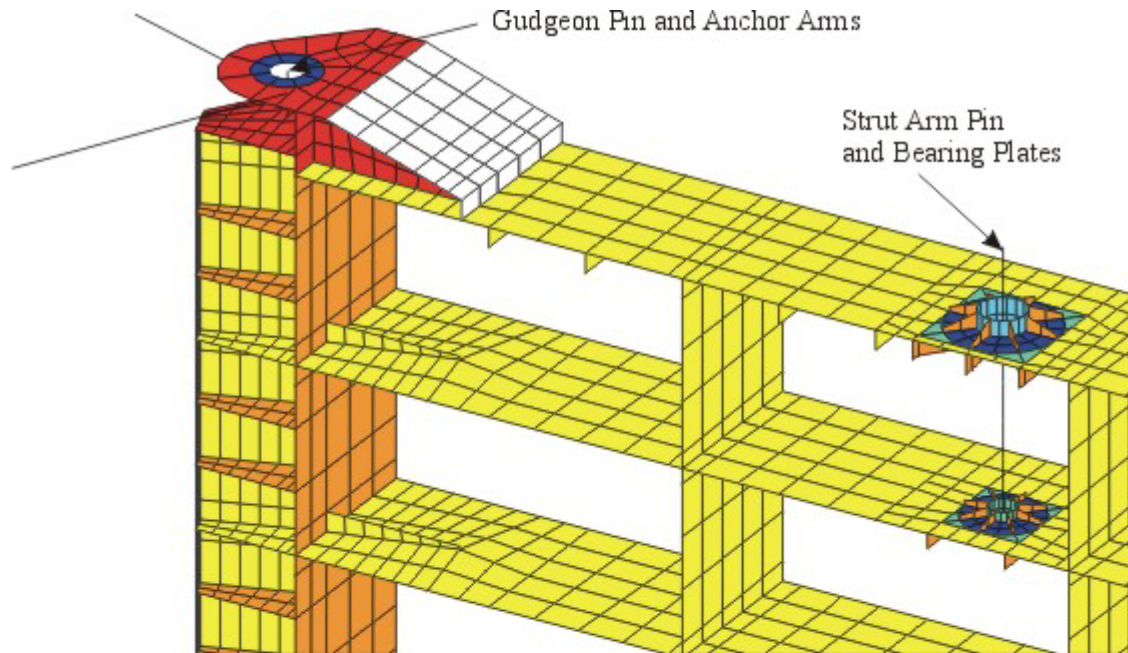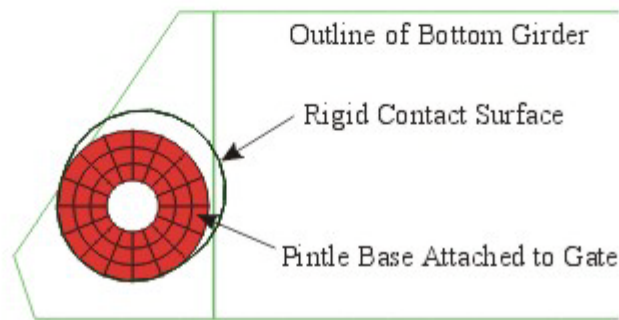
Figure B-6.  Blowup of gudgeon, strut arm connection, and pintle modeling for Snell miter gate

d.  Analyses are performed for the different operating conditions categorized as free hanging, opening and closing, and operation under miter.  Several variations in the diagonal prestressing for the free-hanging condition are considered, including zero prestress in the negative diagonals and zero prestress in the positive diagonals.  For the gate opening loads, the gate is considered in the position just off miter, and pressure loads are applied on the upstream wetted surfaces for the lower pool to represent the resistance of the water as the gate is pulled through the water.  In this case, a node representing the strut arm connection is fixed in the direction of the strut arm to simulate the reaction force of the strut arm on the gate.  For the operating condition with the gate mitered, the nonlinear "contact" springs along the miter and quoin posts are activated, and the hydrostatic loads are incrementally applied to allow the reaction forces to develop along the quoin and miter posts.  Variations in operating conditions,

ETL 1110-2-566
1 Jun 10

such as miter block wear, are considered to establish the performance of the gate under changing operational conditions.  Table B-2 summarizes the cases considered with the global model. Figure B-7 and B-8 illustrate the stress distributions in the downstream flanges and in Girder 20, respectively, for the normal operating condition.

    e.  Eigenvalue buckling analyses are performed on the global model to identify possible limit states for this observed cracking in the stiffener plates.  The buckling analysis identifies the load factor (eigenvalue) on the normal operating loads (gate mitered under hydrostatic pressure) and the elastic buckling shape (eigenmodes) for an elastic instability or bifurcation condition. For these linear perturbation analyses, the nonlinear springs and the contact surfaces must be removed.  The deformations along the quoin and miter posts and at the pintle are "frozen" with the values from the normal operating condition as the boundary condition for the buckling analyses.  Figure B-9 illustrates the lowest buckling mode under pristine gate conditions with web dishing on Girder 9 near the diagonal anchorage connections at midheight.  This buckling would occur at a load factor of 3.74 times the hydrostatic loads for the normal operating condition.  Note that this web dishing in a single bay of a single girder is not cause for concern about the structural integrity or global capacity of the gate.  A global buckling mode affecting several bays would require an even larger load factor, and the effect of the fatigue cracking on the buckling characteristics is based on this lowest buckling mode.  Figure B-10 shows a blowup for the lower portion of the gate near the quoin with cracking damage imposed by removing elements along the direction of cracking.  Here, the cracking is imposed at all the stiffener locations for all girders on the downstream side in the bottom half of the gate and at both the quoin and miter ends.  This cracking simulation renders the stiffeners ineffective in supporting compressive loads.  The buckling analysis with this extensive cracking damage imposed provides a load factor of 3.67 for the same lowest buckling mode with dishing in the web on Girder 9.  Thus, it is concluded that this type of fatigue cracking will not seriously jeopardize the structural integrity of the gate.  There is still significant margin against buckling even with extensive cracking in these stiffeners, and this cracking does not change the buckling mode or performance characteristics of the gate.

B-3.  Local Modeling of Welded Connection.

    a.  A local detailed model of the region around the welded connection of interest is constructed to provider better resolution of the stress concentrations and to introduce the residual stress distribution that is present from the welding operation.  The local model is constructed using continuum-based brick elements and is associated with coordinate locations in the global model.  The displacements from the global model for an analysis case can be extracted and directly applied to the cut surfaces of the local model.  This allows application of any loading condition conducted for the global model to be applied to the local model through the displacement boundary conditions on the local model.  Figure B-11 illustrates the local model assigned to a region around Girder 20 with the associated stiffener plates.  Figure B-12 isolates the local model with a view from the back to illustrate the elements included to represent the weld connecting the stiffener plate to the vertical diaphragm flange plate.  In this figure the elements highlighted in yellow around the cut boundary are used to help simulate the constraint in the connection during the thermal stress analysis to develop the residual stress field at the

**Table B-2  Summary of Parametric Cases for Global Model
of Snell Miter Gates**

| Case No. | Parametric Case | |
|---|---|---|
| Case 1 | Free hanging, equalized lower pool | |
| | 1a | Nominal diagonal prestress |
| | 1b | Zero prestress in negative diagonals |
| | 1c | Zero prestress in positive diagonals |
| Case 2 | Gate opening condition, 30 psf (1.4 kPa) on upstream wetted surface for lower pool | |
| | 2a | Nominal diagonal prestress |
| | 2b | Zero pre-stress in negative diagonals |
| | 2c | 77.5-psf (3.7-kPa) pressure (1.25-ft (0.4-m) head differential surge), normal diagonal prestress |
| Case 3 | 3a | Normal operation, mitered under hydrostatic loads, nominal prestress, nominal head differential, perfect gate conditions |
| Case 4 | 4a | Same as 3a, but with added 2.5-ft (0.8-m) surge head in upper pool |
| Case 5 | Same as Case 3, but with variation in diagonal prestress | |
| | 5a | Zero prestress in negative diagonals |
| | 5b | Zero prestress in positive diagonals |
| Case 6 | 6a | Effect of worn miter block, same as Case 3, except miter can displace 1/4 in. (6-mm) before contact |
| Case 7 | 7a | Effect of head differential same as Case 3, except use maximum upper pool and minimum lower pool |
| Case 8 | Effect of worn quoin block, variations in quoin contact | |
| | 8a | No contact at girders 17,18, 19 |
| | 8b | Fixed contact at girders 17,18,19 (stick conditions) |
| | 8c | No contact at girders 10,11,12 |
| | 8d | Fixed contact at girders 10,11,12 |

welded connection.  By varying the modulus of these elements, the effect of variations in the constraint around the welded connections on the residual stress distribution can be evaluated.

b.  The residual stress distribution at the welded connection is determined using a thermal stress analysis and simulating the weld process as discussed in Chapter 3.  Figure B-13. illustrates the residual stress distribution for a set combination of material properties, welding scheme (order and direction of weld operations), and simulated constraint.  The contour limits are set so that the red areas are close to the nominal yield stress.  Note that a tensile stress field develops at and beyond the corner of the connection, but then dissipates into the stiffener plate toward the thrust plate.  Analyses with variations in these parameters are conducted to characterize this residual stress distribution for uncertainties in the modeling and field conditions.
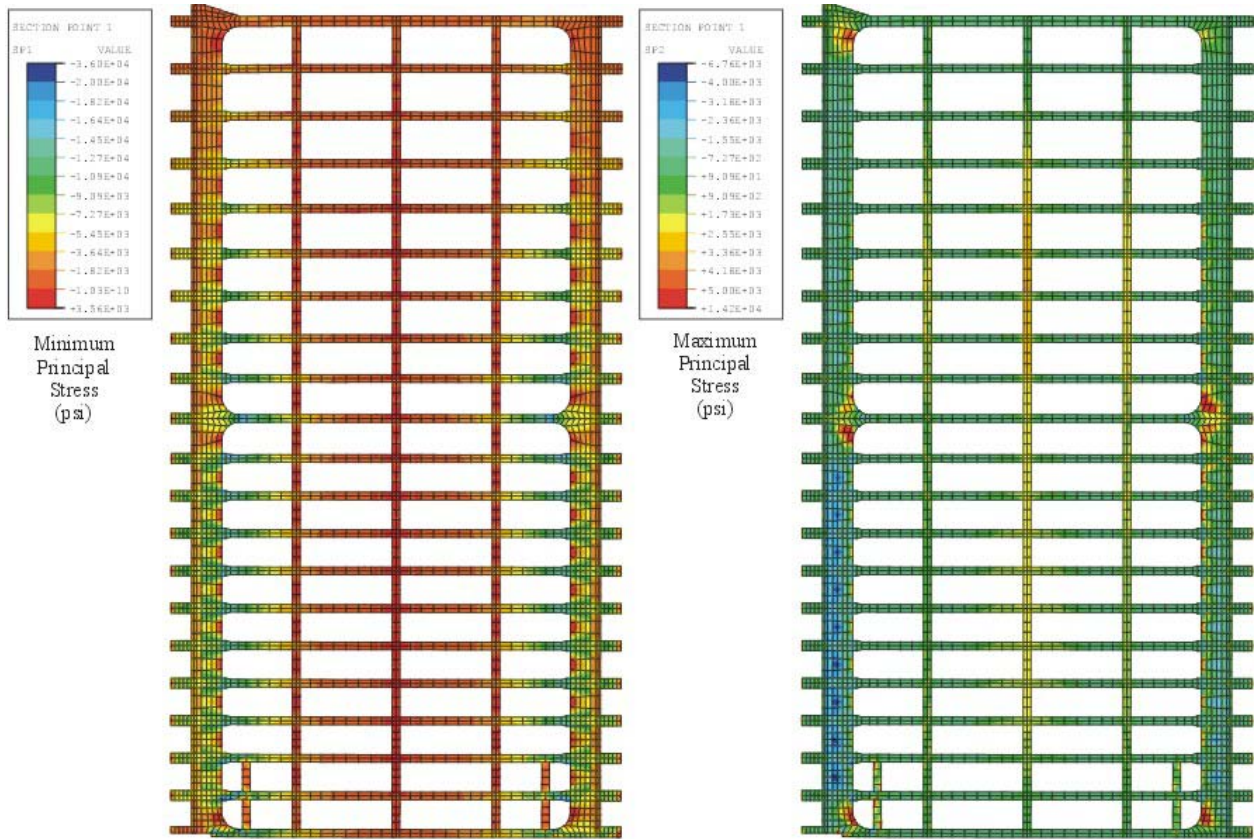
Figure B-7.  Principal stress contours in downstream flanges for normal operating loads
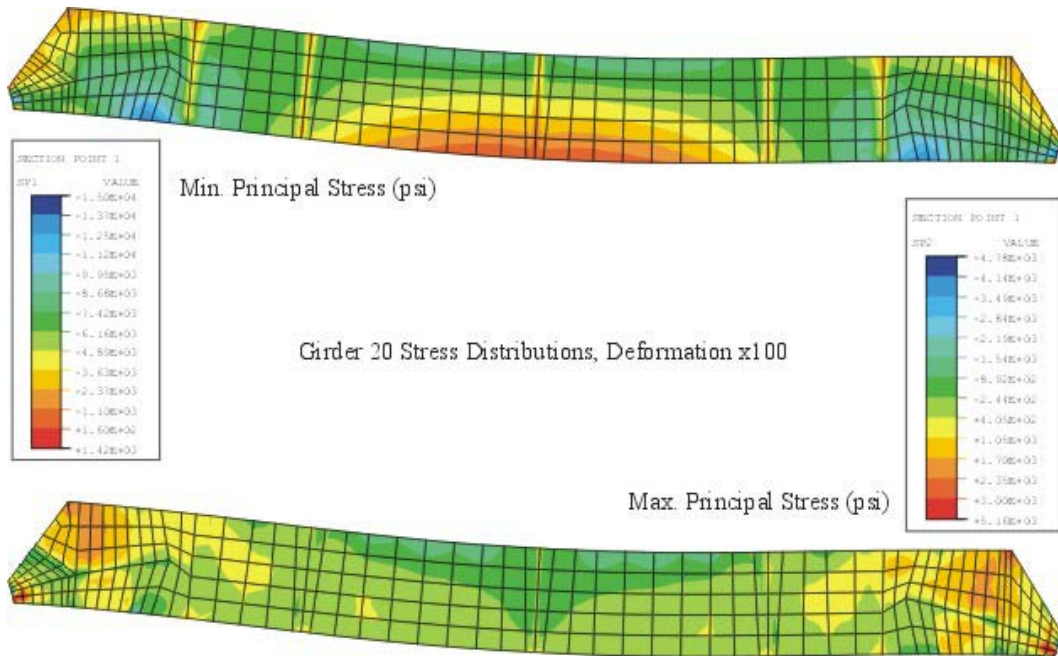(Note: to convert psi to kPa, multiply by 6.894757



Figure B-8.  Principal stress contours for web plate in Girder 20 (Note: to convert
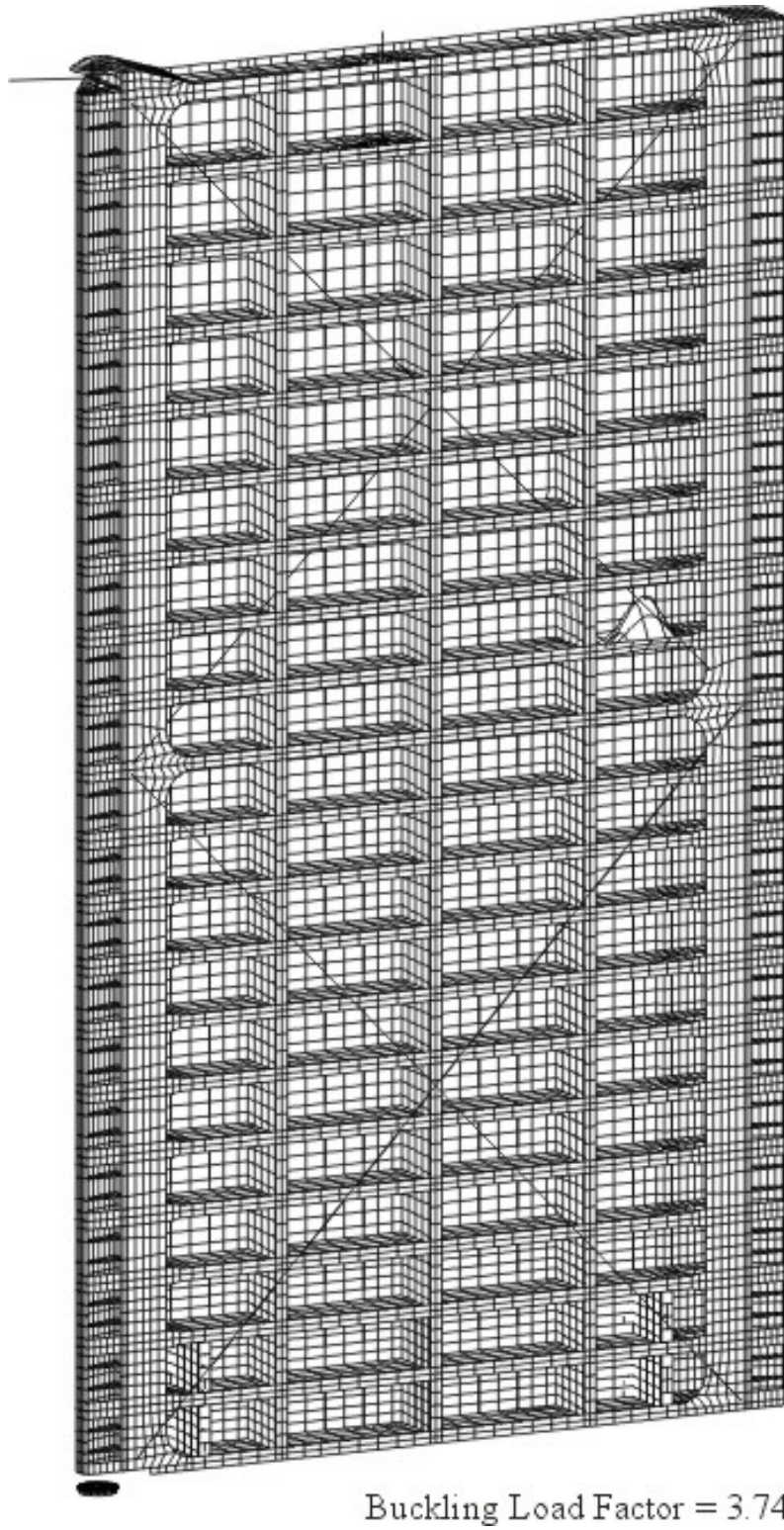psi to kPa, multiply by 6.894757

Buckling Load Factor = 3.74

Figure B-9.  Lowest buckling mode for pristine gate
condition under normal operation, Snell gate

Buckling Load Factor = 3.67

Cracking Damage Imposed at All Stiffener
Connections in Lower Half of Gate
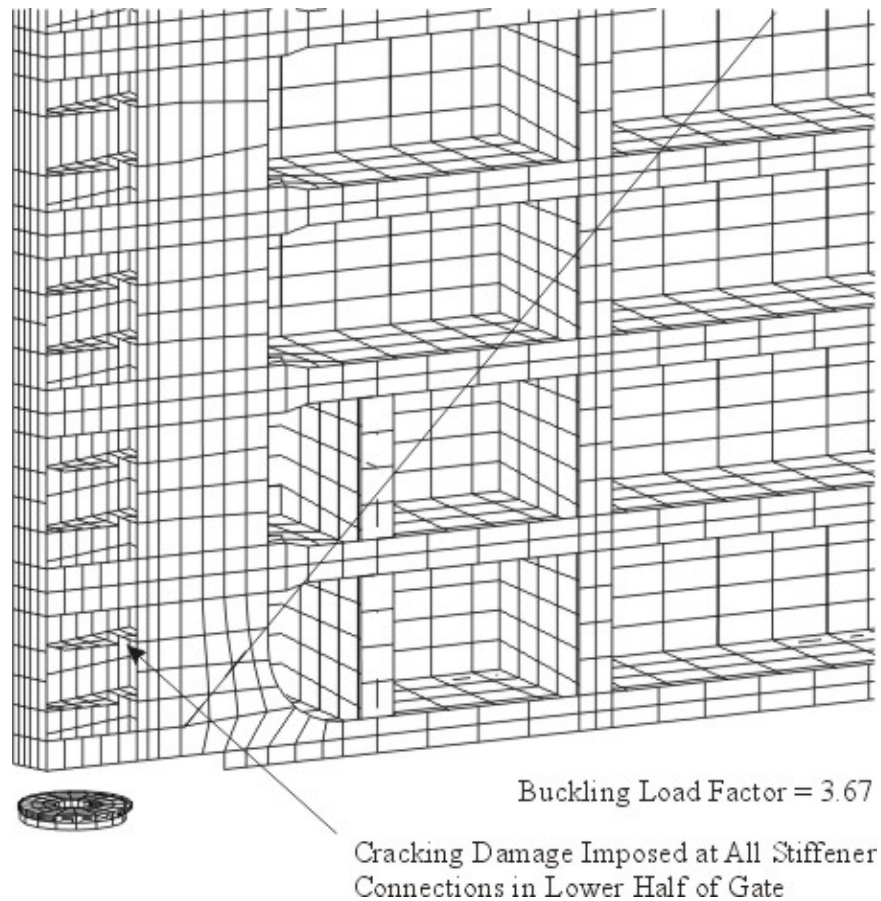
Figure B-10.  Illustration of imposed cracking damage
for evaluation of limit state

c.  The local model is then subjected to loading representing the range of working stresses at the connection.  The displacements corresponding to the cut locations of the local model in the global model are extracted from the global model for the free-hanging condition and for the mitered condition under operating loads (both including the diagonal prestress).  These displacements are then imposed on the cut boundaries of the local model with the residual stresses.  The stress range at the corner of the connection from the local model is used to characterize the conditions leading to initiation of the fatigue cracking.  This local model analysis then includes the residual stresses, the stress concentration caused by geometric configuration, and the stress range for a gate operation cycle.

d.  The local model is then used to establish the crack growth characteristics for a fatigue crack at this welded connection.  A crack is incrementally extended in the local model as illustrated in Figure B-14.  For each increment of crack extension, the local model is subjected to the free-hanging and mitered operation conditions to impose a load cycle for the current crack length.  The stress intensity for the minimum and maximum stress conditions for each crack length is calculated using the J-Integral method as discussed in Chapter 3.  This provides a change in stress intensity versus change in crack length for evaluation of the Paris equation for crack growth with subsequent operating cycles after crack initiation.
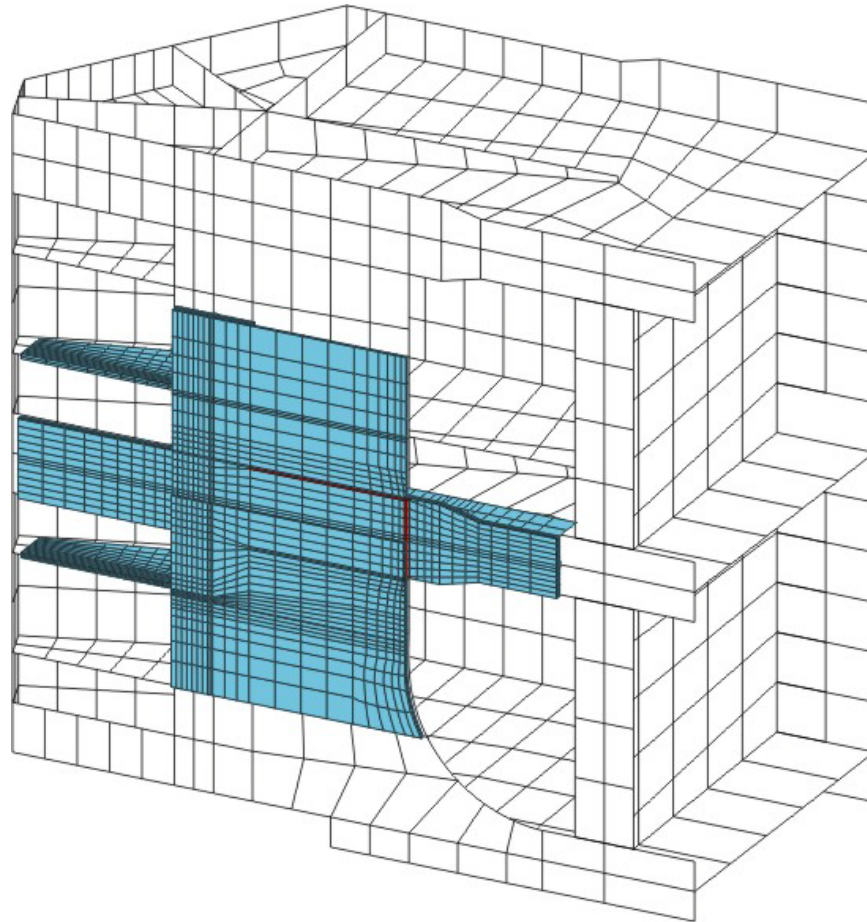
Figure B-11.  Illustration of local model with connection to global model
for Snell gate

B-4.  <u>Reliability Modeling and Evaluation</u>.

a.  The following reliability model is constructed from the results of the global and local
modeling for fatigue cracking at the welded connection of the stiffener plates on the thrust plate.
This model first characterizes the conditions leading to initiation of the fatigue cracks and then to
the growth rate of the cracks with continued operational cycles.

(1)  The stress in the stiffener plate at the connection is found to undergo slight tension
when the gate is open because of sagging under this free-hanging condition.  The stress under
this condition is determined to be primarily a function of corrosion rate and the prestress in the
diagonals, expressed as follows:

$$\sigma_1 = \sigma_0 \cdot F_c \cdot F_d \tag{B-1}$$

where $\sigma_0 = 3.3$ ksi (22.8 MPa) is the nominal value (including the stress concentration from the
connection geometry), and the factors $F_c$ and $F_d$ account for changes caused by corrosion and
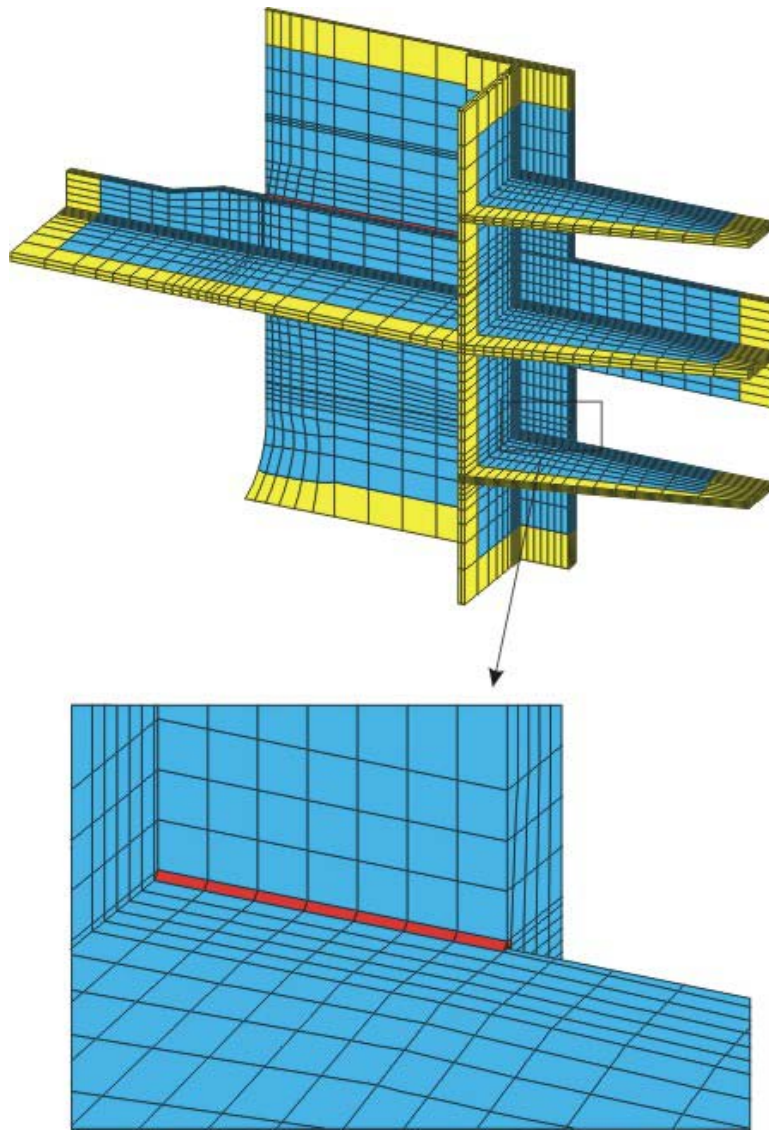diagonal prestress, respectively, as follows:

Figure B-12.  Back view of local model with weld of
stiffener to flange plate

$$F_c = \frac{b}{b - 2r_c t} \tag{B-2}$$

where

    $b =$   nominal plate thickness (in this case $b = 0.75$ in. (19 mm))

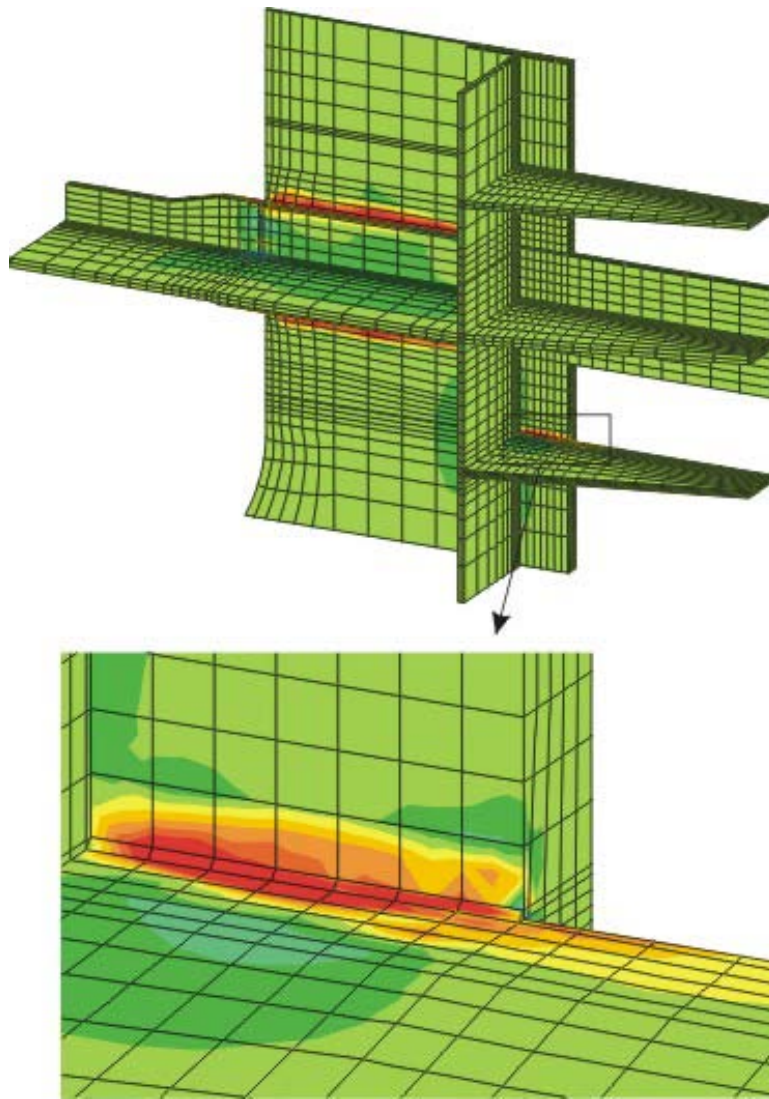    $r_c =$   rate of corrosion (in./year)

    $t =$   time in years

Figure B-13.  Illustration of residual stress distribution
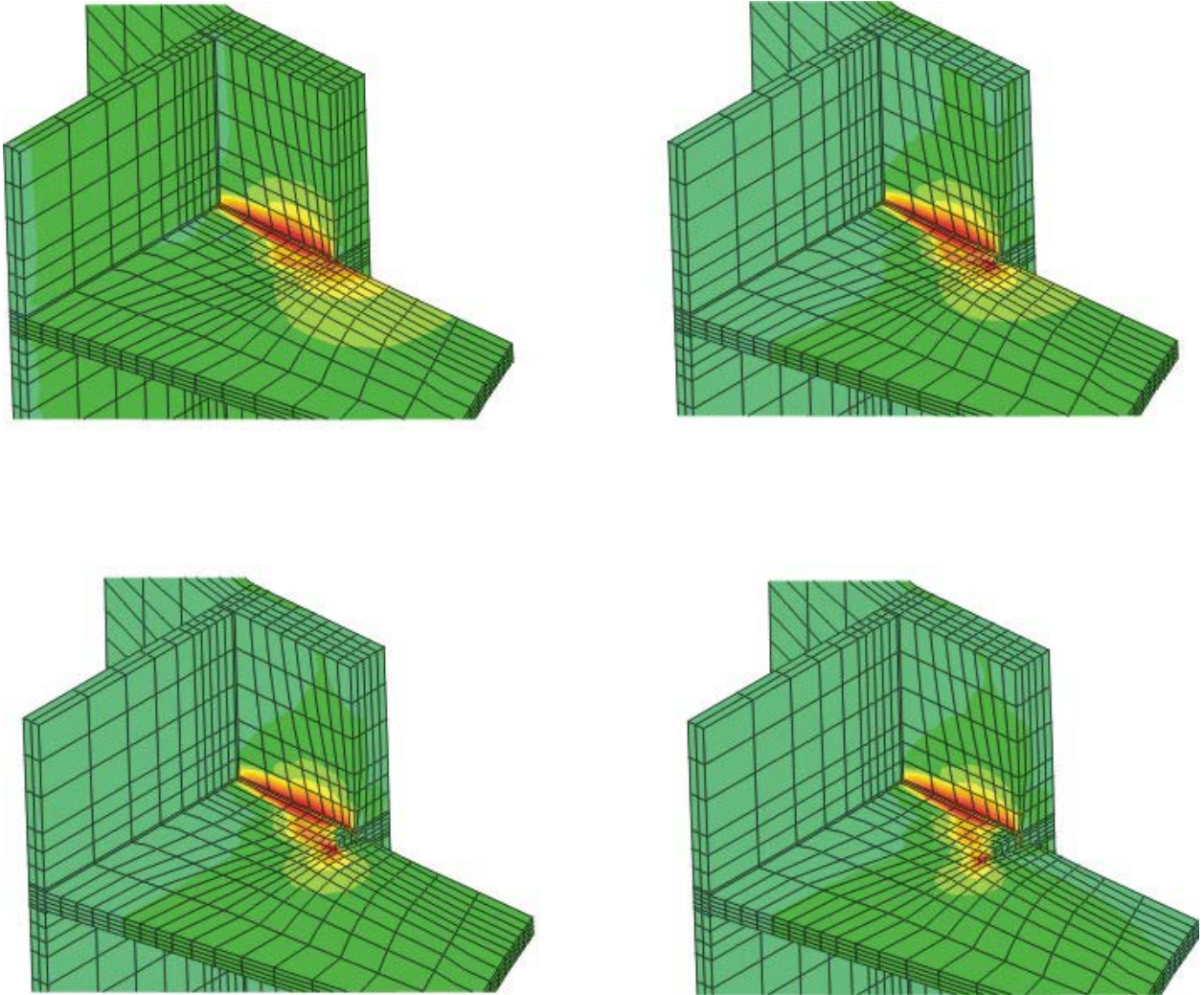at welded connection

Figure B-14. Illustration of crack extension with residual stress field under load cycle

and the multiplier of 2 accounts for corrosion that can occur on both exposed surfaces of the plate:

$$F_d = 1 + 2 \cdot \left(\frac{t}{T_d}\right)^{.5}, \text{ if } t \geq T_d, F_d = 3.0 \tag{B-3}$$

where $t$ again is the time in years, and $T_d$ is the reference time for the stress in the diagonals to relax to zero. This factor is constant once the diagonal prestress is totally dissipated, and the power law form correlates to the observation that relaxation is a direct function of stress, i.e., more relaxation occurs when the diagonals are under higher stress. For this evaluation, it is also assumed that the diagonals are retensioned every 20 years as the baseline condition.

(2) The stiffener plate undergoes high compressive stress under the gate operating conditions as the other extreme in the load cycle. This stress is determined to be primarily functions of the head differential on the gate, the corrosion rate, and the wear on the miter block:

$$\sigma_2 = \sigma_c \cdot F_h \cdot F_c \cdot F_m \tag{B-4}$$

where $\sigma_c = -85$ ksi (586 MPa) is the nominal compressive stress at the corner of the connection, including the stress concentration and $F_h$ is calculated as

$$F_h = {}^h\!/_H \tag{B-5}$$

where $h$ is the head in feet and $H$ is the reference head in fee where the nominal stress is calculated ($H = 44.13$ ft (13.45 m)

(3) Thus, Equation B-4 can be simplified to

$$\sigma_2 = -1.926 \cdot h \cdot F_c \cdot F_m \tag{B-6}$$

$F_c = \dfrac{b}{b - 2r_c t}$ , the same corrosion factor as for $\sigma_1$

$F_m = 1 + 0.2 \cdot r_w \cdot t$ , the factor accounting for wear on the miter block

where $r_w$ is the rate of wear on the miter block with a nominal value of 0.25 in. (6.35 mm) over 20 years, and $t$ is the time in years. Initially, wear in the miter block creates additional compressive stress in the stiffener plate. As the wear approaches 0.5 in. (12.7 mm) on the miter block, the factor starts to decrease in the lower girders because the bottom girder bears on the concrete sill below and reacts some load directly into the sill. For the current model, this effect is ignored, and for the baseline model, this wear factor is reset to 1.0 assuming the miter blocks are repaired during the 20-year maintenance cycle.

(4) The residual tensile stress at the welded connection is primarily a function of the geometric configuration, the yield strength, $\sigma_y$, and the constraint on the connection during the weld:

$$\sigma_w = 1.7 \cdot \sigma_y \cdot F_w \tag{B-7}$$

where $\sigma_y$ is the yield stress of the material, and $F_w$ is a combined factor to account for variations in the yield stress and the constraint during the weld operation. A nominal value of 36 ksi (248 MPa) was used in the local modeling for the A7 steel material, and it is found that a range from 0.85 to 1.2 for $F_w$ provides a good correlation for the variation in residual stress. This range also accounts for the likelihood that the yield stress will be higher than the nominal value.

(5) The effective alternating stress $\sigma_{eff}$ for the load cycle is calculated from the stress range that develops between the open and closed gate positions, and uses the Goodman relation to account for the effect of increased cyclic damage when the mean stress in the cyclic history is in tension. The Goodman relation is a function of the ultimate strength of the steel.

$$\sigma_{max} = \sigma_1 + \sigma_w \tag{B-8}$$

$$\sigma_{min} = \sigma_2 + \sigma_w \tag{B-9}$$

$$\sigma_{alt} = \frac{1}{2}\left(\sigma_{max} - \sigma_{min}\right) \tag{B-10}$$

$$\sigma_{mean} = \frac{1}{2}\left(\sigma_{min} + \sigma_{max}\right) \tag{B-11}$$

$$\sigma_{eff} = \frac{F_b \cdot \sigma_{alt}}{1 - \dfrac{\sigma_{mean}}{\sigma_{ult}}} \tag{B12}$$

where $\sigma_{ult}$ is the ultimate tensile strength of the material. It is found that using a nominal value of 72 ksi (496 MPa) and the factor $F_w$ provides a consistent range and variation of this parameter. ($\sigma_{ult}$ is increased when $\sigma_y$ is increased). $F_b$ is a modeling factor to account for other uncertainties, such as stress corrosion cracking effects, surface roughness, and differences in the configuration of the connection compared to laboratory specimens used to develop fatigue test data. It is found that $F_b = 0.67$ provides a good correlation to field cracking data for this uncertainty.

(6) The damage from cyclic loading is accumulated as

$$D = \Sigma\left(\frac{n_k}{N_k}\right) \tag{B-13}$$

where

$D =$  damage index

$n_k =$  number of cycles imposed at a stress level of $\sigma_{eff}$

$N_k =$  allowable number of cycles at that stress level

When $D$ reaches a value of 1, a fatigue crack initiates. The allowable number of cycles is calculated as

$$N_k = \left\{\frac{E \cdot Ln[100/(100 - RA)]}{4 \cdot (\sigma_{eff} - \sigma_z)}\right\}^2 \tag{B-14}$$

where

$E =$  Young's modulus, psi

$RA =$  68.5%

$\sigma_z =$  21,645 psi

This is the Langer Equation as the best fit to the fatigue data that is used as the basis for the ASME design fatigue relations. Here, RA is also factored by $F_w$ to account for variations in the fatigue data and to correlate the fatigue resistance with variations in yield stress.

(7) The fatigue correlation, described in (6) above, is based on data for cyclic loading on specimens where the number of cycles correlates to complete failure of the specimen. Here it is assumed that the number of cycles to initiate a crack correlates to an initial crack that extends through the thickness of the plate. Thus, when a crack initiates, an initial crack length $a_o$ for that crack is assumed. A nominal initial crack length of 0.10 in. (2.5 mm) is used with a range from 0.05 to 0.20 in. (1.3 to 5 mm).

(8) The crack growth under subsequent stress cycles is then characterized using the Paris equation as described in Chapter 3. The characterization for $\Delta K$ as a function of crack length and loading (i.e., $K_{max}$ and $K_{min}$) is based on detailed local modeling for crack extension within a residual stress field under a cycle of loading. This characterization for $\Delta K$ and $R$ as a function of crack length is defined in Table B-3. Interpolation of the values in this table is used in evaluating the Paris equation for crack growth with increasing crack length. The values are also extrapolated for crack lengths longer than that used in the local models by extending the final values as needed. The characterization of $\Delta K$ is plotted in Figure B-15. Note that the change in stress intensity decreases with longer crack lengths. Thus, while the stress intensity is increased for longer crack lengths, the cracks are growing into regions with less and less residual stress. This will slow down the crack extension as the cracks extend beyond the weld zone.

(9) After the model predicts crack initiation, the crack growth is calculated as follows.

(a) For the current crack length, determine the lower bound values $\Delta K_1$ and $R_1$ and the upper bound values $\Delta K_2$ and $R_2$ from interpolation in Table B-3.

(b) Then, the current value for the change in stress intensity and the stress intensity ratio is calculated.

$$\Delta K = \frac{1}{2}\left[\left(1+\xi\right)\Delta K_2 + \left(1-\xi\right)\Delta K_1\right]$$
(B-15)

$$R = \frac{1}{2}\left[\left(1+\xi\right)R_2 + \left(1-\xi\right)R_1\right]$$
(B-16)

where $\xi$ is a random variable between –1 and 1 with a nominal value of zero. For this evaluation, $\xi$ is also incrementally increased from the base value during subsequent years to account for increasing crack growth with continued gate wear. This factor is 0.025/year and accumulates during the time between maintenance repairs. When maintenance, such as re-tensioning of diagonals, is performed, this factor resets. Note that $\xi$ never exceeds 1.0.

(c) Calculate $\overline{\Delta K}$ and $S$ as described in Chapter 3 based on $\Delta K$ and $R$. Then, calculate the material parameters $C$ and $n$ using $\overline{\Delta K}$ and $S$.

**Table B-3. Characterization of Stress Intensity
for Snell Lock Miter Gate**

| Crack Length | Nominal | | Lower Bound | | Upper Bound | |
|---|---|---|---|---|---|---|
| | $\Delta K$ | R | $\Delta K$ | R | $\Delta K$ | R |
| 0.00 | 0.0 | 0.0 | 0.0 | 0.0 | 0.0 | 0.0 |
| 0.125 | 33.37 | 0.0 | 30.00 | 0.0 | 34.10 | 0.0 |
| 0.525 | 50.37 | 0.0 | 48.00 | 0.0 | 50.00 | 0.0 |
| 0.925 | 43.60 | 0.41 | 31.50 | 0.432 | 53.50 | 0.285 |
| 1.325 | 38.50 | 0.389 | 22.50 | 0.559 | 55.00 | 0.189 |
| 1.725 | 35.00 | 0.356 | 18.00 | 0.608 | 53.00 | 0.120 |
| 2.125 | 31.50 | 0.305 | 15.50 | 0.586 | 49.65 | 0.113 |
| 2.777 | 26.12 | 0.303 | 12.00 | 0.564 | 40.77 | 0.110 |
| 3.697 | 19.40 | 0.327 | 8.00 | 0.560 | 32.43 | 0.094 |
| 4.995 | 13.00 | 0.314 | 2.50 | 0.833 | 25.00 | 0.019 |
| 6.00 | 10.00 | 0.300 | 0.00 | 0.830 | 18.00 | 0.020 |
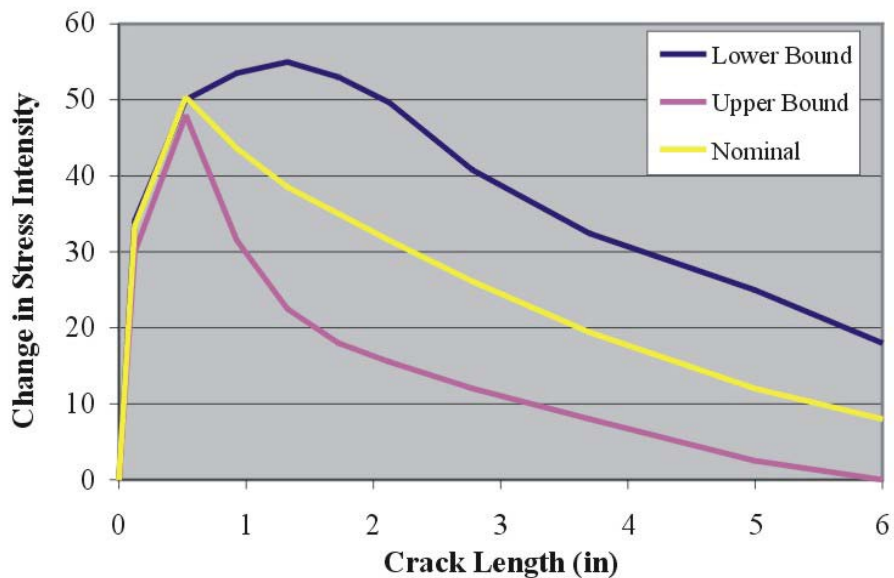


Figure B-15.  Characterization for change in stress intensity,
Snell Lock miter gate (Note:  to convert in. to
mm, multiply by 25.4)

(d) The increment in crack length is computed as

$$da = F_a \cdot C(\Delta K)^n \cdot dN \tag{B-17}$$

where *dN* is the number of cycles over the time period for calculating *da*, the change in crack length.  The factor $F_a$ is a random variable over the range 0.9 to 1.1 to account for uncertainties in the material data and correlations used in defining the Paris equation.

(e) The crack length over time is the initial crack length $a_o$, plus the accumulation of the crack increments *da* from subsequent applied cycles.

b.  Table B-4 provides a summary of parameters and variations used in the reliability evaluations.

**Table B-4.  Summary of Parameters and Variations for Snell Lock Study**

| Parameter/Description | Nominal Value | Range Min | Range Max | Distribution |
|---|---|---|---|---|
| $\sigma_y$, yield stress, ksi | 36 | 30.6 | 43.2 | See $F_w$ |
| $\sigma_{ult}$, Ultimate Tensile Strength (UTS), ksi | 72 | 61.2 | 86.4 | See $Fw$ |
| $F_w$, Material/constraint variation | 1.0 | 0.85 | 1.2 | Lognormal |
| $R_c$, Corrosion rate (in./year) | 1.0E-4 | 0.80E-4 | 1.33E-4 | Normal |
| $T_d$, Time for prestress relaxation, years | 15 | 10 | 20 | Normal |
| $R_m$, miter block wear (in./year) | 0.25/20 | 0.125/20 | 0.375/20 | Normal |
| $F_b$, Fatigue crack data variation/benchmark | 0.67 | -- | -- | -- |
| $a_o$, Initial crack length (in.) | 0.10 | 0.05 | 0.20 | Normal |
| $\xi$, Variation in crack growth modeling | 0.0 | -1.0 | 1.0 | Normal |
| Increment in $\xi$ for continuing gate wear | 0.025/year | -- | -- | -- |
| $F_a$, Variation in crack growth material data | 1.0 | 0.9 | 1.1 | Normal |
| Note:  to convert ksi to MPa, multiply by 6.894757. To convert in. to mm, multiply by 25.4. | | | | |

c.  This structural reliability model was implemented into an Excel spreadsheet and exercised to evaluate the structural reliability from the fatigue cracking being experienced on the miter gates at Snell Lock.  The study considers 82 years of operation, from 1959 to 2040.  Only minor variations in the pool elevations occur for this lock system, and for this study, a constant head on the gate is considered.  For the baseline analyses, the projected traffic is held steady at the current levels.  Figure B-16 plots the crack length at a typical welded joint versus years of operation for the nominal, upper bound, and lower bound limits of the variables.  This evaluation considers that the gate is repaired for diagonal prestress and miter block wear every 20 years. The nominal values of the parameters indicate that the cracks initiated around 1991 and will grow to 6 in. (0.2 m) by 2040.  The maintenance logs indicate that cracks were found and repaired starting in 1996.  This is consistent with the nominal model since the cracks would have been 1-2 in. (0.02-0.05 m) by 1996 and easily detected, assuming that detailed inspections for cracking at these locations were not being performed if the cracking was not expected.  Note that a distribution function has arbitrarily been drawn between the curves to indicate that the lower and upper limits will have a reduced probability of occurrence.  The actual probability for a

given crack length can be established using a Monte Carlo type simulation with random trials for the values of the various variables.
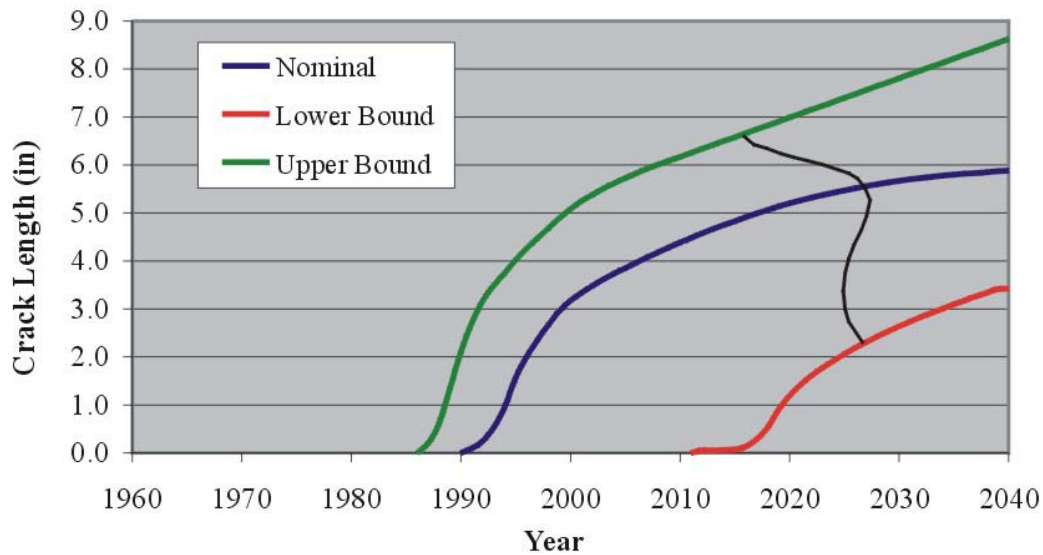


Figure B-16.  Evaluation for crack length and effect of parameter variations
(Note:  to convert in. to mm, multiply by 25.4)

d.  Figure B-17 plots the effect of regular maintenance to adjust miter block and diagonal prestressing on the fatigue crack lengths.  This analysis considers the nominal values of all parameters and adjusts the time interval for periodic maintenance.  This study indicates that maintenance will reduce the fatigue cracking by reducing the stress range during operations.  Because the relaxation of the diagonal prestressing is a persistent problem with the gate and because this does have an effect on the tension side of the load cycle, it may be advantageous to replace the diagonals with larger bars that would minimize the stress relaxation in the diagonals.

e.  Figure B-18 considers the effects of variations in the projected traffic on the fatigue cracking.  Variations for a 2 percent increase per year and a 4 percent increase per year were considered.  These result in factors of about 2 and 4, respectively, in the number of cycles by 2040.  As shown in the figure, this increased traffic does not significantly affect the fatigue crack growth or associated problems with the fatigue cracking.

B-5.  Summary.  The global modeling indicates that the type of fatigue cracking experienced in the Snell Lock miter gates is not critical for compromising the structural integrity of the gate.  Buckling analyses with cracking imposed completely through the width of the stiffener plates over a large extent indicate that there is still good margin against the likelihood of girder buckling under the operational loads.  In addition, the fatigue crack reliability model indicates that extended cracking will require a large number of cycles to extend the cracks completely through the width of the stiffener plates.  The crack growth slows down considerably after extending beyond the weld zone region at the connection.  The largest crack length predicted with all parameters having their worst-case values is about 9 in. (0.2 m) in the year 2040, and the width of the stiffener plate at this location is 14 in. (0.m).  Thus, it would be recommended that the tips of these fatigue cracks be drilled out when found during inspections and maintenance.  Burning out and rewelding these cracks will only make matters worse by introducing new and
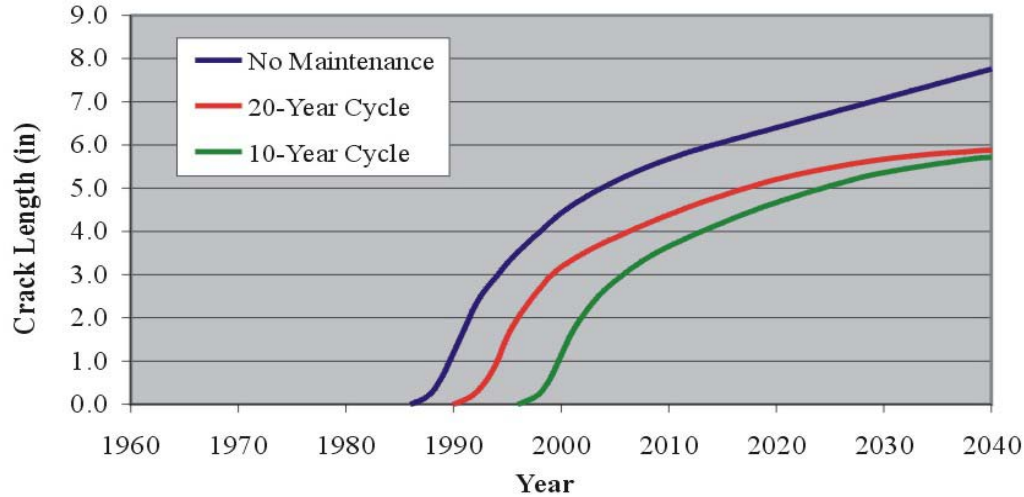
Figure B-17.  Effect of regular maintenance on the fatigue cracking for Snell gate
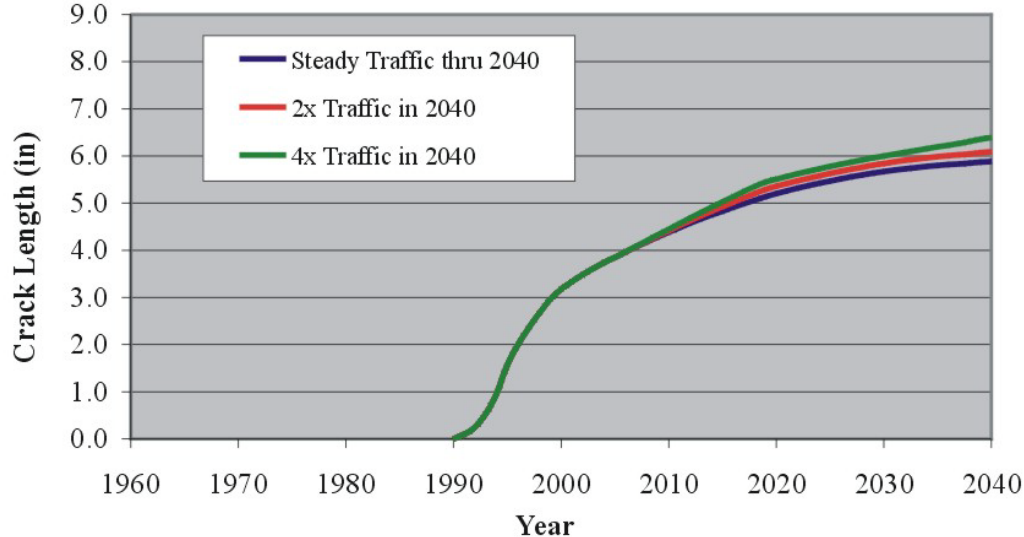


Figure B-18.  Effect of increasing traffic on fatigue cracking for Snell gates
(Note:  to convert in. to mm, multiply by 25.4)

larger residual stress distributions at the connection.  The welds under field conditions would also likely introduce higher geometric stress concentrations for the weld bead geometry, and there is also the possibility of voids or imperfections that would act as crack starters.  It is also found that regular maintenance for retensioning the diagonals and adjusting the miter and quoin blocks will help mitigate the fatigue cracking at these locations.  Even a 10- to 20-year cycle for this maintenance will provide good relief.  Because the diagonals are known to lose prestress consistently and regularly for these gates, it may be advantageous to retrofit the gates with larger diagonals and better tensioning devices to help mitigate the stress relaxation over time.  The cost of this rehabilitation relative to continued maintenance and concern with the cracking could be better defined and optimized by coupling an economic consequence model with the probabilistic reliability model.

**APPENDIX C**
**CASE STUDY FOR MARKLAND LOCKS, OHIO RIVER**

C-1.  Introduction.

a.  This case study considers the cracking found on the miter gates at Markland Locks, Ohio River, in the downstream girder flanges near the pintle.  As described in paragraph 2-1, main text, rather extensive and recurring cracking developed in the welded flange connections with the vertical diaphragm flanges and with the large gusset plates used to anchor the tensioned diagonal bars.  The field data indicates that the fatigue cracks were first found in 1983, on the order of 1/4 to 1/2 in. (6 to 12 mm) long, after some 84,000 cycles of gate operations.  After repairs in 1983-1984, additional and slightly more extensive cracking was found and again repaired in 1987-1988.  Then, in 1994, much more extensive cracking was found.  Cracks 2 to 4 in. (50 to 100 mm) long were found at multiple girder flange connection joints after the 6 years since the previous inspection and repair with about 21,000 additional gate cycles and now about 120,000 total cycles.  Extended cracking in the girder flange at the diagonal anchor plate was also found.  After extensive repairs in 1994, the gates were re-inspected in 1996.  Some additional cracking was found in 1996, generally categorized as 1/4 to 1/2 in. (6 to 12 mm) long. Typically this cracking developed at the welds of the previously repaired cracks.  As illustrated in Figures C-1 and C-2, an area of serious concern was the cracking that initiates at the girder flange connection with the anchor plate for the diagonals.  These cracks are known to extend relatively rapidly across the flange and reach the web plate.  Cracking recurred after repair by burnout and rewelding, and when gusset plates were added at these connections, new cracks developed at the toe of the gusset plate, as illustrated in the figures.  The triangular-shaped anchor plate for this configuration is welded to the webs of the girders and vertical diaphragm beams as part of the downstream flange surfaces.  The horizontal girder flanges are cut and butt-welded to the edges of the anchor plate.  That is, the diagonal anchor plate is not added on top of the girder flanges with fillet welds on the surfaces of the flanges.  For this case study, a reliability model was developed for the cracking in the horizontal girder flanges at the connection with the diagonal anchor plate.

C-2.  Global Modeling of Gate Performance.

a.  A global model for one leaf of a downstream miter gate was constructed to establish the nominal stress range in the flange near the connection of interest and to investigate the effects of variations in operational conditions on this stress range.  The overall modeling and dimensions of the gate are illustrated in Figure C-3.  All major structural sections were modeled with plate bending elements.  Beam elements were used for the anchor arms, and tension-only truss elements were used for the tensioned diagonal bars.  Figure C-4 further illustrates the plate element modeling with colors identifying the various plate thicknesses used in the construction. Figure C-5 is a similar plot for the view from upstream.  Beam elements were employed for the secondary structural components, such as the stiffeners on the girder webs and the thrust plate and the intercostals for the skin plate.  This modeling is illustrated in Figure C-6.

b.  These gates have a floating pintle design, which is modeled as illustrated in Figure C-7. The base of the pintle is explicitly modeled with solid elements and restrained in the horizontal plane within a rigid contact surface representing the shape of the pintle shoe embedded in the

concrete sill.  The pintle base is attached to the bottom girder through a rigid beam element representing the pintle casting and positioning the pintle base at the correct standoff distance from the bottom girder.  This contact surface modeling allows the pintle to move as necessary during the miter as the hydrostatic load is transferred into the wall of the monolith and better captures the reaction loads acting on the pintle.

c.  The vertical displacement at the base of the pintle and all translational displacements at the ends of the anchor arms are fixed as displacement boundary conditions.  The horizontal displacements at the base of the pintle are also restrained to remain within the fixed contact surface described in b above.  The diagonals are pretensioned with the gate in a free-hanging state using several analysis steps to simulate the physical steps taken in the field to pretension the diagonals.  The steps for pretensioning the diagonals are summarized in Table C-1.  Following this procedure, the nominal value of prestress in the negative diagonals is 10 ksi (69 MPa), and the nominal value of prestress in the positive diagonals is 12 ksi (83 MPa) with an out-of-plumb displacement of about 1/16 in. (1.6 mm) along the miter in a free-hanging state.

d.  Analyses are performed for the different operating conditions categorized as free hanging, opening and closing, and operation under miter.  Several variations in the diagonal prestressing for the free-hanging condition are considered, including zero prestress in the diagonals and excessive prestress in the diagonals.  For the gate opening loads, the gate is considered in the position just off miter, and pressure loads are applied on the upstream wetted surfaces for the lower pool to represent the resistance of the water as the gate is pulled through the water.  In this case, a node representing the strut arm connection is fixed in the direction of the strut arm to simulate the reaction force of the strut arm on the gate.  A similar procedure for the gate closing condition is used with the resisting "pressure" load on the downstream wetted surface.  For the operating condition with the gate mitered, the nonlinear "contact" springs along the miter and quoin posts are activated, and the hydrostatic loads are incrementally applied to allow the reaction forces to develop along the quoin and miter posts.  Variations in operating conditions, such as miter block wear and stress relaxation in the diagonals, are considered to establish the performance of the gate under changing operational conditions.  Table C-2 summarizes the cases considered with the global model.

e.  Figure C-8 provides a contour plot for the minimum principal stress under the normal operating conditions with deformations magnified by 100.  The compressive stress of about 12 ksi (83 MPa) flowing through the girder flanges near the quoin and miter in the lower portion of the gate is evident.  Figure C-9 plots a contour for the maximum principal stresses for the normal operating conditions with deformations magnified by 100.  Here some slight tension is seen on some of the downstream flanges near midspan, especially the vertical diaphragm flanges.  Tension stress also develops from bending in the vertical diaphragm webs along the quoin and miter posts under the hydrostatic loads.  Figure C-10 plots the maximum principal stresses in the flanges at the diagonal anchor plate under the free-hanging conditions.  Note that the residual stresses are not included in the global model.  The stress range that is acting on the flange connection with the diagonal anchor plate is illustrated in these figures.  Under the free-hanging state some tension develops in the flange at the anchor plate connection; and during the mitered condition under normal operations, this location experiences compression.  Coupled with tensile residual stresses at the connection from the welding fabrication, a relatively large stress range

can develop. Figure C-11 illustrates the stress distribution in Girder 13 for the normal operating condition.

f. Figure C-12 plots contours for minimum principal stress in the gate for mitered operations with 1/4-in. (6.4-mm) wear on the miter blocks. Here, the increase in the compressive stress in the flanges near the quoin is illustrated for this wear in the gate. The compressive stress is now about 14 ksi (97 MPa). For reference, Figure C-13 plots the maximum principal stresses in the region near the pintle for the normal opening condition. It can be seen that these stresses are very similar to those for the free-hanging condition. Table B-3 summarizes the nominal flange stress in Girder 13 near the diagonal anchorage connection for the various load cases considered. Tension develops in the flange during the free-hanging state and during the opening and closing of the gate. This state of tension is very similar for the free-hanging and for both the normal opening and closing conditions. According to the data in this table, the level of prestress in the diagonals does not appear to affect this flange stress. However, the stress in this table is the nominal flange stress near the midspan of the flange segment, and a closer look at the flange stress near the connection shows that this stress increases by ~15 percent as the diagonal tension relaxes to near zero. The flange segment undergoes in-plane bending, as illustrated in Figure C-10, because of the vertical shear load across the girder span with the support at the pintle acting at the left of the flange segment and the gate weight and the tensioned diagonal load acting on the right of the segment. From Table C-3, the flange undergoes 11.7 ksi (80.7 MPa) compression for the normal mitered operation, and this compression increases by 15 percent as the miter blocks wear by 0.25 in. (6.35 mm). The cases considering no quoin contact or stuck pintle tend to reduce the compressive stress in the girder flange because this load is taken by the pintle. However, this condition is considered more of a temporary state that would not affect the fatigue analysis. For example, if the condition is the result of debris caught between the quoin blocks and operation continues, it is likely to clear after a few gate operations. If the pintle is truly stuck (frozen or broken), then there will be major problems with operating the gate and steps will be taken to correct the problem. Wear on the quoin block will be limited by wear in the pintle. Wear will occur on the quoin block only if there are contact and bearing forces; i.e., if a gap caused by quoin wear occurs, wear will stop until the wear in the pintle contact allows quoin contact. This effect is very similar to that for the worn miter block, that is, a shortening of the gate, which increases the compression in the flange as the gate miters farther downstream. Thus, the flange stress could increase by 25 percent as both the miter and quoin block (and pintle) wear.

C-3. <u>Local Modeling of Welded Connection</u>.

a. A local detailed model of the region around the girder flange to anchor plate connection is constructed to provide better resolution of the geometric stress concentration and to introduce the residual stress distribution that is present from the welding operation. The local model is constructed using continuum based brick elements, and its geometry is associated with coordinate locations in the global model. The displacements from the global model for an analysis case can be extracted and directly applied to the cut surfaces of the local model. This allows application of any loading condition conducted for the global model to be applied directly

to the local model through the displacement boundary conditions on the local model. Figure C-14 illustrates the local model for the girder flange connection at the diagonal anchor plate. The elements plotted in red represent the welds that are simulated to develop the residual stress distribution. The elements highlighted in yellow around the cut boundary are used to help simulate the constraint in the connection during the thermal stress analysis to develop the residual stress field at the welded connection. The local model must be fixed in space for the residual stress calculations since it is part of the overall structure and there is no corresponding global analysis for boundary conditions. If the modulus of these elements is varied, the effect of variations in the constraint around the welded connections on the residual stress distribution can be evaluated.

b. Figures C-15 and C-16 illustrate the comparison of global model results with local model results where the boundary conditions along the cut surfaces of the local model are extracted from the global model analysis. This comparison is done without any residual stress to establish the stress concentration factor (SCF) that can be used to convert the nominal flange stress from the global analyses to the stress acting at the location of crack initiation. The ratio of the average longitudinal stress in the flange at the corner of the local model to the average flange stress in the global analysis is found to have a stress concentration factor of 2.5 for this configuration under the normal operating load.

c. The residual stress distribution at the welded connection is determined using a thermal stress analysis and simulating the weld process as discussed in Chapter 3. Figure C-17 illustrates various stages in the thermal analysis that incrementally heat up the "weld bead" elements to simulate the thermal input for the weld process. Figure C-18 illustrates the residual stress distribution for a set combination of material properties, welding scheme (order and direction of weld operations), and simulated constraint. Analyses with variations in these parameters are conducted to characterize this residual stress distribution for uncertainties in the modeling and field conditions.

d. The local model is then subjected to loading representing the range of working stress at the connection. The displacements corresponding to the cut locations of the local model in the global model are extracted from the global model for the free-hanging condition and for the mitered condition under operating loads (both including the diagonal prestress). These displacements are then imposed on the cut boundaries of the local model with the residual stresses. The stress range at the corner of the connection from the local model is used to characterize the conditions leading to initiation of the fatigue cracking. This local model analysis then includes the residual stresses, the stress concentration caused by geometric configuration, and the stress range for a gate operation cycle.

e. The local model is then used to establish the crack growth characteristics for a fatigue crack at this welded connection. A crack is incrementally extended in the local model as illustrated in Figure C-19. The figure shows a crack under both the gate-closed and gate-open loading conditions and illustrates that the crack closes when the gate is closed and then opens when the gate is open. This is indicative of fatigue loading producing a change in stress intensity that will extend the crack. For each increment of crack extension, the local model is subjected to the free-hanging and mitered operation conditions to impose a load cycle for the current crack

length. The stress intensity for the minimum and maximum stress conditions for each crack length is calculated using the J-integral method as discussed in Chapter 3. This provides a change in stress intensity versus change in crack length for evaluation of the Paris equation for crack growth with subsequent operating cycles after crack initiation.

C-4. Reliability Modeling and Assessment.

a. The following reliability model is constructed from the results of the global and local modeling for fatigue cracking at the welded connection of the girder flange with the large gusset plate used to anchor the diagonal bars. This model first characterizes the conditions leading to initiation of the fatigue cracks and then for the growth rate of the cracks with continued operational cycles.

b. The stress in the flange at the connection is found to undergo slight tension when the gate is open because of sagging under this free-hanging condition. A very similar stress pattern develops during the opening and closing cycle. The stress under this condition is determined to be primarily a function of corrosion rate and the prestress in the diagonals, expressed as follows.

$$\sigma_1 = \sigma_0 \cdot F_c \cdot F_d \tag{C-1}$$

where $\sigma_0 = 3.0$ ksi (20.7 MPa) is the nominal value (not including the stress concentration from the connection geometry), and the factors $F_c$ and $F_d$ account for changes caused by corrosion and diagonal prestress, respectively, as follows.

$$F_c = \frac{b}{b - 2A_c t^{0.667}} \tag{C-2}$$

is the factor that increases the stress in the flange in proportion to the reduction in area caused by corrosion. The corrosion rate (in./year) is based on the power law formula $A_c t^{0.667}$, where $A_c$ is the coefficient for the rate of corrosion and $t$ is the time in years. This formula has been derived based on test data with a nominal value of 1.4 E-4 (in./year) for $A_c$. The variable $b$ is the nominal plate thickness, (in this case $b = 1.0$ in. (25.4 mm)), and the multiplier of 2 accounts for corrosion that can occur on both exposed surfaces of the plate. The factor that increases the flange stress as the stress in the tension bar diagonals relax is defined as

$$F_d = 1 + 0.033 \cdot t^{0.5} \tag{C-3}$$

where $t$ again is the time in years, and the power law form correlates to the observation that relaxation is a function of stress; i.e., more relaxation occurs when the diagonals are under higher stress. This factor is maximum and constant at 1.15 once the diagonal prestress is totally dissipated, and has been scaled for total relaxation over 20 years. For the nominal evaluation case, it is assumed that the diagonals are retensioned every 25 years as a baseline condition, and the factor resets to 1.0 after the maintenance.

c. The flange undergoes high compressive stress under the gate operating conditions as the other extreme in the load cycle. This stress is determined to be primarily functions of the head differential on the gate, the corrosion rate, and wear in the gate components.

$$\sigma_2 = \sigma_c \cdot F_h \cdot F_c \cdot F_m \qquad \text{(C-4)}$$

where $\sigma_c = -11.7$ ksi (80.7 MPa) is the nominal compressive stress in the flange near the connection, again without the stress concentration for the corner geometry of the connection.

$$F_h = h/H \qquad \text{(C-5)}$$

where $h$ is the head in feet and $H$ is the reference head (ft) where the nominal stress is calculated ($H = 35.0$ ft (10.7 m).

$$F_c = \frac{b}{b - 2A_c t^{.667}} \qquad \text{(C-6)}$$

is the same corrosion factor as for $\sigma_1$ and

$$F_m = 1 + r_w \cdot MOD(t - 1, T_m) \qquad \text{(C-7)}$$

is the factor accounting for wear where $r_w$ is the rate of wear on the miter block with a nominal value of 0.25 in. (6.35 mm) over 20 years, and $t$ is the time in years. This factor also accounts for wear in the pintle and quoin block. It increases to 1.25 over 20 years for the nominal wear rate, and is reset to 1.0 after the maintenance time $T_m$.

d. The residual tensile stress at the welded connection is primarily a function of the geometric configuration, the yield strength $\sigma_y$, and the constraint on the connection during the weld:

$$\sigma_w = 1.5 \cdot \sigma_y \cdot F_w \qquad \text{(C-8)}$$

where $\sigma_y$ is the yield stress of the material, and $F_w$ is a combined factor to account for variations in the yield stress and the constraint during the weld operation. A nominal value of 36 ksi (248 MPa) was used in the local modeling for the A36 steel material, and it is found that a range of 0.85 to 1.2 for $F_w$ provides a good correlation for the variation in residual stress. This range also accounts for the likelihood that the yield stress will be higher than the nominal value.

e. The effective alternating stress for the load cycle is calculated from the stress range that develops between the open and closed gate positions, and uses the Goodman relation to account for the effect of increased cyclic damage when the mean stress in the cyclic history is in tension. The Goodman relation is a function of the ultimate strength of the steel:

$$\sigma_{max} = C \cdot \sigma_1 + \sigma_w \qquad \text{(C-9)}$$

$$\sigma_{min} = C \cdot \sigma_2 + \sigma_w \tag{C-10}$$

where $C$ is the stress concentration factor relating the nominal flange stress from the global model to the local stress in the corner. This factor is found to have a nominal value of 2.5.

$$\sigma_{alt} = \frac{1}{2}\left(\sigma_{max} - \sigma_{min}\right) \tag{C-11}$$

$$\sigma_{mean} = \frac{1}{2}\left(\sigma_{min} + \sigma_{max}\right) \tag{C-12}$$

$$\sigma_{eff} = \frac{F_b \cdot \sigma_{alt}}{1 - \dfrac{\sigma_{mean}}{\sigma_{ult}}} \tag{C-13}$$

where $\sigma_{ult}$ is the ultimate tensile strength of the material. It is found that using a nominal value of 72 ksi (496 MPa) and the factor $F_w$ provides a consistent range and variation of this parameter. ($\sigma_{ult}$ is increased when $\sigma_y$ is increased). $F_b$ is a modeling factor to account for other uncertainties, such as stress corrosion cracking effects, surface roughness, and differences in the configuration of the connection compared to laboratory specimens used to develop fatigue test data. It is found that $F_b = 1.15$ provides a good correlation to field cracking data for this uncertainty.

   f. The damage from cyclic loading is accumulated as

$$D = \Sigma\left(\frac{n_k}{N_k}\right) \tag{C-14}$$

where

   $D =$   damage index

   $n_k =$   number of cycles imposed at a stress level of $\sigma_{eff}$

   $N_k =$   allowable number of cycles at that stress level

When $D$ reaches a value of 1, a fatigue crack initiates. The allowable number of cycles is calculated as

$$N_k = \left\{\frac{E \cdot Ln\left[100/(100 - RA)\right]}{4 \cdot (\sigma_{eff} - \sigma_z)}\right\}^2 \tag{C-15}$$

where

$E =$ Young's modulus, psi

RA = 68.5%

$\sigma_z =$ 21,645 psi

This is the Langer Equation as the best fit to the fatigue data that is used as the basis for the American Society of Mechanical Engineers (ASME) design fatigue relations.

g. The fatigue correlation, described in f above, is based on data for cyclic loading on specimens where the number of cycles correlates to complete failure of the specimen. Here it is assumed that the number of cycles to initiate a crack correlates to an initial crack that extends through the thickness of the plate. Thus, when a crack initiates, an initial crack length $a_o$ for that crack is assumed. A nominal initial crack length of 0.10 in. (2.5 mm) is used with a range from 0.05 to 0.20 in. (1.3 to 5 mm).

h. The crack growth under subsequent stress cycles is then characterized using the Paris equation as described in Chapter 3. The characterization for $\Delta K$ as a function of crack length and loading (i.e., $K_{max}$ and $K_{min}$) is based on detailed local modeling for crack extension within a residual stress field under a cycle of loading. This characterization for $\Delta K$ and $R$ (defined in Chapter 3) as a function of crack length is defined in Table C-4. Interpolation of the values in this table is used in evaluating the Paris equation for crack growth with increasing crack length. The values are also extrapolated for crack lengths longer than that used in the local models by extending the final values as needed. The characterization of $\Delta K$ is plotted in Figure C-20. Note that the change in stress intensity remains relatively high with some increase for longer crack lengths and with increasing uncertainty with longer crack lengths. This type of relation for change in stress intensity with crack length will predict continuing crack extensions with load cycles, and implies that once the crack starts, it will continue to grow rather rapidly across the flange.

i. After the model predicts crack initiation, the crack growth is calculated as follows.

(a) For the current crack length, determine the lower bound values $\Delta K_1$ and $R_1$ and the upper bound values $\Delta K_2$ and $R_2$ from interpolation in Table C-4.

(b) Then, the current value for the change in stress intensity and the stress intensity ratio is calculated:

$$\Delta K = \frac{1}{2}\left[(1+\xi)\Delta K_2 + (1-\xi)\Delta K_1\right] \tag{C-16}$$

$$R = \frac{1}{2}\left[(1+\xi)R_2 + (1-\xi)R_1\right] \tag{C-17}$$

where $\xi$ is a random variable between –1 and 1 with a nominal value of zero. For this evaluation, $\xi$ is also incrementally increased from the base value during subsequent years to account for increasing crack growth with continued gate wear. This factor is 0.025/year and

accumulates during the time between maintenance repairs.  When maintenance is performed this factor resets.  Note that $\xi$ never exceeds 1.0.

j.  Calculate $\overline{\Delta K}$ and $S$ as described in Chapter 3 based on $\Delta K$ and $R$.  Then, calculate the material parameters $C$ and $n$ using $\overline{\Delta K}$ and $S$.

k.  The increment in crack length is computed as

$$da = F_a \cdot C(\Delta K)^n \cdot dN \tag{C-18}$$

where $dN$ is the number of cycles over the time period for calculating $da$.  The factor $F_a$ is a random variable over the range 0.9 to 1.1 to account for uncertainties in the material data and correlations used in defining the Paris equation.

l.  The crack length over time is the initial crack length $a_o$ plus the accumulation of the crack increments $da$ from subsequent applied cycles.

m.  Table C-5 provides a summary of parameters and variations used in the reliability evaluations.

n.  This structural reliability model was implemented into an Excel spreadsheet and exercised to evaluate the structural reliability based on the fatigue cracking being experienced on the miter gates at Markland Lock.  The study considers 82 years of operation, from 1959 to 2040.  For this example study, a constant head, based on the median value as calculated from the historical seasonal variations in upper and lower pool elevations, is used.  For a more detailed assessment, each year could be broken into subincrements using recorded head differentials for the fraction of time they occur per year.  For the baseline analysis, the projected traffic is based on that developed for the Ohio River Main Stem System Study.  Figure C-21 plots the crack length at the girder flange to diagonal anchor plate welded joint versus years of operation for the nominal, upper bound, and lower bound limits of the variables.  Note that a variation for the probability of the prediction at the limit state values is added to illustrate that the limit state values also have reduced probability.  This evaluation considers that the gate has maintenance performed for diagonal prestress and miter block wear every 25 years.  The nominal values of the parameters indicate the cracks will initiate around 1981 and grow rapidly across the flange to the web.  This is consistent with the maintenance logs that indicate that cracks about 1/2 in. (12 mm) long were found and repaired in 1983-84.  As a simulation, the crack lengths for the nominal values of the reliability model were reset to zero following the repair history of the gates.  For the repairs in 1983 and 1987 only 1 and 2 years, respectively, were assumed for the effectiveness of the repair since these repairs just welded the cracks in 1983 and then also applied gusset plates in 1987.  For the window frame repairs performed in 1994-96, the reliability was reset with no additional cracking for a nominal 12-year period.  This simulation of tracking the repair history and projection with upper and lower bounds is shown in Figure C-22.  This also provides good correlation for the crack growth rate developed for the model since the reported crack lengths agree well with the projected values.  Note that the projected crack growth rate for cracking with the window frame repair is arbitrarily reduced in this simulation example.

o. Figure C-23 plots the effect of variations in the maintenance period to adjust miter block and diagonal prestressing on the initiation of fatigue cracking in the model. This analysis considers the nominal values of all parameters and adjusts the time interval for periodic maintenance as indicated. This study indicates that reducing the time between scheduled maintenance will not have a large impact on the propensity for cracking at this connection. The stress range, including the residual stresses, acting on the joint along with the normal wear rate appears to control the fatigue cracking. Figure C-24 considers variations in the magnitude of residual stress at the joint for the effect on the fatigue cracking. Variations of 10 percent in the peak residual stress show relatively large variations in the projected fatigue crack initiation. While this can be benchmarked with field data and accounted for in probabilistic assessments for a particular site, it also shows the difficulty in developing a more generic predictive tool for fatigue cracking at arbitrary connection configurations.

C-5. Summary.

a. A reliability model for fatigue cracking in the downstream girder flange at the diagonal anchor plate for the Markland miter gates is constructed and exercised. The model is benchmarked with field data for cracking repairs and captures premature fatigue crack initiation followed by relatively rapid growth across the width of the flange. Once initiated, the crack will extend across the flange and reach the web of the girder in about 32,000 load cycles or about 10 years of operations if not repaired. Once the crack reaches the connection of the flange to the web, the crack will likely grow into the web of the girder. Similar cracking has been observed at the other welded connections of the horizontal girder flanges in these regions. Thus, this type of cracking must be carefully monitored and repaired to ensure continued reliability of the miter gate. The window frame type of repair implemented on the Markland gates has thus far proved effective in mitigating this cracking.

b. As an alternative repair, the cover plate technique, where a prefabricated plate spanning multiple girders and welded to the flange surfaces, is evaluated. An example of the cover plate repair is pictured in Figure 2-19, and Figure C-25 illustrates the modeling where a 3/4-in. (19-mm) thick plate is attached over the bottom four girders on both the quoin and miter ends of the Markland gate. The plate overlays are modeled separately with plate elements and connected to the downstream flanges of the global model at the weld locations. Short plate elements perpendicular to the flanges are used to position the center line of the plate overlay at the correct standoff and simulate the welds, illustrated in red in the figure. The welds connecting the free edges of the flanges to the back of the plate overlay around the openings are ignored because of mesh size limitations.

c. Figure C-26 plots the maximum principal stress contours for the gate with the plate overlay repair under the normal mitered operation load. Figure C-27 plots the maximum principal stresses in the original downstream flanges with the plate overlays removed. The reduction in the compressive stresses in the downstream flange surfaces near the quoin and miter posts is evident. For reference, the principal stress contours in the plate overlays are plotted in Figure C-28. In addition to the added flange area, the plate overlay also provides additional shear stiffness, and the flange stresses in the quoin area are also reduced for the free-hanging condition caused by sagging. Figure C-29 plots the maximum principal stresses in the quoin

region for the free-hanging condition with the plate overlay removed. The tension stress acting on the flange to anchor plate connection is reduced. With the plate overlay repair, the nominal flange compressive stress is –8 ksi (-55 MPa) during mitered operation, and the nominal tension stress during free-hanging conditions is only 1.6 ksi (11.03 MPa). If this stress range is plugged into the reliability model for crack initiation, the onset of fatigue cracking would not be predicted until 2043 or about 80 years of operations under the projected traffic levels. In addition, the plate overlay should reduce the stress concentrations (radius inside corners and added strength to the original corner configuration), and the welded connections are somewhat removed from the free surfaces where cracking tends to originate. Thus, the plate overlay repair technique should be very effective in mitigating the problem with fatigue cracking in this region.

**Table C-1.  Summary of Steps for Pre-tensioning
Diagonals on Markland**

| | |
|---|---|
| Step 1 | Support gate at pintle and top anchorage.  Retrain bottom of miter end. Apply dead loads with slack in all diagonals. |
| Step 2 | Push top of miter block upstream 4 in. (0.1 m).  Remove slack from positive diagonals. |
| Step 3 | Push top of miter block downstream 3 in. (0.08 m).  Remove slack from negative diagonals. |
| Step 4 | Release top of gate. Adjust diagonals if necessary to keep miter post within 0.25 in. (6 mm) plumb top to bottom. |

**Table C-2.  Summary of Parametric Cases for Global Model at
Markland Lock**

| Case No. | Parametric Case | |
|---|---|---|
| Case 1 | Free hanging, equalized lower pool | |
| | 1a | Nominal diagonal prestress |
| | 1b | Zero prestress in diagonals |
| | 1c | ~2x nominal prestress in diagonals |
| Case 2 | Normal operation, nominal prestress, perfect gate conditions | |
| | 2a | Nominal head differential |
| | 2b | Low head differential, high lower pool, low upper pool |
| | 2c | High head differential, high upper pool, low lower pool |
| Case 3 | Normal operation but with miter block wear | |
| | 3a | 0.25 in. (6.4 mm) wear on miter block |
| | 3b | 0.50 in. (12.7 mm) wear on miter block |
| Case 4 | Normal operation but with quoin and pintle wear | |
| | 4a | Stuck pintle, no quoin contact G12 to G14 |
| | 4b | No quoin contact for G9 to G14 |
| | 4c | Excessive friction at quoin, G9 to G14 |
| | 4d | Worn pintle |
| Case 5 | Opening and closing | |
| | 5a | Normal closing, 30 psf (1.4 kPa) resistance |
| | 5b | Normal opening, 30 psf (1.4 kPa)  resistance |
| | 5c | Open against surge head, 78 psf (3.7 kPa) resistance |
| | 5d | Normal closing, zero tension in diagonals |

**Table C-3.  Summary of Stresses for Global Model at Markland Lock**

| Analysis Case | Analysis Conditions | Nominal Flange Stress, Girder 13 (ksi)[a] | Negative Diagonal (ksi)[a] | Positive Diagonal (ksi)[a] |
|---|---|---|---|---|
| 1a | Nominal Prestress and Gravity | 2.95 | 10.12 | 11.63 |
| 1b | Zero Prestress with Gravity | 1.19 | 0.0 | 4.26 |
| 1c | ~2x Nominal Prestress and Gravity | 5.73 | 22.93 | 20.31 |
| 2a | Normal Operation, 35-ft (11-m) Head Differential | -11.67 | 12.06 | 9.68 |
| 2b | Low Head (31 ft (10 m)) | -10.25 | 12.01 | 9.78 |
| 2c | High Head (39 ft (12 m)) | -13.03 | 12.06 | 9.61 |
| 3a | 0.25-in.(6.35-mm) Wear on Miter Block | -13.48 | 12.12 | 9.81 |
| 3b | 0.50-in. (12.7-mm) Wear on Miter Block | -14.44 | 12.18 | 9.93 |
| 4a | Stuck Pintle, No Contact G12 to G14 | -2.81 | 12.21 | 9.46 |
| 4b | Worn Quoin, No Contact G9-G14 | -0.40 | 12.53 | 7.79 |
| 4c | High Quoin Friction, G9-G14 | 10.82 | 11.98 | 9.63 |
| 4d | Worn Pintle, No Contact | -11.89 | 12.16 | 9.66 |
| 5a | Normal Closing, 30 psf (1.4 kPa) on DS Wetted Surface | 3.04 | 8.87 | 12.93 |
| 5b | Normal Opening, 30 psf (1.4 kPa) on US Wetted Surface | 2.87 | 11.40 | 10.29 |
| 5c | Open with Surge Head, 78 psf (3.7 kPa) on US Surface | 2.72 | 13.70 | 7.89 |
| 5d | Normal Closing, Zero Diagonal Prestress | 1.66 | 0.0 | 6.29 |
| [a] To convert ksi to MPa, multiply by 6.894757. | | | | |

**Table C-4.  Characterization of Stress Intensity for Markland Lock
Miter Gate**

| Crack Length | Nominal | | Lower Bound | | Upper Bound | |
|---|---|---|---|---|---|---|
| | $\Delta K$ | $R$ | $\Delta K$ | $R$ | $\Delta K$ | $R$ |
| 0.00 | 30.51 | 0.00 | 27.46 | 0.00 | 33.56 | 0.00 |
| 0.20 | 34.20 | 0.00 | 30.44 | 0.00 | 37.96 | 0.00 |
| 1.13 | 51.30 | 0.00 | 45.14 | 0.00 | 57.46 | 0.00 |
| 2.05 | 63.32 | 0.00 | 55.09 | 0.00 | 71.55 | 0.00 |
| 2.98 | 51.80 | 0.27 | 39.11 | 0.36 | 64.49 | 0.21 |
| 3.90 | 46.50 | 0.41 | 29.93 | 0.55 | 63.08 | 0.30 |
| 4.83 | 45.50 | 0.46 | 25.58 | 0.64 | 65.42 | 0.34 |
| 5.75 | 47.85 | 0.48 | 24.94 | 0.67 | 70.76 | 0.34 |
| 6.68 | 50.69 | 0.47 | 25.11 | 0.68 | 76.27 | 0.33 |
| 7.61 | 50.00 | 0.49 | 22.26 | 0.72 | 77.74 | 0.33 |
| 8.53 | 49.59 | 0.50 | 19.74 | 0.75 | 79.44 | 0.33 |

**Table C-5.  Summary of Parameters and Variations for Markland Lock Study**

| Parameter/Description | Nominal Value | Range | | Distribution |
|---|---|---|---|---|
| | | Min | Max | |
| $\sigma_y$, Yield Stress (ksi) | 36 | -- | -- | See $F_w$ |
| $\sigma_{ult}$, Ultimate Tensile Strength, (ksi) | 72 | -- | -- | See $F_w$ |
| $F_w$, Material/Constraint Variation | 1.00 | 0.85 | 1.20 | Lognormal |
| $A_c$, Corrosion Rate Coefficient (in./year) | 1.4E-04 | 5.6E-05 | 2.2E-04 | Lognormal |
| $R_m$, Miter Block Wear Rate (in./year) | 0.25/20 | 0.125/20 | 0.375/20 | Normal |
| $T_m$, Maintenance Period, years | 25 | 20 | 30 | Discrete |
| $C$, Stress Concentration, Global to Local | 2.5 | 2.25 | 2.75 | Normal |
| $F_b$, Fatigue Data Variation/Benchmark | 1.15 | 1.035 | 1.265 | Normal |
| $\sigma_w$, Residual Stress (ksi) | 1.5 | 1.5 | 1.5 | See $F_w$ |
| $\sigma_1$, Maximum Flange Stress (ksi) | 3.0 | -- | -- | See $C$ |
| $\sigma_2$, Minimum Flange Stress (ksi) | -11.7 | -- | -- | See $C$ |
| $a_o$, Initial Crack Length (in.) | 0.1 | 0.05 | 0.2 | Normal |
| $\xi$, Variation in Crack Growth Modeling | 0.0 | -1.0 | 1.0 | Normal |
| $F_a$, Variation in Crack Growth Material Data | 1.00 | 0.90 | 1.10 | Normal |
| Increment in $\xi$ for Continuing Gate Wear | 0.025/year | -- | -- | -- |

Figure C-1.  Fatigue cracking in girder flange at diagonal anchor plate
in Markland miter gates



Figure C-2.  Fatigue cracking in girder flange near diagonal anchor plate
after gusset plate repairs
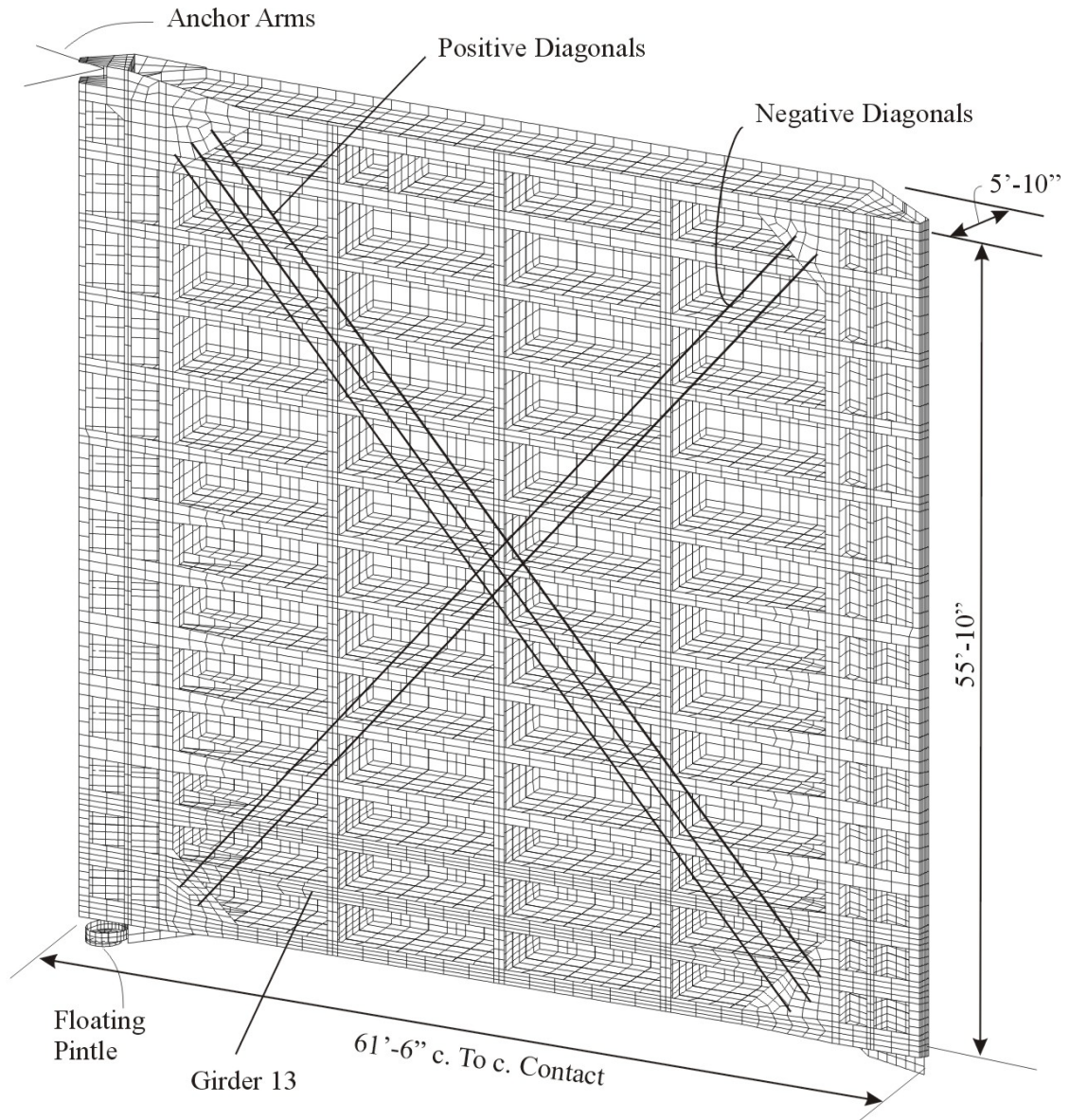
Figure C-3. Global model of Markland miter gate with overall dimensions
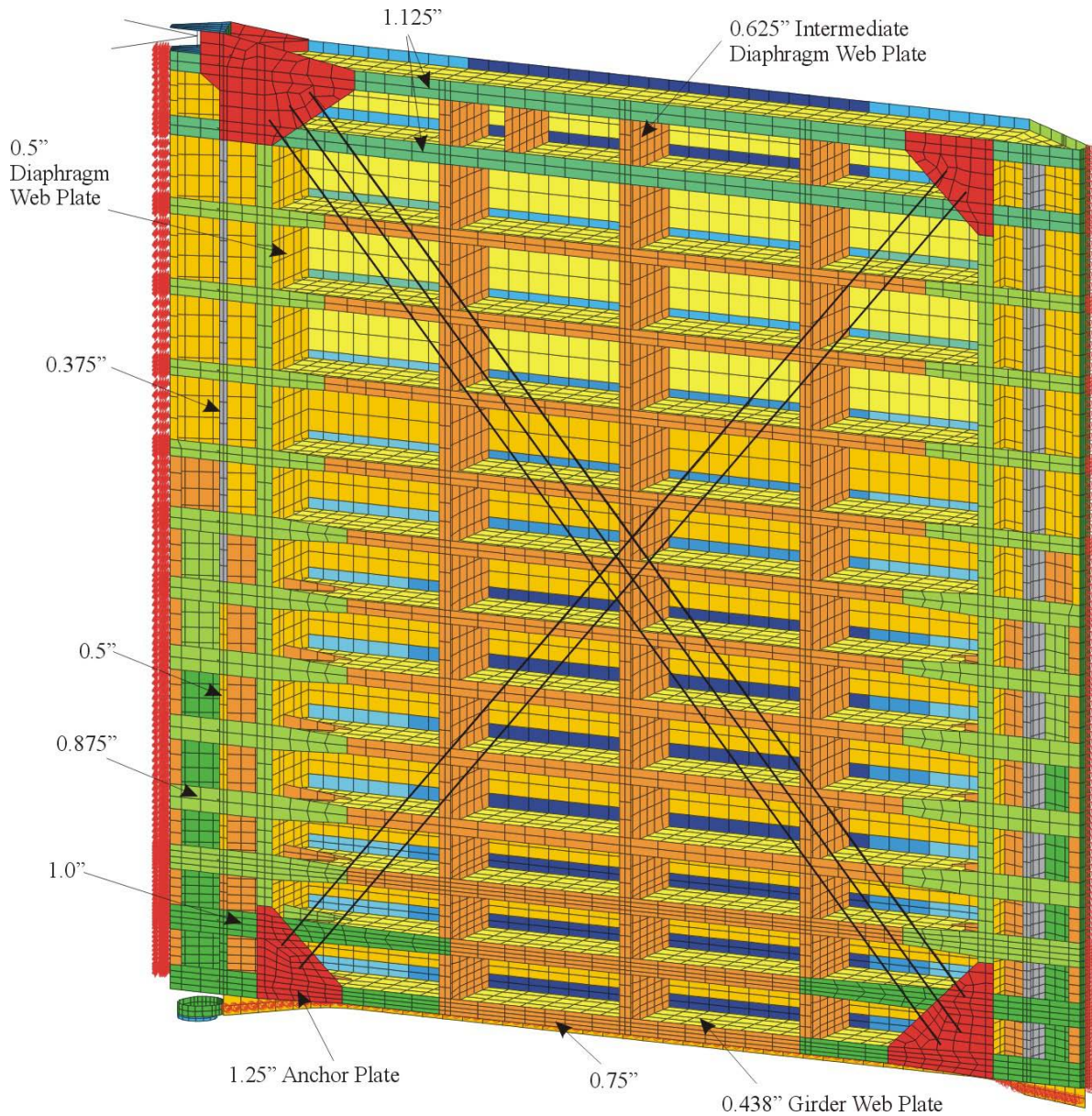
Figure C-4.  Schematic for plate element modeling, viewed from downstream
(Note:  to convert in. to mm, multiply by 25.4)
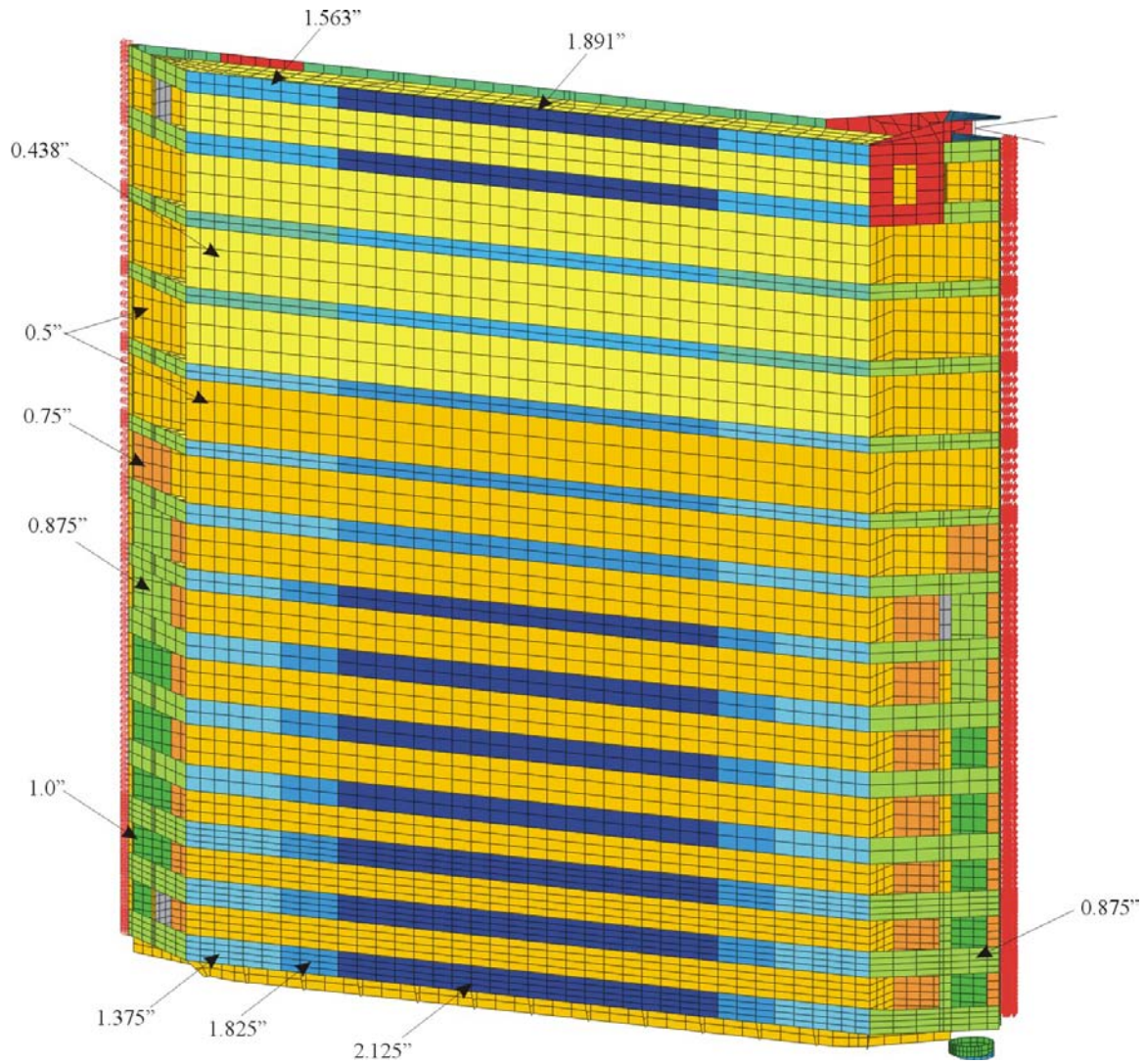
Figure C-5.  Schematic for plate element modeling, viewed from upstream
(Note:  to convert in. to mm, multiply by 25.4)

Intercostals

Thrust Plate
Stiffeners

Girder Web Stiffeners
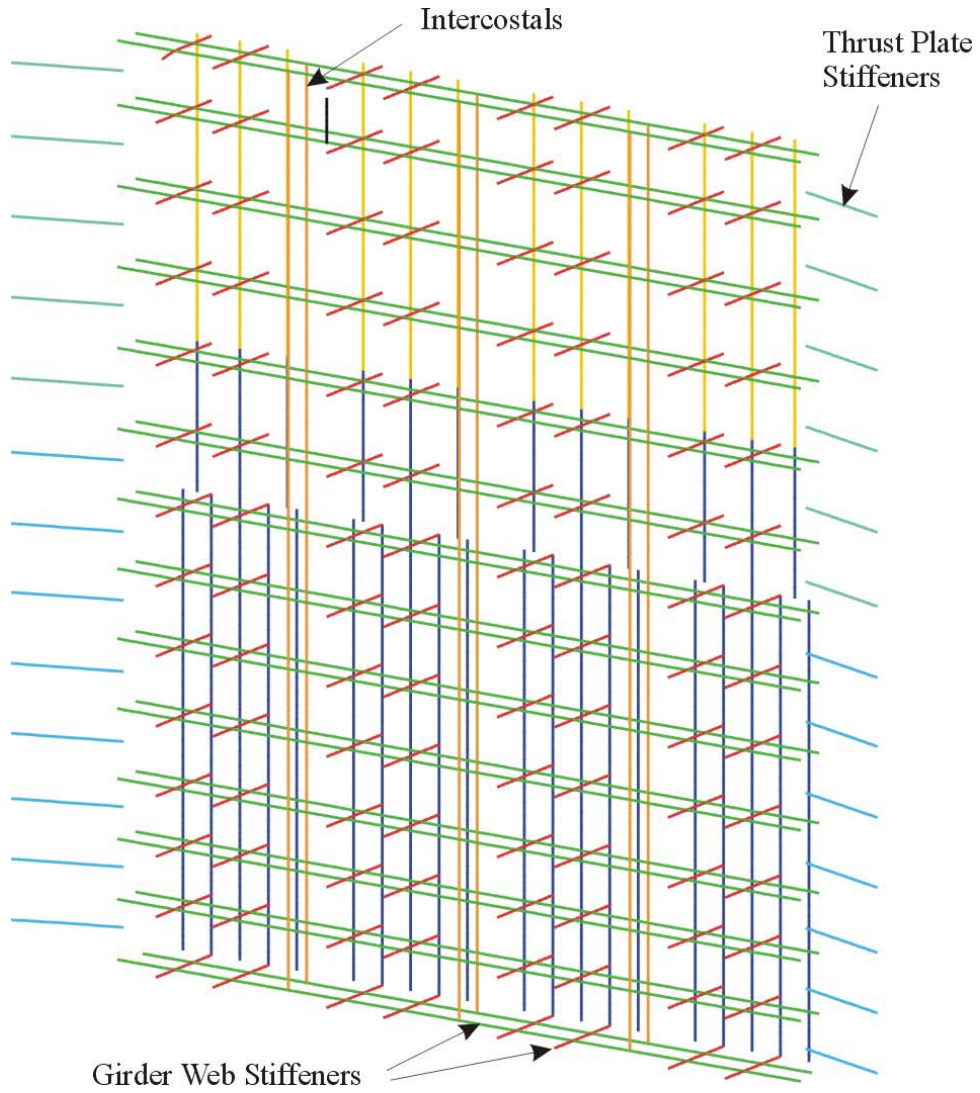
Figure C-6. Illustration of beam element modeling for secondary components

Outline of Bottom Girder

Rigid Contact Surface for
Embedded Pintle Base

+

Pintle Base Attached to Gate
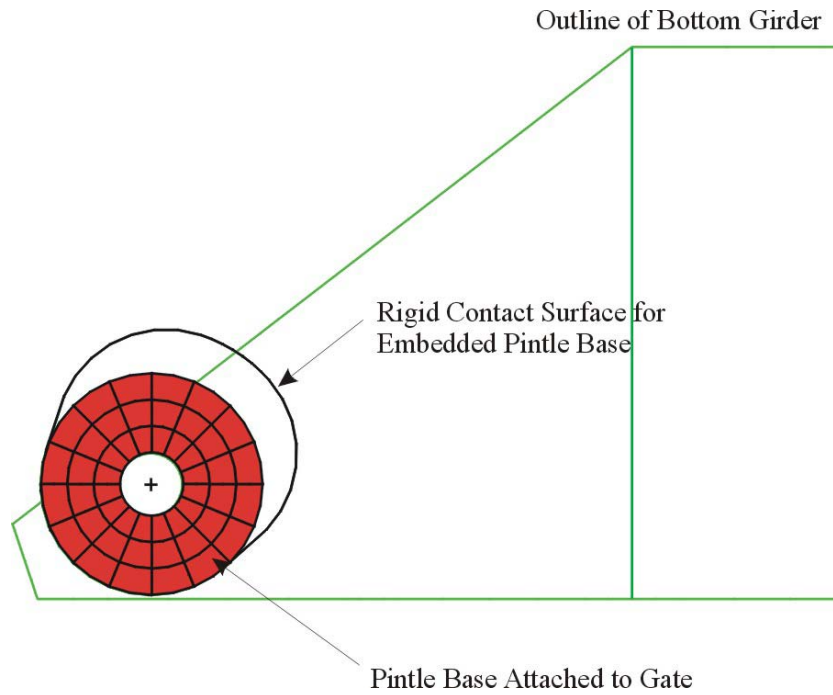
Figure C-7.  Schematic for modeling used to simulate floating pintle

SECTION POINT 1

| SP1 | VALUE |
|---|---|
| | -4.16E+04 |
| | -3.72E+04 |
| | -3.28E+04 |
| | -2.84E+04 |
| | -2.40E+04 |
| | -1.96E+04 |
| | -1.52E+04 |
| | -1.08E+04 |
| | -6.42E+03 |
| | -2.01E+03 |
| | +2.39E+03 |
| | +6.79E+03 |
| | +1.12E+04 |
| | +1.56E+04 |

Case 2a
Deformation x100
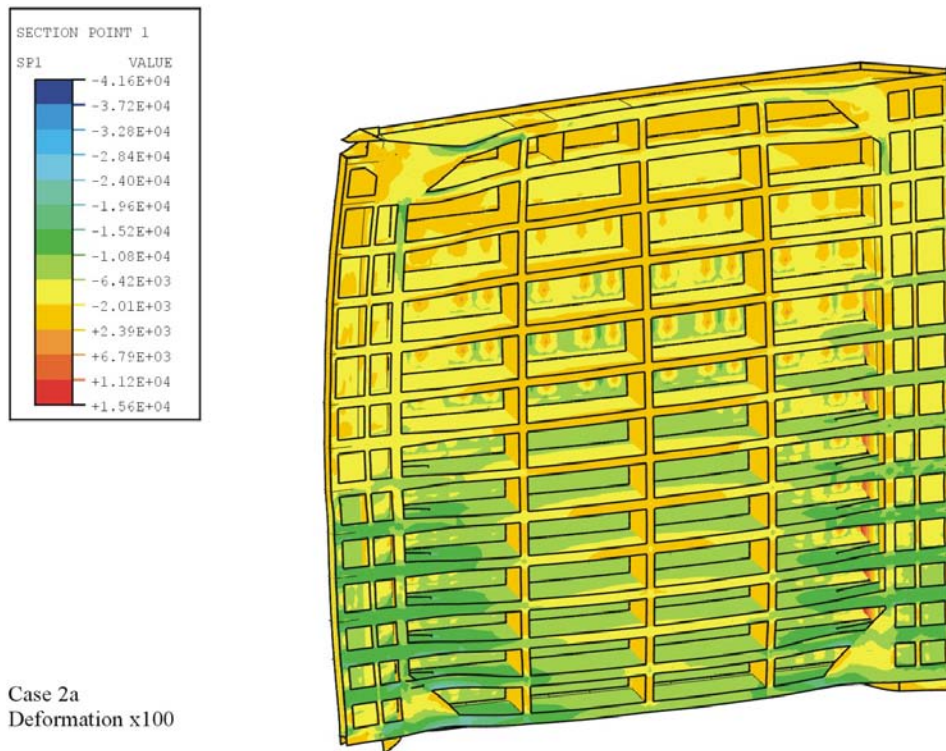
Figure C-8.  Minimum principal stress for normal operating condition,
Case 2a, Markland Gate

**SECTION POINT 1**

| SP2 | VALUE |
|---|---|
| | -1.60E+04 |
| | -1.32E+04 |
| | -1.04E+04 |
| | -7.53E+03 |
| | -4.69E+03 |
| | -1.85E+03 |
| | +9.83E+02 |
| | +3.82E+03 |
| | +6.66E+03 |
| | +9.49E+03 |
| | +1.23E+04 |
| | +1.52E+04 |
| | +1.80E+04 |
| | +4.68E+04 |

Case 2a
Deformation x100
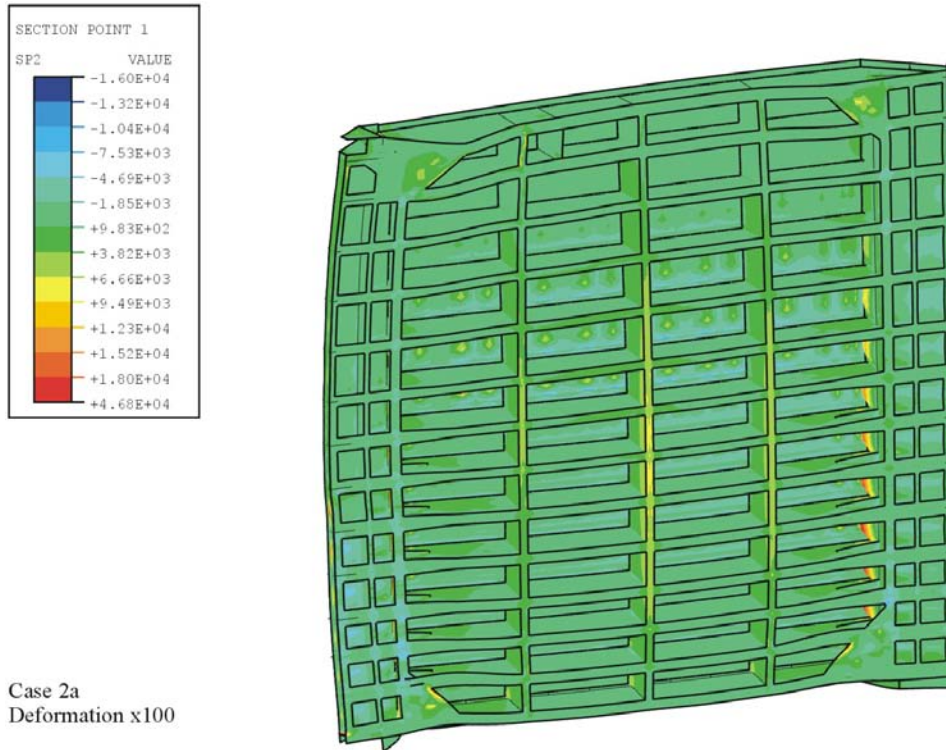
Figure C-9.  Maximum principal stress for normal operating condition, Case 2A,
Markland Gate



**SECTION POINT 1**

| SP2 | VALUE |
|---|---|
| | -3.07E+03 |
| | -2.12E+03 |
| | -1.16E+03 |
| | -2.00E+02 |
| | +7.57E+02 |
| | +1.71E+03 |
| | +2.67E+03 |
| | +3.63E+03 |
| | +4.59E+03 |
| | +5.55E+03 |
| | +6.50E+03 |
| | +7.46E+03 |
| | +8.42E+03 |
| | +9.38E+03 |

Case 1a
Deformation x100
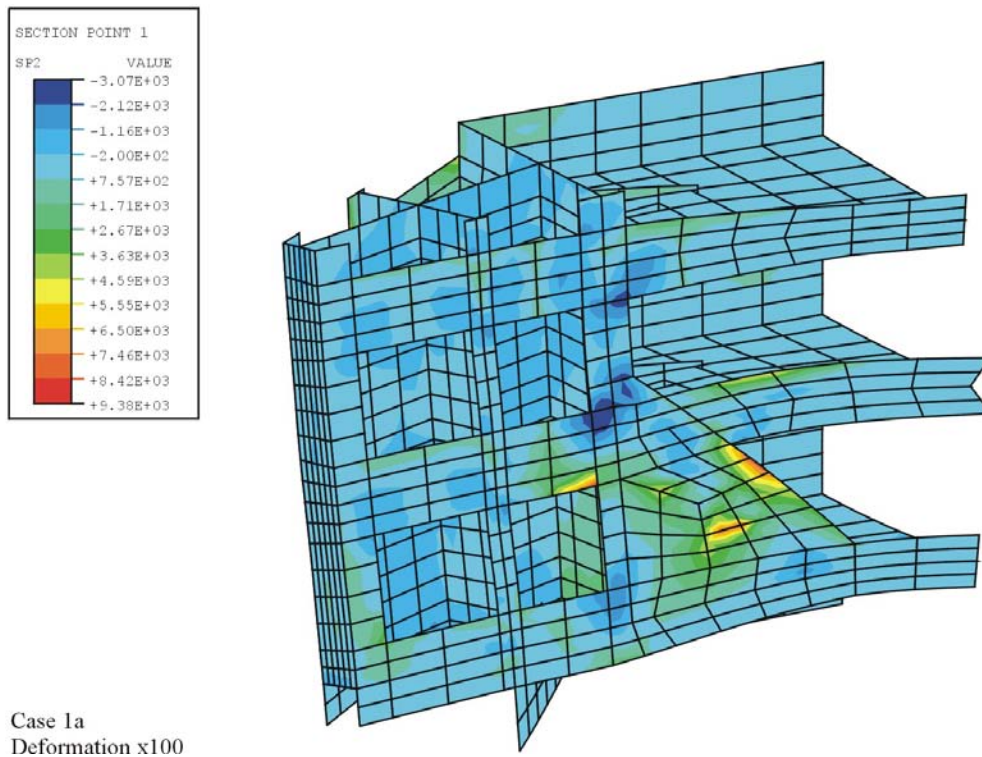
Figure C-10.  Maximum principal stress near lower quoin for free hanging condition, Case 1a
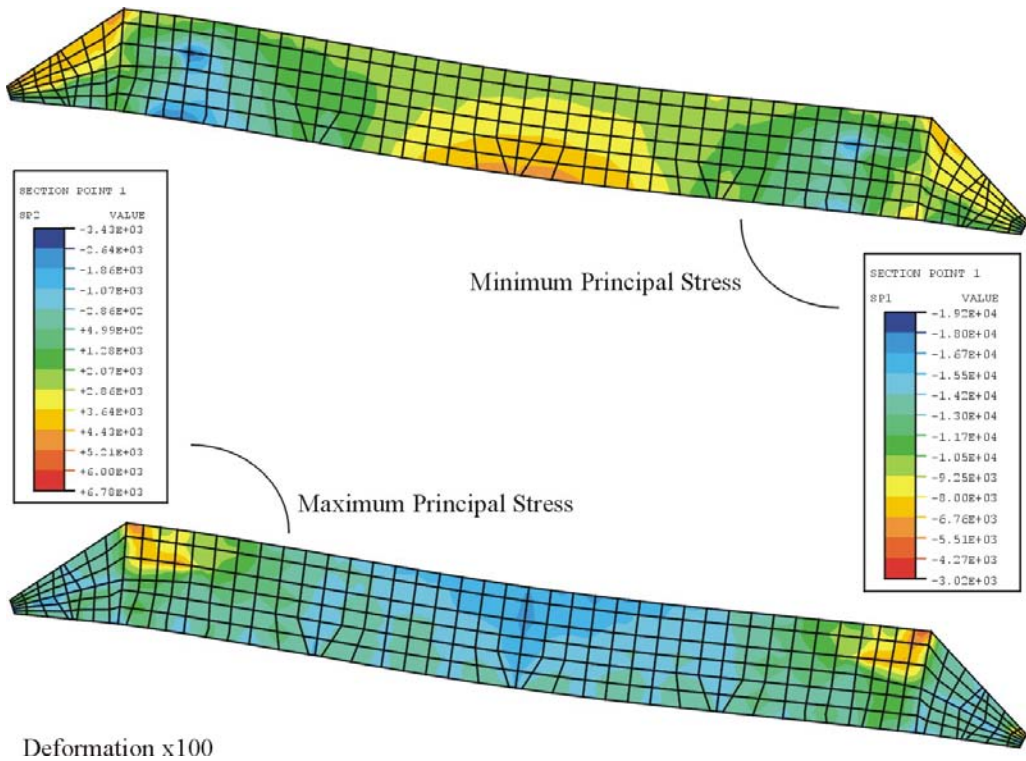
Figure C-11.  Stress contours in Girder 13 web for normal operating conditions
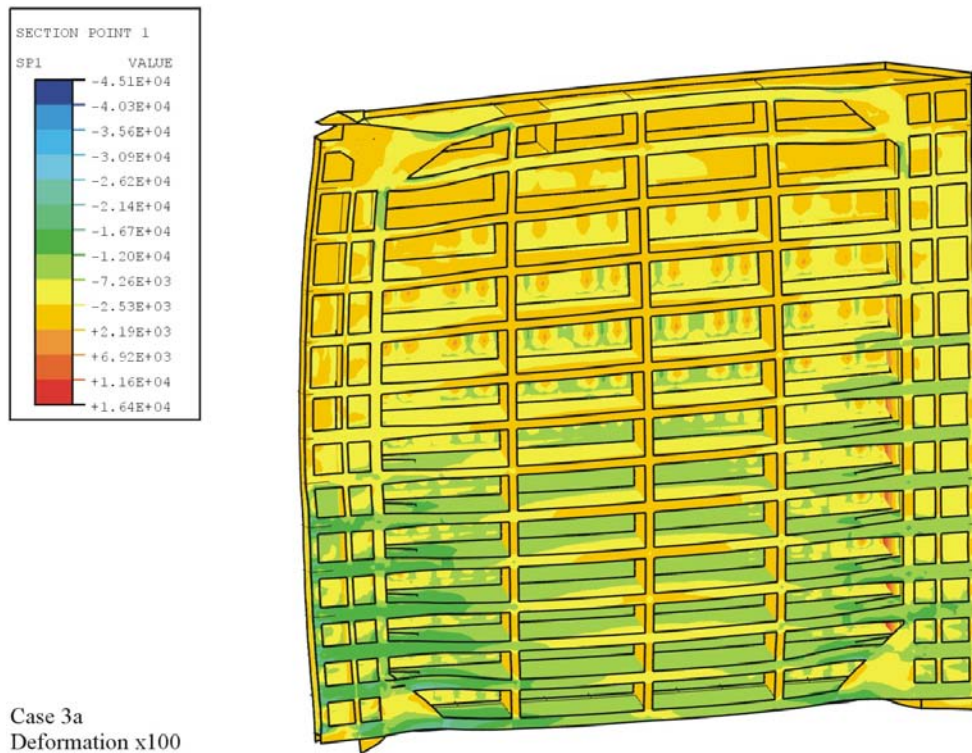
Figure C-12.  Minimum principal stress with wear on miter block, Case 3a
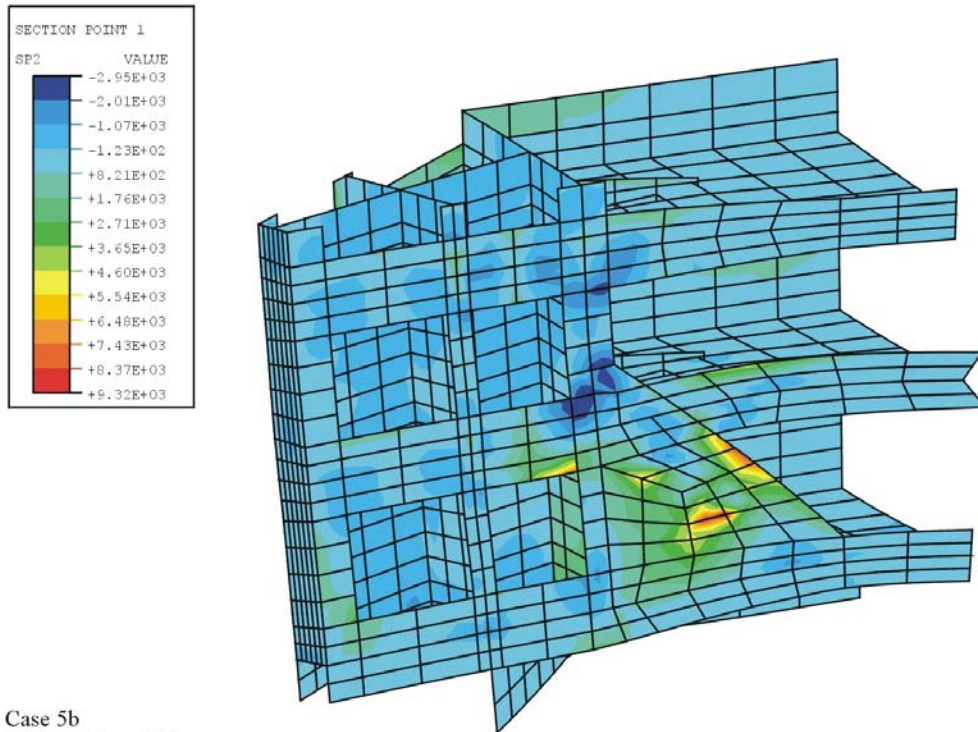


Figure C-13.  Maximum principal stresses in quoin region at pintle for normal opening case, Case 5b
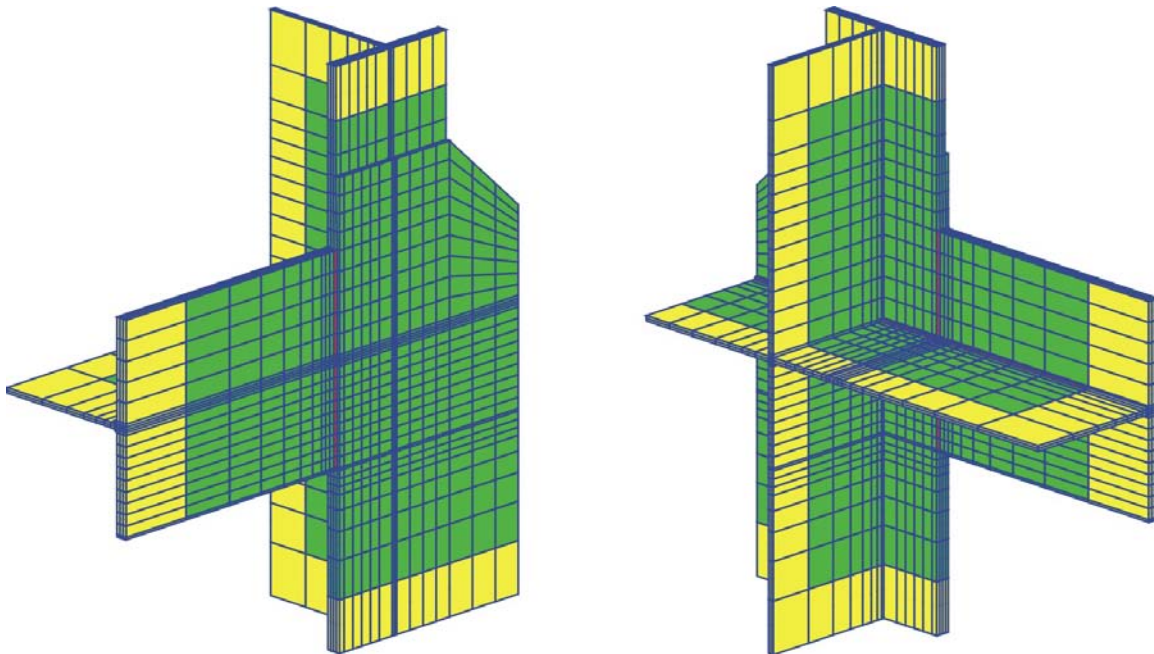


Figure C-14.  Local model for girder flange connection with diagonal anchor plate
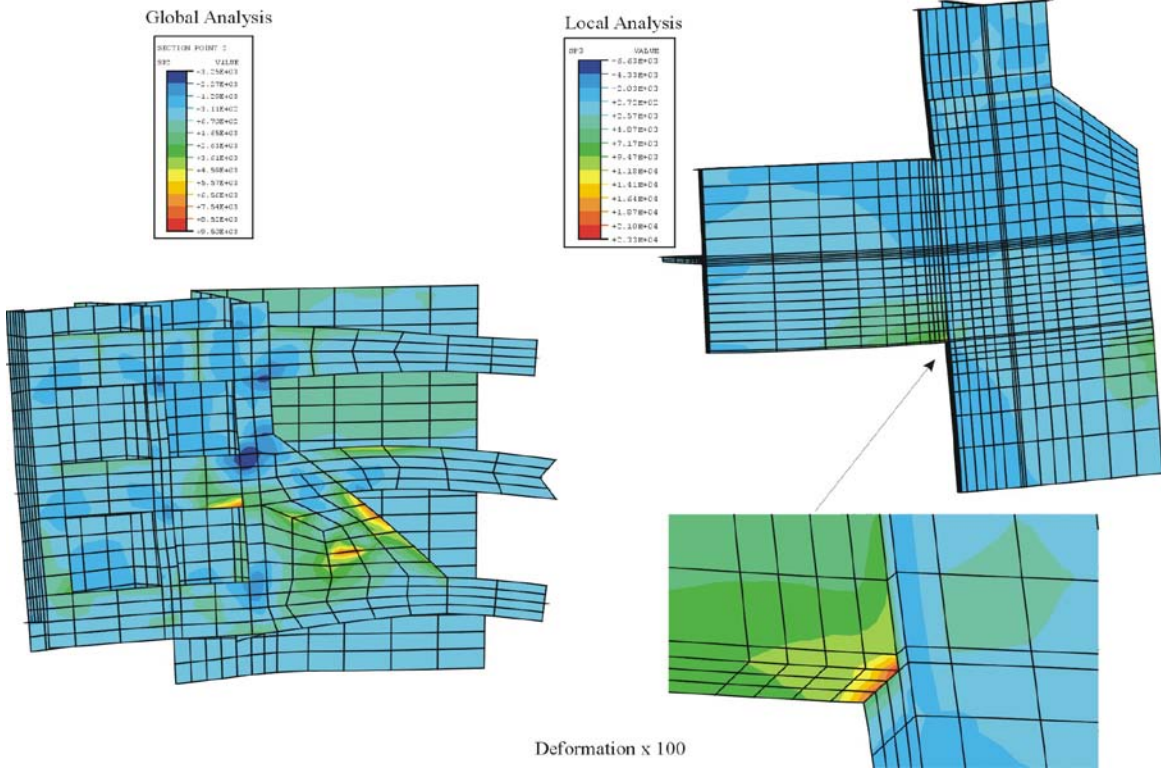
Figure C-15.  Global to local model stress concentration factor, Case 1a
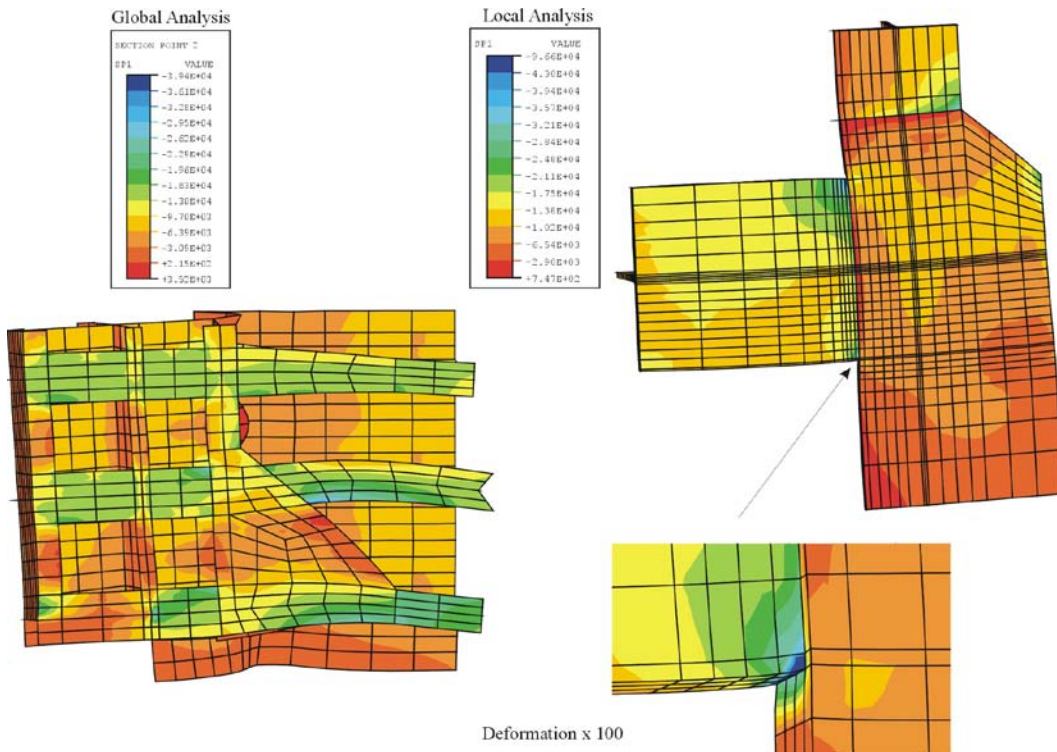


Figure C-16.  Global to local model stress concentration factor, Case 2a
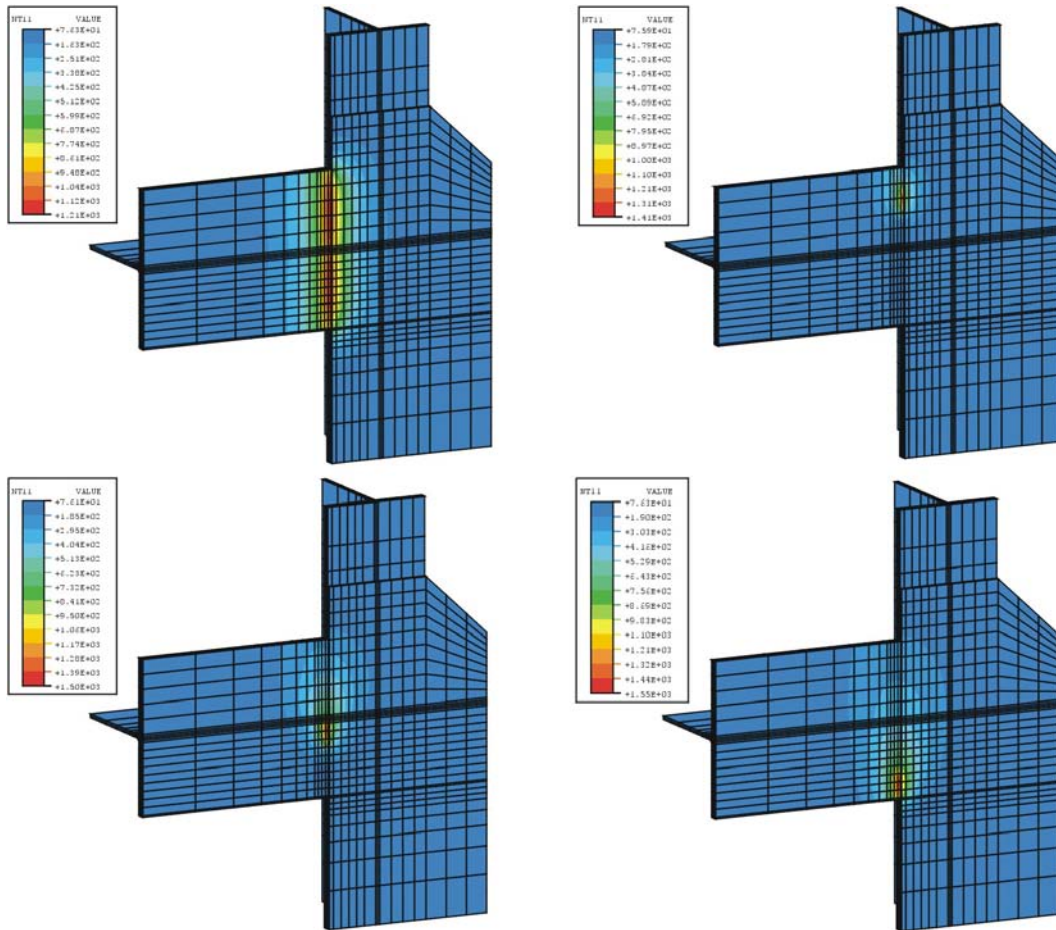
Figure C-17.  Illustration of thermal analysis for simulation of weld procedure
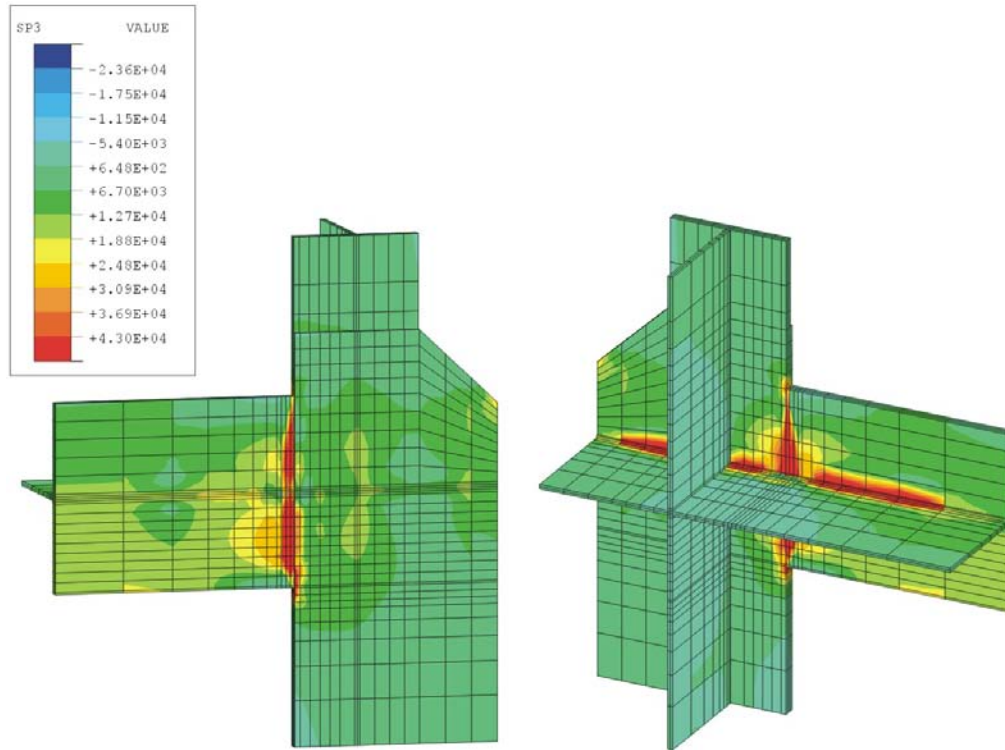
Figure C-18.  Illustration of residual stress distribution at welded joint

Gate Open

Gate Closed
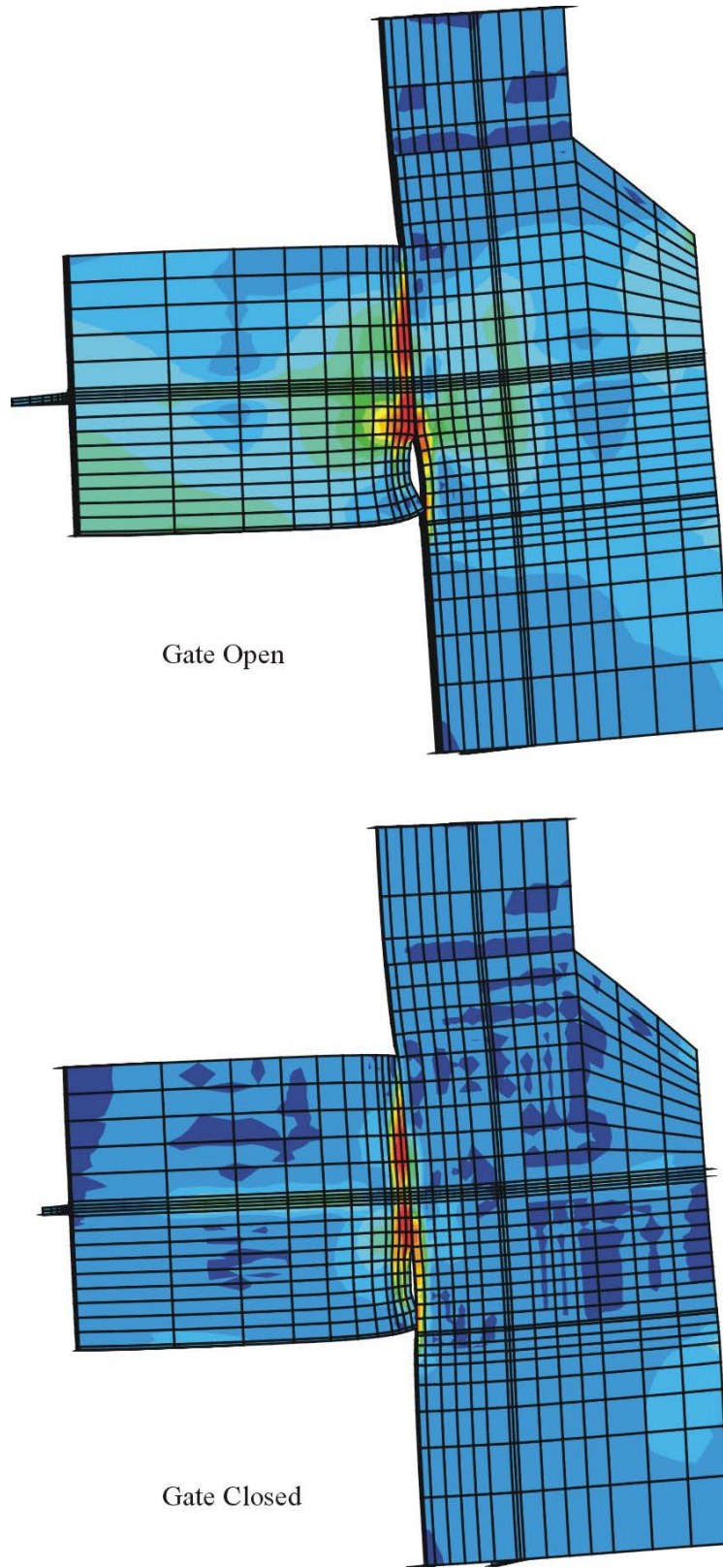
Figure C-19.  Simulation of crack extension with
residual stresses under load cycle
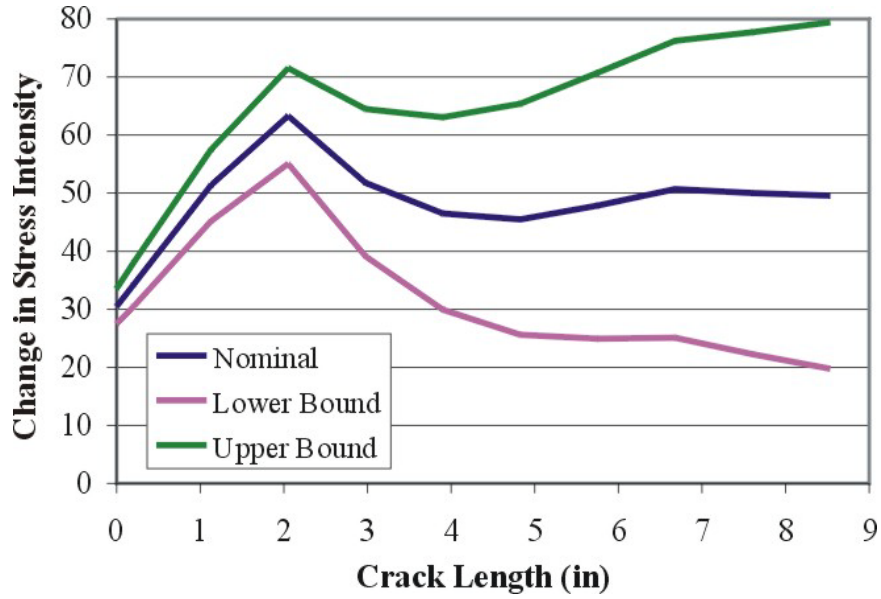
Figure C-20.  Characterization for change in stress intensity,
Markland Lock miter gate (Note:  to convert in. to mm,
multiply by 25.4)
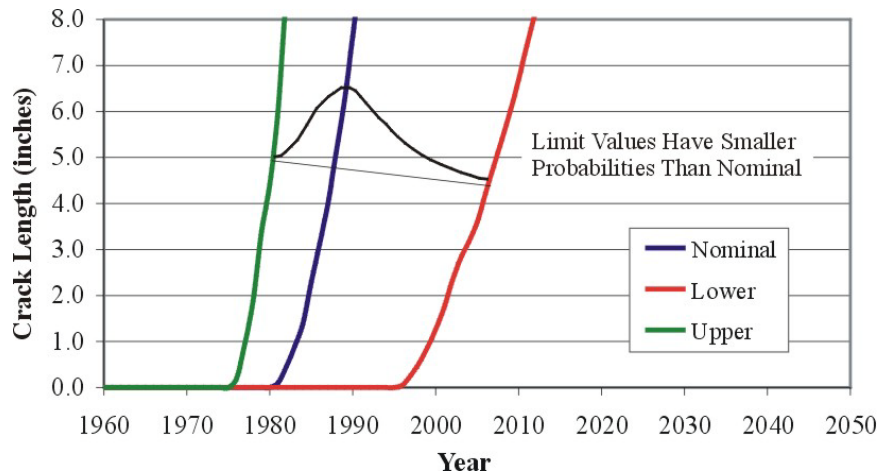


Figure C-21.  Evaluation for crack length and effect of parameter
variations for Markland Gate (Note:  to convert in. to mm,
multiply by 25.4)
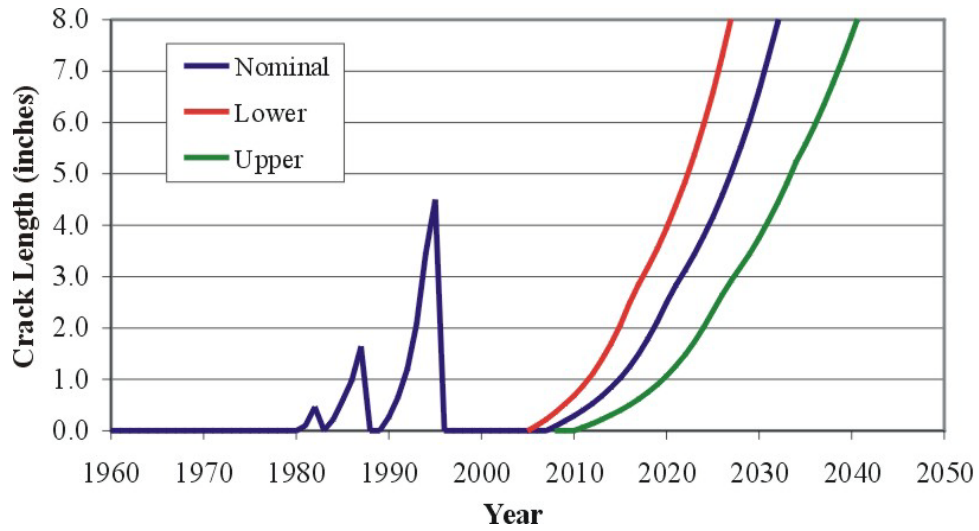
Figure C-22.  Simulation of tracking repair history with reliability model
(Note:  to convert in. to mm, multiply by 25.4)
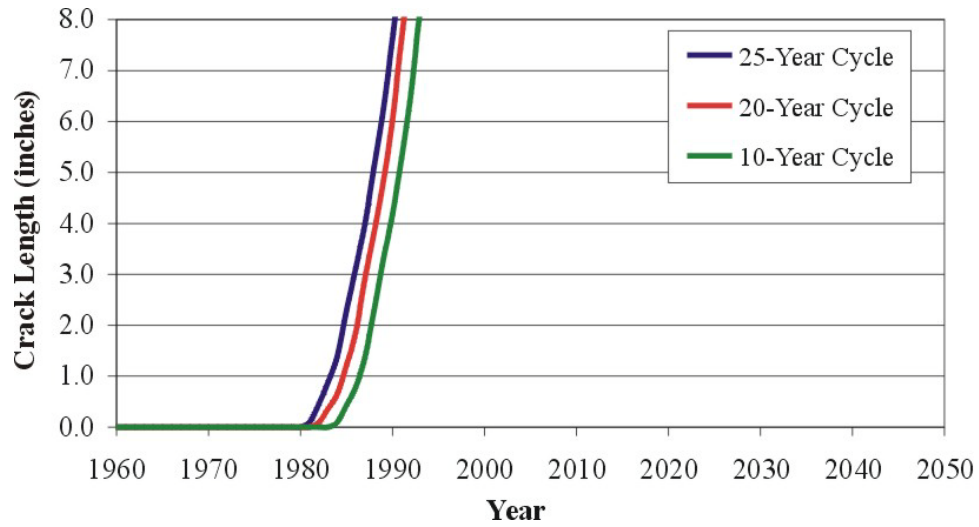
Figure C-23.  Effect of regular maintenance on the fatigue cracking
for Markland Gate (Note:  to convert in. to mm, multiply by 25.4)
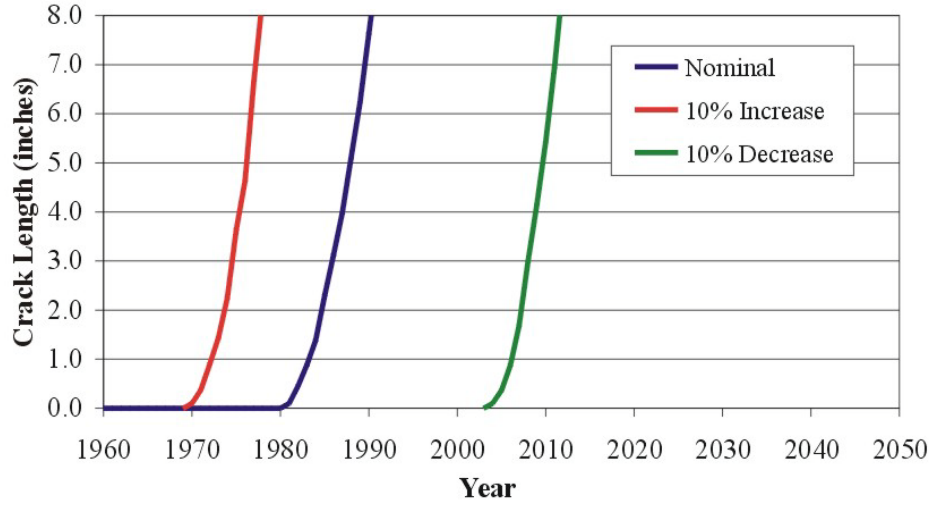
Figure C-24.  Effect of variation in residual stress
(Note:  to convert in. to mm, multiply by 25.4)
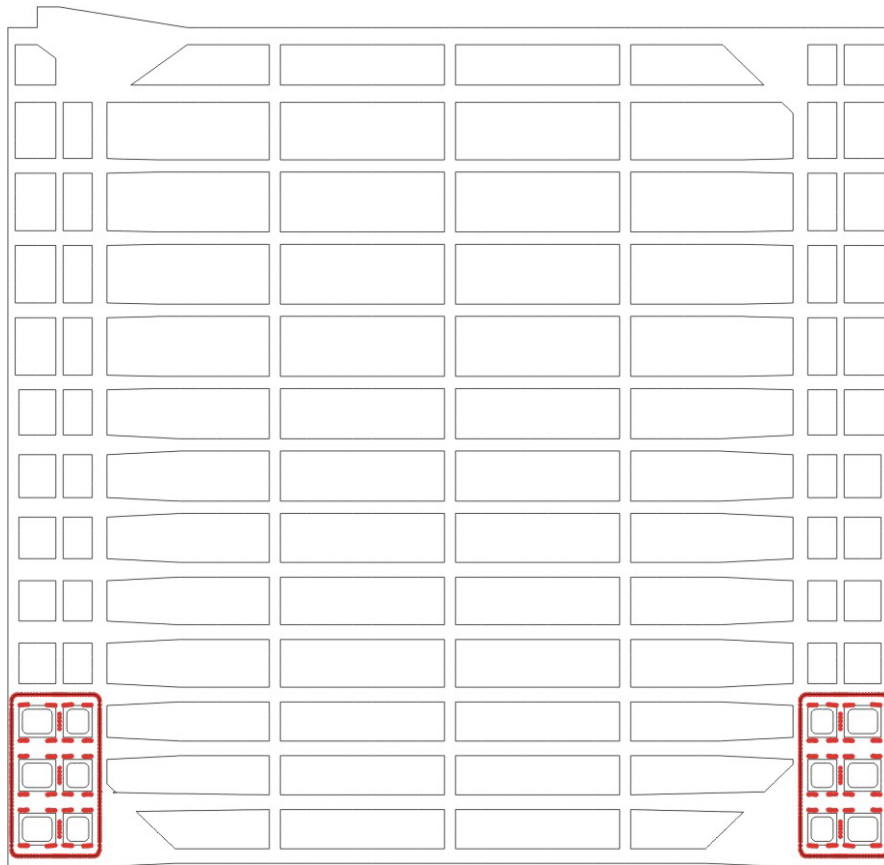


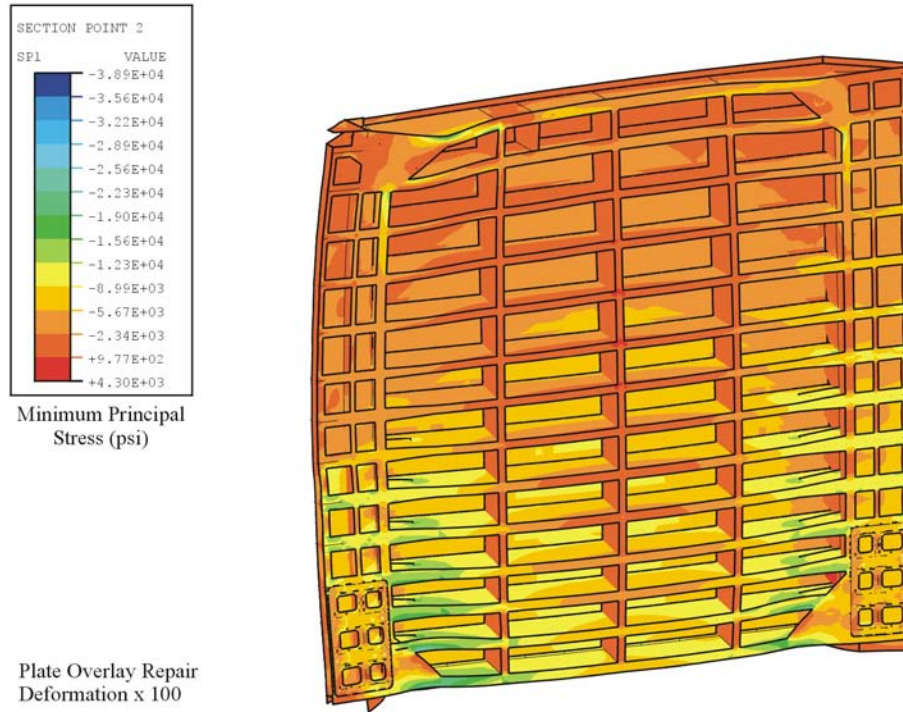Figure C-25.  Illustration of modeling used to simulate plate overlay repair

Figure C-26. Maximum principal stresses with plate overlay repair for normal operating condition (to convert psi to MPa, multiply by 6.894757)
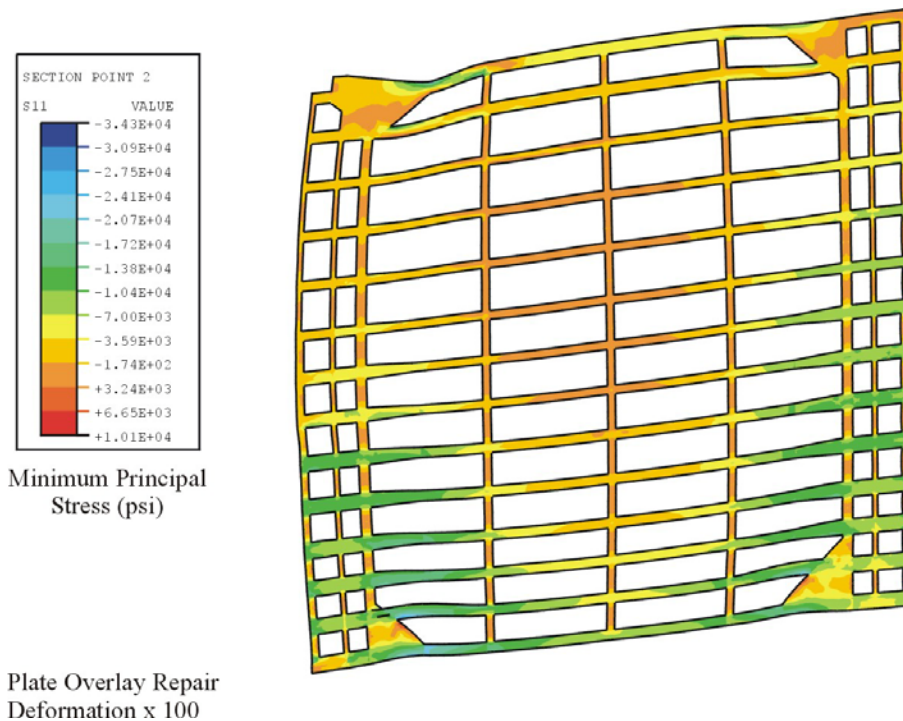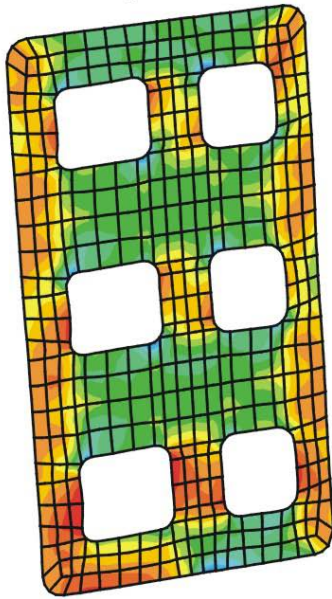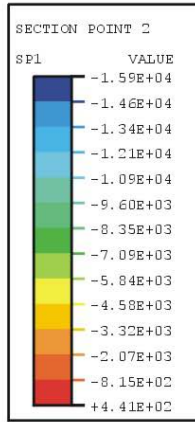


Figure C-27. Maximum principal stresses in downstream flanges with plate overlay repair for normal operating condition (to convert psi to MPa, multiply by 6.894757)
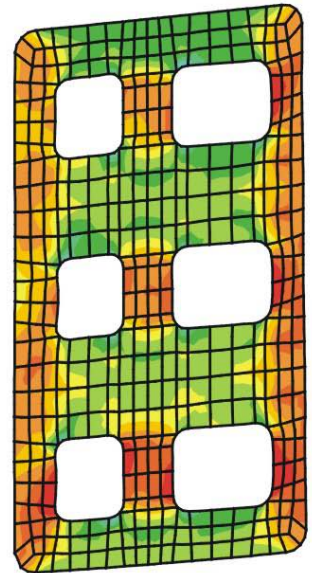
At Quoin End

Minimum Principal
Stress (psi)

At Miter End

```
SECTION POINT 2
SP1          VALUE
        -1.59E+04
        -1.46E+04
        -1.34E+04
        -1.21E+04
        -1.09E+04
        -9.60E+03
        -8.35E+03
        -7.09E+03
        -5.84E+03
        -4.58E+03
        -3.32E+03
        -2.07E+03
        -8.15E+02
        +4.41E+02
```

Maximum Principal
Stress (psi)

```
SECTION POINT 2
SP2          VALUE
        -3.58E+03
        -2.76E+03
        -1.93E+03
        -1.11E+03
        -2.83E+02
        +5.42E+02
        +1.37E+03
        +2.19E+03
        +3.02E+03
        +3.84E+03
        +4.67E+03
        +5.49E+03
        +6.32E+03
        +7.14E+03
```
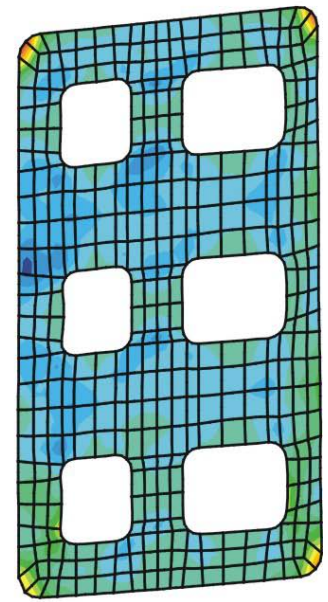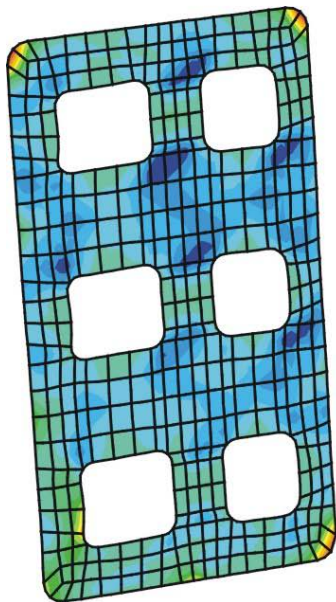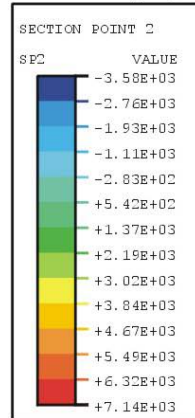
Plate Overlay Repair
Deformation x 100

Figure C-28. Principal stresses in plate overlay for normal operations(to convert psi to MPa, multiply by 6.894757)

SECTION POINT 1

SP2          VALUE
    -2.89E+03
    -2.03E+03
    -1.18E+03
    -3.20E+02
    +5.36E+02
    +1.39E+03
    +2.25E+03
    +3.10E+03
    +3.96E+03
    +4.82E+03
    +5.67E+03
    +6.53E+03
    +7.39E+03
    +8.24E+03

Maximum Principal
Stress (psi)
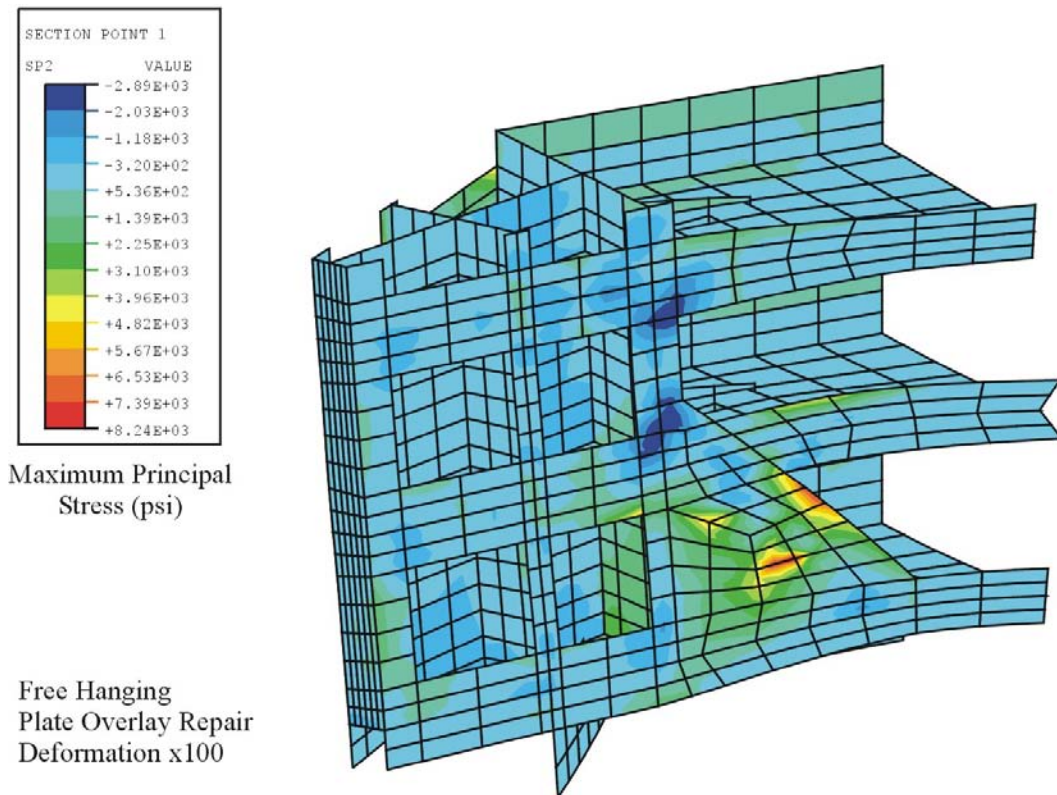
Free Hanging
Plate Overlay Repair
Deformation x100

Figure C-29.  Maximum principal stresses in quoin region with plate overlays
removed for free hanging condition (to convert psi to MPa,
multiply by 6.894757)